An Evaluation of the Contributions of Short and Long Range Pollutant Transport on Southern Ontario's Atmospheric Sulfur Content

Austin Pritchard-Oh

A Thesis submitted to the Faculty of Graduate Studies in Partial Fulfillment of the Requirements for the Degree of Master of Science

Graduate Program in Atmospheric Chemistry

York University

Toronto, Ontario

February 17th, 2023

Abstract

Sulfur dioxide (SO_2), particle sulfate ($p\text{-}SO_4^{-2}$), and total sulfur (SO_x) was evaluated at York University, in Toronto, Canada, using a Thermo Fisher SO_2 analyzer and an Aerodyne Aerosol Mass Spectrometer. These measurements were compared with a historical dataset from 2002-2020, which demonstrated a downward trend in atmospheric sulfur. Toronto's atmospheric sulfur decline has plateaued in recent years. Current mean SO_2 was 0.37 ppb, $p\text{-}SO_4^{-2}$ was 0.60 $\mu g/m^3$, and SO_x was 1.6 $\mu g/m^3$. There were no significant seasonal, daytime, or nighttime differences. The effects of pollutant transport and major contributors to Toronto's sulfur were determined. Major contributors to SO_2 included Hamilton metal refineries, Greater Toronto Area chemical production facilities, the Nanticoke petroleum refinery, and vehicle emissions. Major contributors to $p\text{-}SO_4^{-2}$ are Sarnia petroleum and chemical production, Sudbury metal refineries, and long-range transport from the Ohio River Valley. A field study mass-balance determination of Sarnia's SO_2 emissions was estimated at 0.18 tonnes/hr (4,300 kg/day).

Acknowledgements

To my supervisor, Professor Robert McLaren, I would like to extend my utmost thanks for your endless wisdom, patience, humor, and support through this project. I could not have had a more seamless transition into atmospheric chemistry and graduate studies without your support.

To my committee members, Dr. John Liggio, and Professor Cora Young, I thank you for your guidance and insight over the course of my research, as well as your enthusiasm and kindness for my project.

To my colleagues at York University, who put as much (if not more) blood, sweat, and tears into our work alongside me. My group members, Yeuhyun Kim (who I thank for patiently explaining everything I needed to know, twice, thrice, and endlessly more) and Nicole Badiali (who I thank for her dedication and support with assisting my research). A special thank you to Dr. Shira Joudan from Professor Young's group, for helping troubleshoot any issues I came across, and for graciously offering her data to help my project, as well as Stefan Miller and Rhythm Reet for providing meteorological data.

To the many wonderful people at Environment and Climate Change Canada who made this project possible, with a special appreciation for Dr. Katherine Hayden and Dr. Cristian Mihele, I thank you for teaching me so much about atmospheric chemistry and troubleshooting analytical instruments, as well as providing the essential equipment required for this study.

To my loving parents, I thank you for the incredible support and patience through this project. I thank you for, all the way from my very earliest memories, instilling in me a love and passion for science, learning, and investigation. Most of all, I thank you for your unconditional love my entire life.

To my partner and darling love, Riley, without whom none of this would be possible, I thank you for providing the unwavering love that carried me through this project. Your help and support in every aspect of my life made the endlessly long days and nights of work seem effortless, and I could not have done this without you.

Table of Contents

List of Tables

List of Figures Fix Page Numbers

Chapter 1 - Introduction

1.1 Contextualizing Atmospheric Sulfur

To understand the current state of atmospheric sulfur in southern Ontario, we must first contextualize the historical significance, as well as the anthropogenic and environmental relevance of sulfur. Two of the most important sulfur species in the atmosphere are sulfur dioxide (SO_2) and the particle sulfate ($p\text{-}SO_4^{-2}$), each with important, negative implications for human health and the environment.[1] Note that $p\text{-}SO_4^{-2}$ is a component of particulate matter under 2.5 micrometers in diameter ($PM_{2.5}$). In the context of human health, SO_2 causes respiratory irritation and inflammation and exacerbates existing respiratory and cardiac conditions,[2] while increased $p\text{-}SO_4^{-2}$ levels are positively correlated with increasing hospital admissions for respiratory illness.[3] Both pollutants are positively correlated with increases in all-cause deaths (total number of recorded deaths attributed to any reason).[2,3] In addition, SO_2 oxidizes in the atmosphere to $p\text{-}SO_4^{-2}$, and $PM_{2.5}$ has well-established links to negative effects on human health.[3,4,5] In the context of the environment, SO_2 is a precursor species to acid rain, which is significantly destructive to lakes, forests, and agricultural sectors through acid deposition on water and soil.[6] Sulfur also has important implications for climate change; aerosols (including $p\text{-}SO_4^{-2}$) engage in solar radiation scattering, and alter global mean radiative forcing.[1] This radiation-scattering effect results in global cooling, correlated with aerosol concentration.[1]

From a historical perspective, sulfur has been a significant factor in high pollution air quality events. It is capable of forming a sulfurous smog (as opposed to ozone-driven smog common in modern urban environments, such as those commonly seen in Los Angeles[7]), the most famous and notable of which being the Great Smog of London.[8] Over a period of 5 days in 1952, a sulfurous smog formed over London, driven by coal-burning stoves and factories, and caused widespread illness. Up to 12,000 deaths were attributed to the smog over this short time period. While we would not expect such an extreme event in modern times due to environmental and fuel content regulations, sulfur's smog-forming capabilities and its subsequent detriments to human health must still be considered. From a local perspective, high

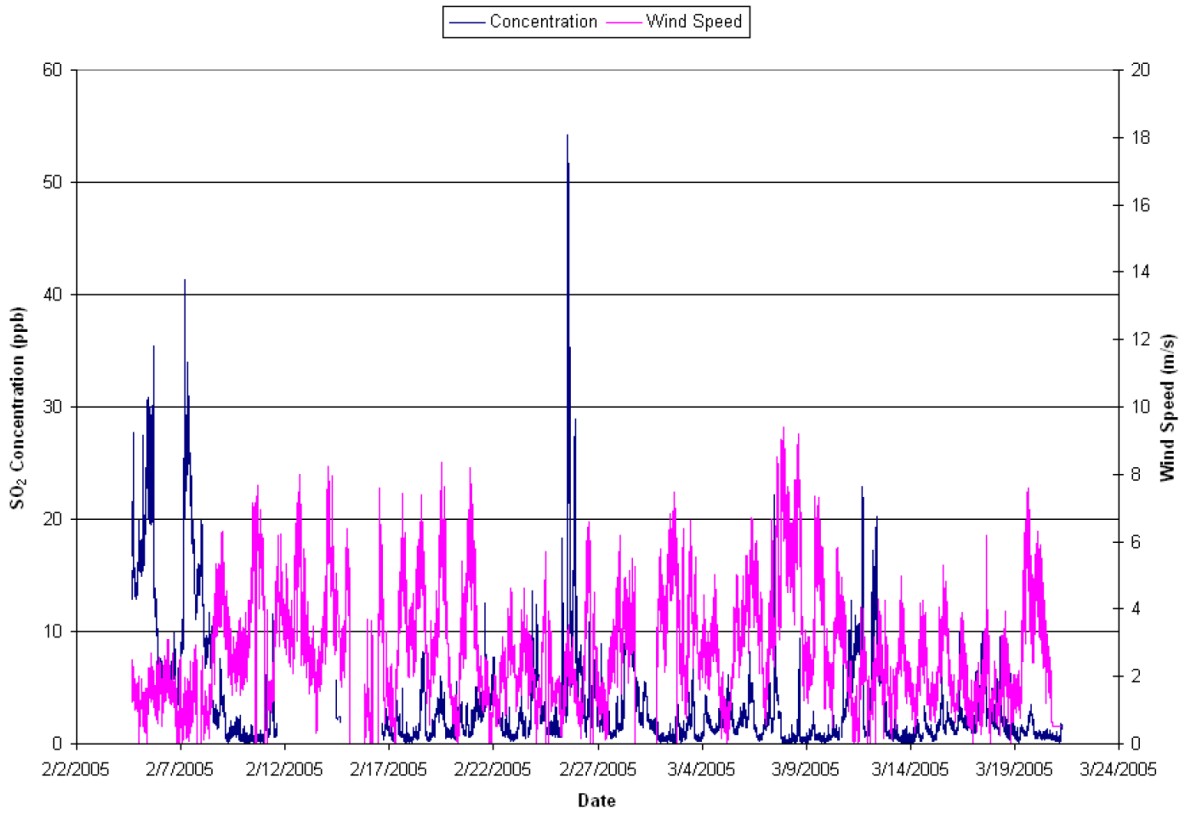

Figure 1. A graph depicting SO_2 and wind speed measurements over a nearly 2-month time period in 2005, taking place on the roof of the Petrie Science and Engineering Building at York University.

pollution air quality events in Ontario have been traditionally dominated by high concentrations of atmospheric sulfur.[9] A previous measurement from 2005 at York University measured SO_2 levels as high as 50 parts-per-billion (ppb) during the first wintertime air quality warning issued by the Ontario Ministry of the Environment, for example (see Figure 1).[10] The current Ontario Ambient Air Quality Criteria (the Ontario Ministry of the Environment-established upper mixing ratio limit for a given pollutant, selected to be protective against health and environmental effects) for SO_2 are presented as follows, for comparison: the 10-minute limit is 67 ppb, the 1-hour limit is 40 ppb, and the annual limit is 4 ppb.[11] The 10-minute and 1-hour limits were established to be preventative against negative health effects, while the annual limit is preventative against environmental damage.[11]

To fully understand the current state of atmospheric sulfur in Ontario, it is important to first examine any notable, historic sources, while also accounting for environmental regulations that may limit sulfur emissions. Fairbridge's report on SO_2 at York University noted that, in 2002, SO_2 emissions were largely driven by power generation and industrial activity (such as oil refining and metal smelting), with the vast majority (~74%) coming from Ontario Power

Generation, and much of the remainder coming from St. Lawrence Cement, Petro-Canada, and Tonolli Canada LTD.[10] In that same year, the National Pollutant Release Inventory database lists the highest polluters for $PM_{2.5}$ as industrial plants largely dealing with fiberglass, glass, and metallic alloys (Owens Corning, O-I Canada Corp., and Indalloy, respectively.)[12] We can also examine the NPRI 2002 emissions inventory for sulfuric acid, as this contributes directly to atmospheric p-SO_4^{-2} concentrations. In 2002, the significant contributing sectors were very similar to SO_2, with the majority of emissions originating from the exact same sectors and facilities.[12]

Petroleum and coal produce sulfur through combustion - hydrocarbon resources are formed through the geological transformation of organic matter and, upon combustion, release and oxidize sequestered sulfur deposits that originated from the cells of biological organisms, as well as seawater sulfate.[13] Similarly, metal smelting processes release sulfur species trapped in ores. Copper, for example, is refined and smelted partially from chalcopyrite ($CuFeS_2$), a cupric sulfide compound; when raw ore is heated, sulfur is released and oxidized into SO_2.[14] - Chemical production facilities are a broad term to refer to any manufacturing site which generates an industrial product through a chemical process with a sulfur byproduct. A relevant example of this is carbon black production, such as with Cabot Canada Ltd. In Sarnia, Ontario: through the pyrolysis of precursor reagents containing hydrogen sulfides, sulfur is oxidized and released into the atmosphere as SO_2.[15]

Note that direct SO_2 emissions were far higher than sulfuric acid and $PM_{2.5}$ (of which p-SO_4^{-2} is only a partial component). Direct sulfate emissions can be approximated as the sum of sulfuric acid and roughly 25% of $PM_{2.5}$ emissions (proportion based on a 2007 study of the annual average composition of $PM_{2.5}$ across the entire United States by Bell et al.).[16] In 2002, the total emitted SO_2 was 562,227 tonnes, the total emitted sulfuric acid was 6,045 tonnes, and the total emitted $PM_{2.5}$ was 23,398 tonnes.[12] From this, we can see that SO_2 emissions are roughly 50x higher than sulfate. Thus, it can be seen that the bulk of direct emissions of sulfur to the atmosphere are in the form of SO_2, which subsequentially oxidizes to p-SO_4^{-2}, rather than being emitted directly as sulfate.

Since the 1980s, many regulations have been enacted under the Environmental Protection Act of Ontario in the interest of curtailing atmospheric sulfur emissions. Specifically and recently, by the start of 2015, all power generation facilities in Ontario were no longer allowed to use coal.[17] In addition, limits on sulfur content in gasoline were added to keep it below 12 mg/kg sulfur by mass.[18] A final example would be that, by 2019, petroleum facilities would have specific limits of 225 kg/day for their SO_2 emissions.[19] Given these changes, and the historic sources of SO_2 being dominated by power generation and petroleum companies, we would expect measurements to show significant decreases in atmospheric sulfur in more recent times. Per the National Pollutant Release inventory, it can be observed that the contribution of power generation to atmospheric sulfur has dropped to negligible levels, and is now dominated only by metal smelting, petroleum refining, and chemical production (see **Tables 1 and 2**).[12]

Table 1. Top SO_2 contribution point sources in Southern Ontario per the NPRI data set for 2020. Includes every source contributing at least 1% of the total SO_2 emissions for Ontario. Included for comparison is the current contribution of Ontario Power Generation Inc.

Company	Facility	City	Total Emissions (tonnes)	Contribution (%)	Sector
Vale Canada Limited	Copper Cliff Smelter	Copper Cliff	27686	24.9	Metals
Glencore Canada Corporation	Sudbury Integrated Nickel Operations Smelter	Falconbridge	26217	23.6	Metals
Imperial Oil	Sarnia Refinery Plant	Sarnia	7190	6.47	Petroleum
St. Mary's Cement Inc. (Canada)	Bowmanville Cement Plant	Bowmanville	6085	5.48	Chemical Production
Vale Canada Limited	Copper Cliff Nickel Refinery	Copper Cliff	5935	5.34	Metals
Imperial Oil	Imperial Oil Nanticoke Refinery	Nanticoke	4788	4.31	Petroleum
ArcelorMittal Canada MP Inc.	ArcelorMittal Dofasco	Hamilton	4672	4.21	Metals
Cabot Canada Limited	Cabot Canada Limited	Sarnia	4098	3.69	Chemical Production

Table 1. (Continued)

Company	Facility	City	Total Emissions (tonnes)	Contribution (%)	Sector
Birla Carbon Canada Ltd.	Birla Carbon Canada Ltd.	Hamilton	2737	2.46	Chemical Production
Algoma Steel Inc.	Algoma Steel Inc	Sault Ste. Marie	2540	2.29	Metals
Stelco Inc.	Hamilton	Hamilton	2444	2.20	Metals
Stelco Inc.	Lake Erie	Haldimand County	2033	1.83	Metals
Lehigh Hanson Materials Limited	Picton Plant	Picton	1700	1.53	Chemical Production
Carmeuse Lime Canada	Dundas Operations	Dundas	1460	1.31	Chemical Production
Shell Canada Products	Sarnia Manufacturing Centre	Corunna	1434	1.29	Petroleum
CRH Canada Group Inc.	Mississauga Cement Plant	Mississauga	1185	1.07	Chemical Production
Produits forestiers Résolu	Resolute Forest Products - Thunder Bay Operations	Thunder Bay	1183	1.06	Chemical Production
Ontario Power Generation Inc.	Lennox Generating Station	Greater Napanee	107.0	0.10	Power Generation

Table 2. Total percent contribution by sector of the point sources listed in **Table S1**. The remaining ~13% is made up of a roughly even mixture of the 3 sectors, with around 0.1% of the total contribution stemming from power generation.

Sector	Total Contribution (%)
Metals	64.4
Petroleum	12.1
Chemical Production	11.1

Overall, environmental regulations for the reduction of atmospheric sulfur over the last few decades has been very successful on a global scale, particularly in North America and Europe. From 1990 to 2015, SO_2 emissions in these regions have decreased by roughly 70-80%, based on legislation and pollution controls.[1] Modeling results indicate an associated decrease in p-SO_4^{-2} concentrations with reduced SO_2, which would positively correlate with improved health and environmental outcomes.[1]

An important note for this project is conventional units used for SO_2, which differ from units used for particulate matter. SO_2 (as well as other gas-phase single species) are given in a mixing ratio, which describes the number of moles of gas divided by the number of moles of air (in this case, SO_2 is typically given in units of ppb, as recorded by the analytical instrument used in this project). Since $PM_{2.5}$ represents a mixed collection of various species, it is not well-represented as a mixing ratio, and is instead given as mass-per-unit-volume concentration (in this case, μg/m^3). At 25 °C and 1 atm of pressure, SO_2 can be converted to a concentration unit (μg/m^3) by multiplying the mixing ratio value in ppb by 2.62.

1.2 Important Chemistry of Atmospheric Sulfur

Broadly speaking, atmospheric particles are airborne clusters of solid and liquid material that coagulate matter around a stable, solid nucleus in the air to form dense particles.[20] These particles further agglutinate and continually grow in size before eventually becoming cloud condensation nuclei, or becoming too heavy to sustain their lift, depositing to the earth below.[20] Atmospheric particles typically range from 0.003 – 100 μm in diameter, with fine

particles defined as being below 1 µm, and coarse particles being defined as above 1 µm.[20] Fine particles can sustain their lift and continue their airborne transport for several weeks, crossing the span of oceans and continents, facilitating long-range transport of pollutants.[20] While particles can form around solid material (such as dust, soot, sea salt spray, etc.), they can also be generated from oxidated species, such as the SO_2 to p-SO_4^{-2} oxidation pathway.[20]

There are 3 important reaction pathways to consider for the oxidation of SO_2 to SO_4^{-2}, the first being the dry, homogenous reaction of SO2 with hydroxyl radical, the second being the reaction between SO_2 with ozone and peroxide in aqueous solutions (clouds, fog precipitation, etc.), and the third being the reaction between SO_2 and NO_2. The proposed reaction scheme for the first pathway is as follows[21]:

$$OH + SO_2 \overset{M}{\rightarrow} HOSO_2 \quad (\boldsymbol{Eq.1})$$

$$HOSO_2 + O_2 \overset{M}{\rightarrow} HO_2 + SO_3 \ (\boldsymbol{Eq.2})$$

$$H_2O + SO_3 \overset{M}{\rightarrow} H_2SO_4 \quad (\boldsymbol{Eq.3})$$

This reaction forms sulfuric acid in the atmosphere, which readily condenses to form particle sulfate.[22]

The proposed reaction scheme for the second pathway with ozone is as follows, where SO_2 in cloud droplets forms an equilibrium with SO_3^{-2}, with subsequent O_3 oxidation occurring with the latter species[23]:

$$SO_2 + H_2O \rightleftharpoons {SO_3}^{-2} + 2H^+ \ (\boldsymbol{Eq.4})$$

$${SO_3}^{-2} + O_3 \rightarrow SO_4^{-2} + O_2 \ (\boldsymbol{Eq.5})$$

The proposed reaction scheme for the second pathway with peroxides is as follows[24]:

$$SO_2 + H_2O_2 \rightarrow H_2SO_4 \quad (\boldsymbol{Eq.6})$$

This reaction again forms sulfuric acid, which condenses to p-SO_4^{-2}. The third reaction pathway will be discussed shortly, in the context of smog formation. These reactions are key for understanding how p-SO_4^{-2} levels are maintained in the environment, as direct $PM_{2.5}$ emissions

are far lower than direct SO_2 emissions. **Reactions (5)** and **(6)** in particular are thought to contribute to over 80% of the global formation of particle sulfate.[23] Thus, the conversion of SO_2 via **Reactions (1) - (6)** is a critical factor in determining air quality.

Sulfur is also important for determining smog events. Photochemical smog in urban environments is primarily driven by ozone and is also mixed with $PM_{2.5}$.[25] It follows that high SO_2 emissions would directly result in increased smog severity through the production of p-SO_4^{-2}. There is another important chemical consideration: the interactions between SO_2, ozone, and nitrogen compounds. During the day, NO_x (representing NO + NO_2) catalytically forms ozone via the oxidation of volatile organic compounds.[26] In addition, there is some limited suggestion in recent literature that, during high relative humidity periods, SO_2 undergoes rapid aqueous oxidation by NO_2 to form p-SO_4^{-2} (often known as 'winter haze' events due to its seasonal dependence).[27] This would, in turn, decrease air quality through the direct addition of $PM_{2.5}$ to smog clouds. It would also, however, decrease the amount of ozone, by consuming available reactive NO_2, which paradoxically reduces smog.

Another indirect link between p-SO_4^{-2} and ozone is suggested by Brown et al. (2006).[26] In that study they showed that increased p-SO_4^{-2} concentrations at night can decrease the lifetime of N_2O_5, giving rise to less NO_x available the next day for NO_x catalyzed ozone formation. The implication is that decreases in SO_2 emissions (and thus p-SO_4^{-2}) could lead to longer lifetimes of N_2O_5 at night, more NO_x the next day, and thus more NO_x available for NO_x catalyzed ozone formation. Thus, one can conclude that atmospheric sulfur content is a delicate balance in terms of air quality. Increased sulfur emissions directly result in increased $PM_{2.5}$, while decreased emissions ultimately can result in decreased ozone formation (in winter), but perhaps increased O3 formation in summer. It will be important to precisely examine current concentrations of SO_2 and p-SO_4^{-2} to determine if atmospheric sulfur is still an important factor in air quality, and whether decreased SO_2 emissions have been a net benefit.

1.3 Effects of Temporal and Seasonal Variation

There are expected seasonal variations in SO_2 and p-SO_4^{-2}, likely due to a combination of climate, meteorological, and anthropogenic effects (such as changes in power generation for

climate control). For example, in 1998, a monitoring site on Mt. Sonnblick, Austria, noted similar SO_2 levels in winter and summer, and highly elevated SO_2 levels in the springtime.[28] It is likely that trends in seasonal variability are dependent on local climate patterns, and so the seasonal variance of SO_2 and p-SO_4^{-2} will be further investigated in this report. A study of SO_2 emissions in 6 European cities also showed seasonal variation, demonstrating higher levels in the winter compared to the summer.[29] This was attributed to higher use of fuel for heating, as well as cold temperature inversions in the boundary layer trapping SO_2 emissions.[30] Thus, while electricity usage would be high in the summer due to air conditioning usage, meteorological factors may result in higher winter mixing ratios. A study in the eastern U.S noted some long-term seasonal dependence of p-SO_4^{-2} after SO_2 emissions regulations.[30] Specifically, the authors noted that decreases in p-SO_4^{-2} followed decreases in SO_2 at a slower rate in winter than in summer, suggesting a significant effect of a wintertime production pathway for p-SO_4^{-2} from the oxidation of SO_2 with ozone in pH-sensitive clouds.[30] SO_2 is also expected to display diurnal patterns. The European cities study showed consistently lower levels of SO_2 later in the day and overnight when compared to early morning measurements, likely related to vehicle emissions.[29]

Overall, SO_2 mixing ratios are very highly influenced by anthropogenic activity. In seasons of high electricity consumption (i.e., summer air conditioning usage and winter heating, versus spring and fall seasons), SO_2 emissions from power generation would be at their highest. Meteorological factors have major influences on seasonal variation, and thus, SO_2 mixing ratios per season are regionally dependent.

1.4 Research Objectives

The main objective of this research is to evaluate the current levels of SO_2 and p-SO_4^{-2} in Southern Ontario, their seasonal and temporal transformations, their impacts on air quality, and to trace their significant sources of origin, in an attempt to determine the current relative impacts of short- and long-range transport on Toronto's atmospheric sulfur levels. Due to constraints related to the COVID-19 pandemic, the first year of research was spent analyzing historical data on SO_2 and p-SO_4^{-2}, to contextualize the current findings. Measurements were

conducted with a ThermoFisher 43i-TLE UV Fluorescence Sulfur Dioxide Analyzer (43i), and a High-Resolution Time of Flight Aerodyne Aerosol Mass Spectrometer in V-Mode (V-Mode HR-TOF-AMS), beginning on August 12th, 2021. Note that due to hardware-related issues with the first 43i instrument, a second, replacement 43i instrument was used beginning on July 18th, 2022 (See **Chapter 2.2**).

Additional data has been provided from auxiliary instruments (see **Acknowledgements** for sources). CO_2, CO, and methane data was collected from a Picarro G2401 Gas Concentration Analyzer Cavity Ringdown Spectrometer (Picarro CRDS) while p-SO_4^{-2} data was collected from a URG Corp. and ThermoFisher Scientific ambient ion monitor-ion-chromatography-mass-spectrometer (AIM-IC-MS). In addition, meteorological data has been provided. Historic and current atmospheric sulfur data will also be used as a point of comparison from Environment Canada's National Air Pollution Surveillance Program (NAPS) Data Mart,[31] as well as the Ontario Ministry of the Environment.[32]

The advantage of the data collected through this thesis project when compared to the NAPS and Ontario Ministry data is two-fold: first, the time-resolution is much higher from our data collection period. The SO_2 data provided by NAPS and the Ontario Ministry was given as hourly-averages, while the p-SO_4^{-2} data was a 3-day-average. Our data collected occurs every 10 seconds for SO_2, and every minute for p-SO_4^{-2}, allowing for much more precise analysis of the origins of high-concentration sulfur plumes, as well as the peak concentrations, which are often lost during broad averaging times. The second advantage is data availability – it often takes significant time for NAPS and the Ontario Ministry to release their datasets. For example, the 2022 data set for SO_2 is currently unavailable at the time of writing this report, and the 2022 Ontario Ministry data is viewable on a day-to-day basis but is not available for bulk analysis.

The current research objective is to analyze the collected data for specific trends, as well as to investigate high pollution air quality events to determine their nature and source. For trend data, we will determine the following parameters about SO_2 and p-SO_4^{-2}: overall means and uncertainty, hourly means, seasonal and temporal variations, and origin directions of pollutants. This will be supported with non-particle-sulfate data collected by the AMS (such as

ammonia, nitrate, and organic aerosols), meteorological data, and the Picarro data. Pollution event analysis will involve examining high pollutant concentration periods and investigating their sources and causes. This will be accomplished through the use of National Oceanic and Atmospheric Administration (NOAA) HYSPLIT backwards trajectory modeling and NPRI point source data.

Of particular interest is the role of long-range transport in local sulfur mixing ratios and concentrations, for SO_2 and p-SO_4^{-2}; given the recent trends in sulfur reduction from environmental regulations, it is expected that local sulfur levels will have decreased over the last few years. It is therefore likely that long-range transport will now have a greater effect on local sulfur in Toronto when compared to pre-regulation measurements, especially considering the ban on coal-fired power plants. Now that Ontario Power Generation is not expected as a source of SO_2, the sources of interest will include steel factories in the south in Hamilton, Ontario, metal smelting in the north in Sudbury, Ontario, petroleum refining and chemical production in the west in Sarnia, Ontario, and coal-fired power plants from the Ohio River Valley south-west across the border with the United States (where Ontario's environmental regulations are irrelevant).

This project was supported by a field study campaign conducted in Sarnia, Ontario, from July 21-22, 2022. Since it is known that a significant portion of Ontario's sulfur emissions are sourced from petroleum refining in Sarnia, it is theorized that Sarnia's emissions would have a long-range transport effect and influence local sulfur levels in Toronto.[12] To this end, a two-day trip was taken to Sarnia with the 43i instrument to evaluate SO_2 emissions from the city. The measurements taken were applied to a mobile mass-balance method for the calculation of the total mass of sulfur emitted from Sarnia. This value can be compared to historic SO_2 inventory numbers to determine the relative influence of Sarnia to Ontario's sulfur emissions in 2022, to better support the analysis of any high SO_2 HYSPLIT trajectories originating from the south-west.

Chapter 2 - Experimental Methods & Instrumental Setup

2.1 Description of Historical Data

All data used for the preliminary evaluation of atmospheric sulfur was taken from the NAPS Data Mart,[31] as well as the Ontario Ministry of the Environment.[32] NAPS operates 286 monitoring sites across Canada, reporting continuous measurements of SO_2, NO_2, particulate matter, ozone, and CO.[33] SO2 data was given as hourly average measurements in units of ppb. Particle sulfate data was given as speciated $PM_{2.5}$ data and was collected through ion chromatography of PM collected on Teflon filters. The NAPS $PM_{2.5}$ data was given as a daily-average measurement, roughly twice a week at various stations. The Ontario Ministry of the Environment data for SO_2 is given as hourly averages from an ambient air monitoring station in the north side of Toronto.

Three different NAPS site locations were selected for our preliminary analysis: Toronto, Windsor, and Simcoe. Toronto was selected to best mimic the conditions that will be applicable to new measurements at York University and is also representative of a typical urban environment. Windsor was selected as it will likely be indicative of sulfur emissions coming from Detroit, Michigan (a location known for being highly industrialized, and likely a large source of transported sulfur). Simcoe was selected due to the fact that local sources of sulfur will be very low, as a relatively non-industrialized, rural region. It is also on the transport path from Ohio and other Midwestern states, a historic source of long-range transport of sulfur into Ontario[30], and so Simcoe may be used as an indicator for any changing trends in long-range pollutant transport over time.

For SO_2, yearly means were calculated for all sites, along with seasonal means and daytime and nighttime intervals for Toronto. For this purpose, spring season was defined to be the months of March, April, and May, summer defined as June, July, and August; Autumn was defined as September, October, and November and winter was defined as December, January, and February. Daytime intervals were set as the 12-hour period from 8:00 AM to 8:00 PM, with the other 12-hour interval being the nighttime period. For p-SO_4^{-2}, yearly means were calculated for all sites and seasonal means were calculated for Toronto, but due to the nature

of the data, daytime and nighttime measurements could not be separated. Total SO_x (SO_2 + SO_4^{-2}) was calculated as well as the ratio of SO_4^{-2}/SO_x, for all chosen sites. The time period examined was from 2003-2020, as this was the widest range of data available at the chosen sites. Note that little data was available before 2007 for Simcoe, and in 2003 for Windsor's p-SO_4^{-2}.

2.2 43i-TLE UV Fluorescence Sulfur Dioxide Analyzer

The 43i-TLE SO2 Analyzer works via UV fluorescence spectroscopy, by exciting SO2 molecules with UV light, and capturing their decaying emissions at a longer wavelength (See **Figure 2** for schematic diagram).[34] It is possible to quantify the amount of SO2 present, as the emitted light is proportional to the concentration of SO2.[34] The sample gas is introduced to the instrument and passed to a heated kicker, which removes the hydrocarbon components without affecting the SO2 molecules (since hydrocarbon species will produce a falsely high background signal).[34] Next, the sample flows to a chamber with a pulsating UV lamp, which

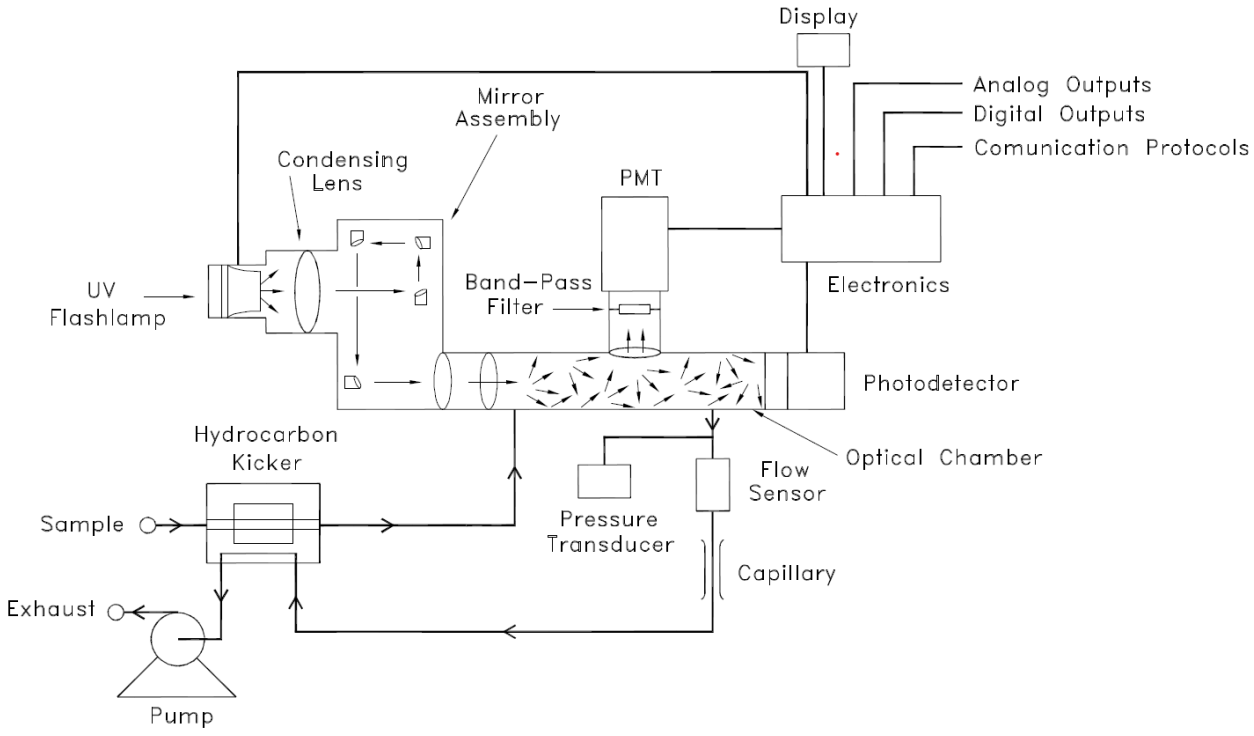

Figure 2. A schematic diagram for a ThermoFisher 43i-TLE UV Fluorescence SO_2 Analyzer Instrument.[34]

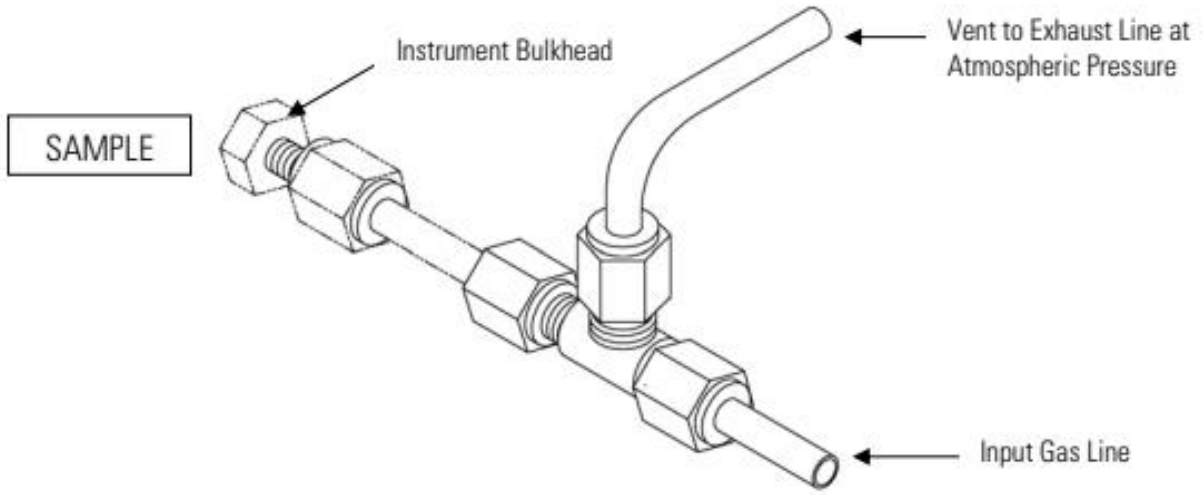

Figure 3. A schematic diagram for an atmospheric bypass setup for the Thermo Fisher Model 43i.[34] © Thermo Fisher Scientific.

starts the aforementioned excitation and decay process, which is captured by a selective mirror assembly attuned to the UV emission wavelength of SO2 and a photomultiplier tube.[34]

This instrument operates on a 300-second running average, with sampling points taken every 10 seconds; this setup provides smoother trend data by eliminating sampling variance. The theoretical lower detectable limit for the instrument at a 300-second averaging time is 0.05 ppb.[34] Data has been collected near-continuously from August 12th, 2021, to October 18th, 2022, with only minor interruptions in data collection. The ideal sampling flow rate for this instrument is 0.480 L/min. Ambient air sampling is performed through 1/8" diameter Teflon tubing which is attached to the "SAMPLE" port of the 43i via Swagelok fittings. The sampling line for this instrument is affixed to the roof of the Petrie Science and Engineering atmospheric chemistry lab and is outfitted with a Pall Zefluor™ 2 μm particulate filter (47 mm diameter).

The 43i is zeroed through the use of an ultra-zero-air compressed gas cylinder from Linde Gases. The zero-air gas cylinder is attached via 1/8" Teflon tubing to the "ZERO" port of the 43i, with an atmospheric bypass line attached with a T-junction fitting to ensure the instrument is sampling air at atmospheric pressure (See **Figure 3)**. The instrument is calibrated once weekly by switching the active intake valve to the "ZERO" port and flowing zero air into the 43i for 10 minutes, at which point this reading is stored as the background SO_2

concentration using the instrument's on-board controls. Linde gases does not provide a minimum guaranteed SO_2 concentration for their ultra-zero air. To ensure minimal SO_2 contamination, an activated carbon scrubber was fabricated out of ¼" Teflon tubing, activated carbon, and Swagelok fittings. As the zero-air passes through the Teflon tube packed with activated carbon (secured in place with cotton at each end of the tube), any SO_2 present will be scrubbed from the zero-air and adsorbed onto the carbon. The zero-air background correction value (i.e., the signal quantity read by the 43i during a sampling of zero-air) for the instrument typically varies around 1.62 ppb, though this value is known to drift by up to 1% per week, and requires weekly correction.[34] The experimental blank limit-of-detection of the analytical technique can be determined, which is equal to 3 times the standard deviation of the blanks (σ_{blank}), as well as the blank limit-of-quantitation, which is equal to $10\sigma_{blank}$. Since the blank values represent the background noise, $3\sigma_{blank}$ is the minimum threshold for 3 times the signal to noise ratio, a typical metric of detection limit. This 'blank' data is derived from 60 data points taken during two routine zeros of the instrument in July 2022, which should roughly vary around 0 ppb. The blank limit-of-detection limit for this analytical technique is 0.07 ppb (0.19 $\mu g/m^3$), and the limit of quantitation is 0.24 ppb (0.63 $\mu g/m^3$) (See **Tables 3 and 4**).

Table 3. Statistical analysis of the blanks data operating at a 300-second running average.

Statistical Parameter	Mixing Ratio (ppb)	Concentration ($\mu g/m^3$)
Mean	-0.005	-0.012
± CI (95%)	0.006	0.016
σ	0.024	0.063
3σ	0.072	0.188
10σ	0.239	0.625

Table 4. Collected blanks data from two zero-air calibrations in July 2022.

Timestamp	Blank Value	Timestamp	Blank Value
7/6/2022 11:56:45	0.008	7/13/2022 12:36:42	-0.011
7/6/2022 11:56:55	0.003	7/13/2022 12:36:52	-0.015
7/6/2022 11:57:05	-0.001	7/13/2022 12:37:02	-0.017
7/6/2022 11:57:15	-0.004	7/13/2022 12:37:12	-0.020
7/6/2022 11:57:25	-0.006	7/13/2022 12:37:22	-0.025
7/6/2022 11:57:35	-0.002	7/13/2022 12:37:32	-0.028
7/6/2022 11:57:45	-0.007	7/13/2022 12:37:42	-0.028
7/6/2022 11:57:55	-0.005	7/13/2022 12:37:52	-0.023
7/6/2022 11:58:05	-0.011	7/13/2022 12:38:02	-0.024
7/6/2022 11:58:15	-0.005	7/13/2022 12:38:12	-0.027
7/6/2022 11:58:25	0.002	7/13/2022 12:38:22	-0.024
7/6/2022 11:58:35	0.002	7/13/2022 12:38:32	-0.027
7/6/2022 11:58:45	0.002	7/13/2022 12:38:42	-0.026
7/6/2022 11:58:55	0.001	7/13/2022 12:38:52	-0.027
7/13/2022 12:34:02	0.058	7/13/2022 12:39:02	-0.030
7/13/2022 12:34:12	0.058	7/13/2022 12:39:12	-0.037
7/13/2022 12:34:22	0.049	7/13/2022 12:39:22	-0.036
7/13/2022 12:34:32	0.042	7/13/2022 12:39:32	-0.036
7/13/2022 12:34:42	0.042	7/13/2022 12:39:42	-0.041
7/13/2022 12:34:52	0.032	7/13/2022 12:39:52	-0.036
7/13/2022 12:35:02	0.032	7/13/2022 12:40:02	-0.037
7/13/2022 12:35:12	0.031	7/13/2022 12:40:12	-0.030
7/13/2022 12:35:22	0.023	7/13/2022 12:40:22	-0.025
7/13/2022 12:35:32	0.017	7/13/2022 12:40:32	0.000
7/13/2022 12:35:42	0.003	7/13/2022 12:40:42	0.003
7/13/2022 12:35:52	0.000	7/13/2022 12:40:52	0.003
7/13/2022 12:36:02	0.002	7/13/2022 12:41:02	0.001
7/13/2022 12:36:12	-0.003	7/13/2022 12:41:12	-0.003
7/13/2022 12:36:22	-0.006	7/13/2022 12:41:22	-0.004
7/13/2022 12:36:32	-0.006	7/13/2022 12:41:32	-0.001

Multipoint and span calibrations are performed to maintain instrument performance; both of these procedures rely on Mass Flow Controllers (MFCs) and a source of SO_2 gas to generate calibration gas in the appropriate mixing ratios. MFCs are from CCR Process Products (MKS GA50A MFCs with CCR SR5 digital readouts and power supplies), while a cylinder of 10.2 ±0.4 ppm SO_2 gas balanced in nitrogen is used from Linde gases. The concentration of calibration gas is calculated with the following equation[34]:

$$[SO_2]_{Out} = \frac{[SO_2]_{Std} * F_{SO_2}}{F_D + F_{SO_2}} \ (\boldsymbol{Eq.7})$$

Where $[SO_2]_{Out}$ is the concentration of SO_2 after dilution in ppm, $[SO_2]_{Std}$ is the concentration of the SO_2 gas in the cylinder used for dilution in ppm, F_{SO2} is the flow rate of the standard SO_2 gas at standard temperature and pressure, and F_D is the flow rate of the zero-air dilutant gas at standard temperature and pressure.

The previously mentioned zero-air cylinder is connected to a Teflon tube passing through one of the MFCs, while the SO_2 calibration gas cylinder is connected to a separate Teflon tube that passes through a second MFC; the outputs of these MFCs are blended together at a T-junction connected to a third Teflon tube, which transports this gas to the "ZERO" port.

A multipoint calibration was performed to check the validity of the readings of the instrument, and to correct for any deviations. This calibration procedure involves the generation of 6 known concentrations of SO_2 gas in zero air, evenly spaced between 0 ppb and the full-scale range of the instrument (set to 20 ppb). The response of the instrument at each of these points was used to create a calibration curve by which all incoming measurements were compared to and corrected by (see **Figure 4**). The equation of the line-of-best-fit is given by:

$$y = 1.0039x + 0.025714 \ (\boldsymbol{Eq.8})$$

$$\text{or: } [SO_2]_{Adjusted} = \frac{([SO_2]_{Raw} - 0.025714)}{1.0039} \ (\boldsymbol{Eq.9})$$

Incoming data was therefore adjusted by **Equation (9)**, where $[SO_2]_{Raw}$ is the raw signal recorded by the detector in ppb, and $[SO_2]_{Adjusted}$ is the multipoint-calibrated 'true' value in ppb.

In addition, weekly span calibrations were performed to adjust for drift in the instrumental readings. A calibration gas of SO_2 in zero-air was generated at a mixing ratio corresponding to 80% of the full-scale (16 ppb, in this case). This generated gas is used to calibrate the instrument's internal coefficient value, which is a multiplicative factor that adjusts the signal created by sampled SO_2 to an ideal value determined by the calibration gas.[34] For example, a calculated span gas of 16 ppb may display a signal of 15.94 ppb on the 43i at a coefficient of 1; performing a span calibration will adjust the coefficient to 16/15.94 = 1.004, so that the 16 ppb span gas signal will be adjusted upwards by the coefficient factor, and will now record a signal output of 16 ppb.

Initial calibrations of the instrument during the first few months of the data collection period were difficult, owing to outdated equipment with unverifiable accuracy. Attempts to

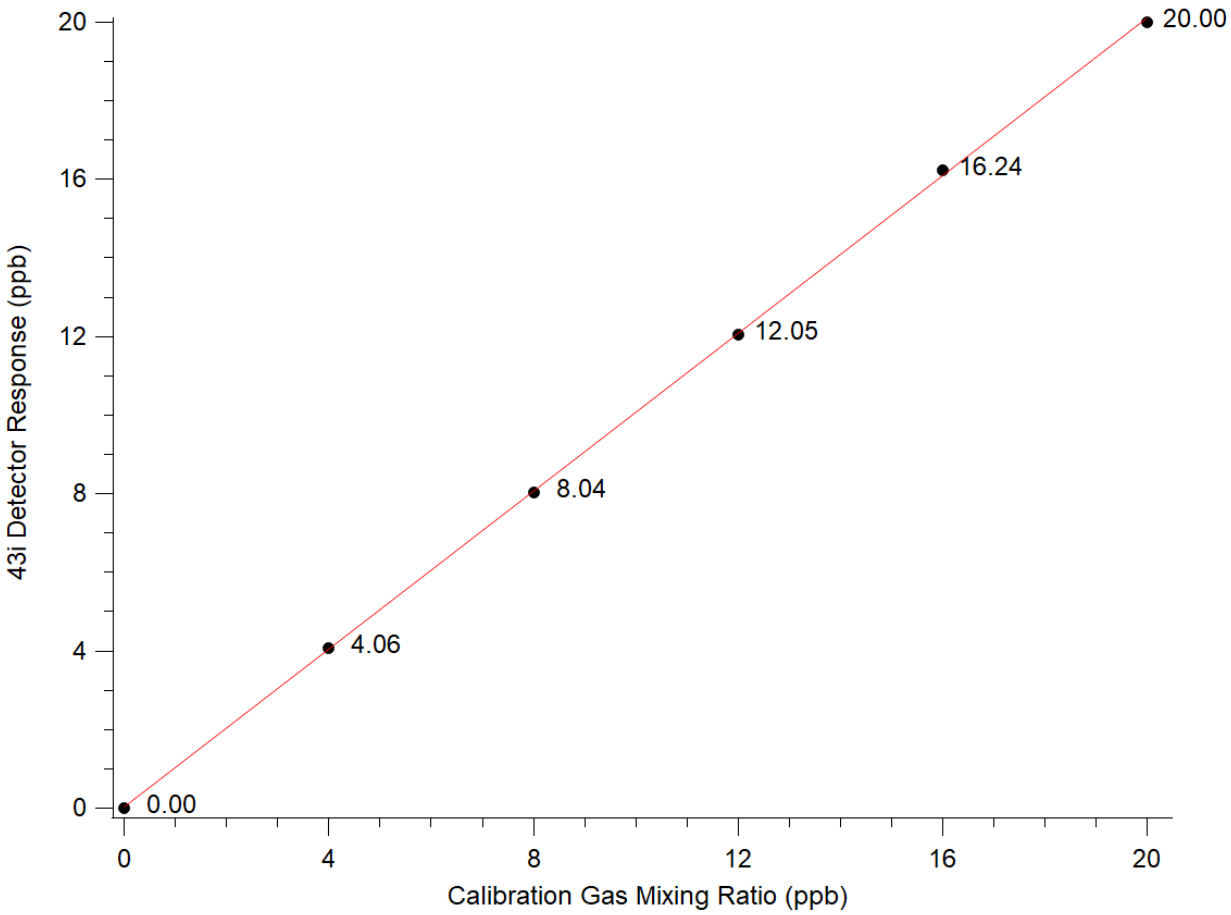

Figure 4. Multipoint calibration curve for the second 43i-TLE instrument. The chosen points were as follows: 0, 4, 8, 12, 16, and 20 ppb. The response of the instrument at each point is labeled. Note that $r^2 > 0.99$, indicating that the variability in the response of the instrument is nearly completely explained by a linear regression model.

generate calibration gases at specific mixing ratios were inconsistent, and the 43i did not respond as expected to high SO_2, as it was often less than half of the theoretical SO_2 mixing ratio.

It was discovered that there was a hardware failure in the instrument, which was the most probable reason for the inconsistent response of the 43i. The instrument was replaced with an identical-model 43i-TLE. This second instrument was used to experimentally demonstrate that the first 43i, as of July 2022, had an inadequate signal response to an inputted calibration gas (See **Figure 5**). Based on this calibration curve, it is possible to create a conversion factor to correct the data from the old 43i, according to the following equation:

$$[SO_2]_{New} = 2.7762[SO_2]_{Old} + 0.17702 \ (\boldsymbol{Eq.10})$$

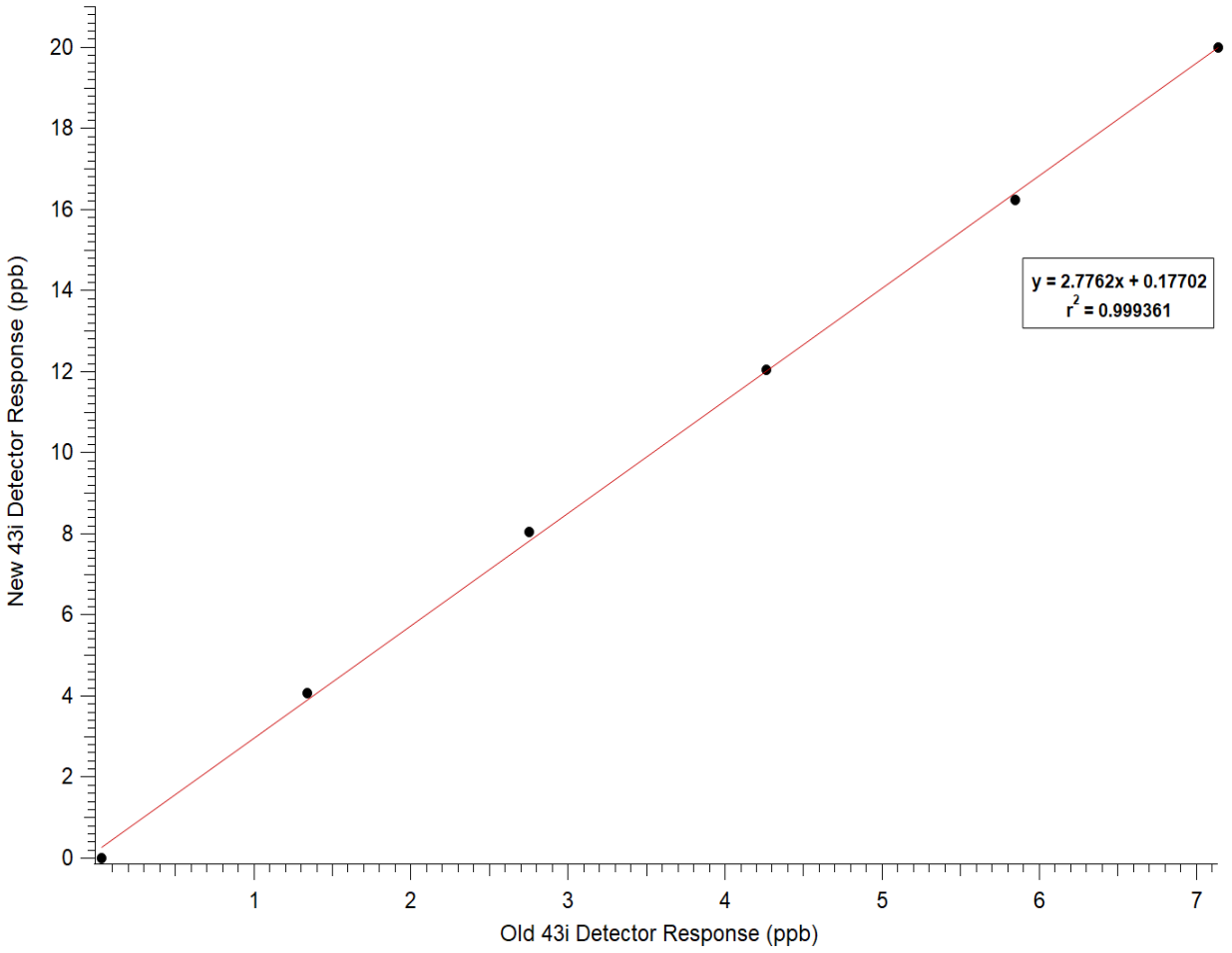

Figure 5. Multipoint calibration curve response ratio of the first (old) 43i instrument vs. the second (new) 43i. The chosen points were as follows: 0, 4, 8, 12, 16, and 20 ppb. Note that $r^2 > 0.99$, indicating that the variability in the response of the instrument is nearly completely explained by a linear regression model.

where $[SO_2]_{New}$ is the adjusted value for the SO_2 signal from the first 43i instrument calibrated to the multipoint response of the new, functional 43i instrument, and $[SO_2]_{Old}$ is the raw signal from the first 43i instrument. It is unclear when exactly the response of the first 43i instrument deteriorated; while there had been calibration issues since the beginning of this thesis project, it was possible (albeit difficult) to generate an appropriate, full-scale response at the detector from a set calibration gas as late as December 8th, 2021, and so applying the correction to the entire dataset does not seem valid. Based on the collected data and comparing with both historical data and hourly data from the Ontario Ministry of the Environment,[31, 32] it seems most likely that the corrections should be applied to the April - July 2022 datasets.

There was an additional source of signal variation during the data collection period: from the months of November 2021 to April 2022, the flow rate of the 43i instrument was inconsistent, and often operated far below the ideal value of 0.480 L/min (See **Figure 6**). On April 20th, 2022, this flow rate error was fixed by changing the filter used in the atmospheric sampling inlet, as well as correcting the position of the inlet on the roof. It is currently unclear

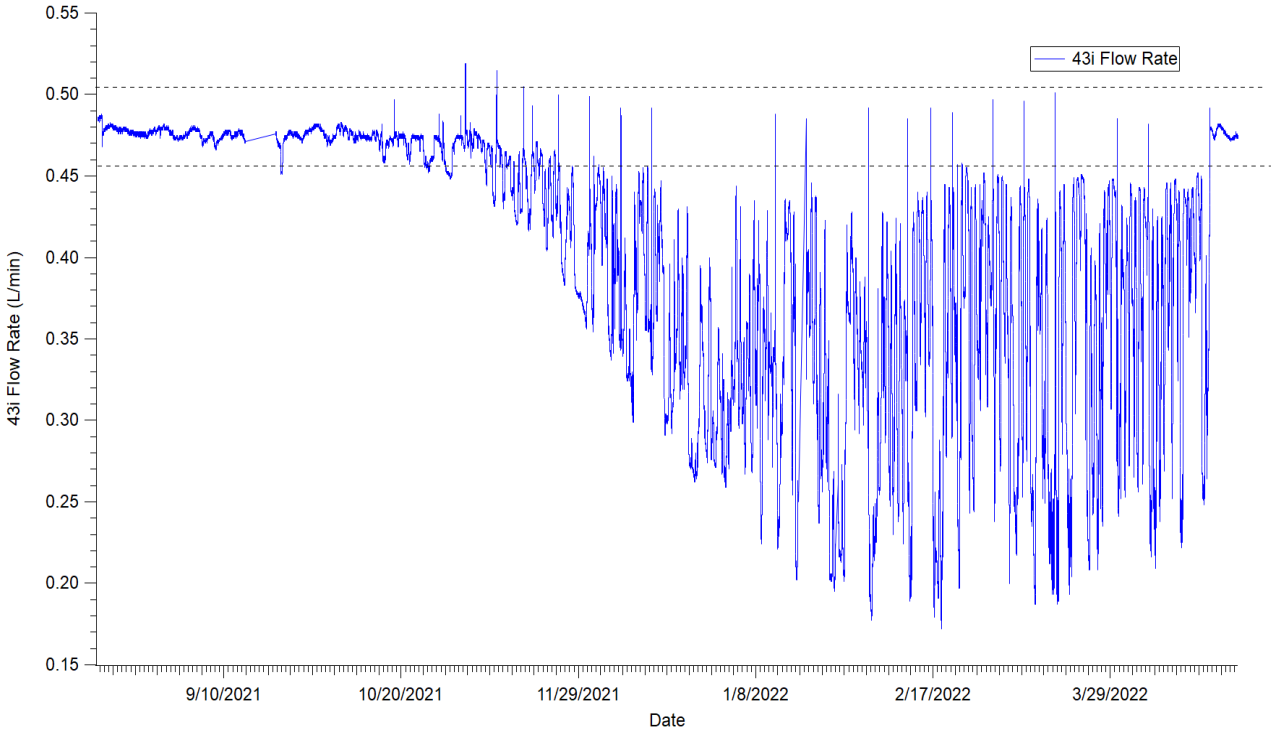

Figure 6. Collected sample flow rate data for the first 43i instrument from August 21st, 2021, to April 26th, 2022. Note that dashed lines have been added at ± 5% of the ideal flow rate, 0.48 L/min, to represent the acceptable operational bounds of the instrument.

as to why the flow rate was inconsistent; initially, it was theorized that unchanged filter paper caused a slow degradation of the flow rate over time, as it got steadily "dirtier" through the filtration of atmospheric contaminants. This theory was tested by directly comparing a 'clean' filter and a 'dirty' filter with 16 ppb SO_2 calibration gas, and it was found that the flow rates for the clean and dirty filter were near identical (0.438 L/min vs 0.439 L/min respectively, within 1% difference), as was the measured mixing ratio of SO_2 (16.00 ppb vs 16.03 ppb, within 1% difference). This indicates that a dirty filter has no impact on the flow rate of SO_2 and causes no chemical effects that would alter the sampled mixing ratio.

Figure 7. Position of the atmospheric sampling line on the roof of the Petrie Science and Engineering Building at York University on April 20th, 2022. The inlet for the line is circled in red for visibility.

The second theory for the reduced flow rate has to do with the position of the sampling line for the 43i instrument (See **Figure 7**). It is possible that the sampling inlet was covered by snow and ice over the winter months, blocking the flow of sampled air to the instrument.

Based on the operating principles of the 43i, we would expect that a reduced flow rate would lower the incoming signal from any sampled SO_2. The reaction cell is pressurized at roughly 760 mmHg of pressure; any less than that would create a vacuum and reduce the number of molecules of SO_2 within the cell, and a lower number of SO_2 molecules would result in a reduced fluorescence signal. The internal pressure of the instrument correlates with the flow rate, and so the reduced flow rate during the compromised sampling period also reduced the pressure (see **Figure 8**). Thus, it follows that a reduced flow rate would result in a lower amount of SO_2 fluorescence in the cell.

It is likely that the conditions leading to a reduction in SO_2 in a low-cell-pressure environment cannot be easily explained by a single factor; instead, it is likely a competition of variables such as an increased residence time and oversampling of SO_2 fluorescence due to a

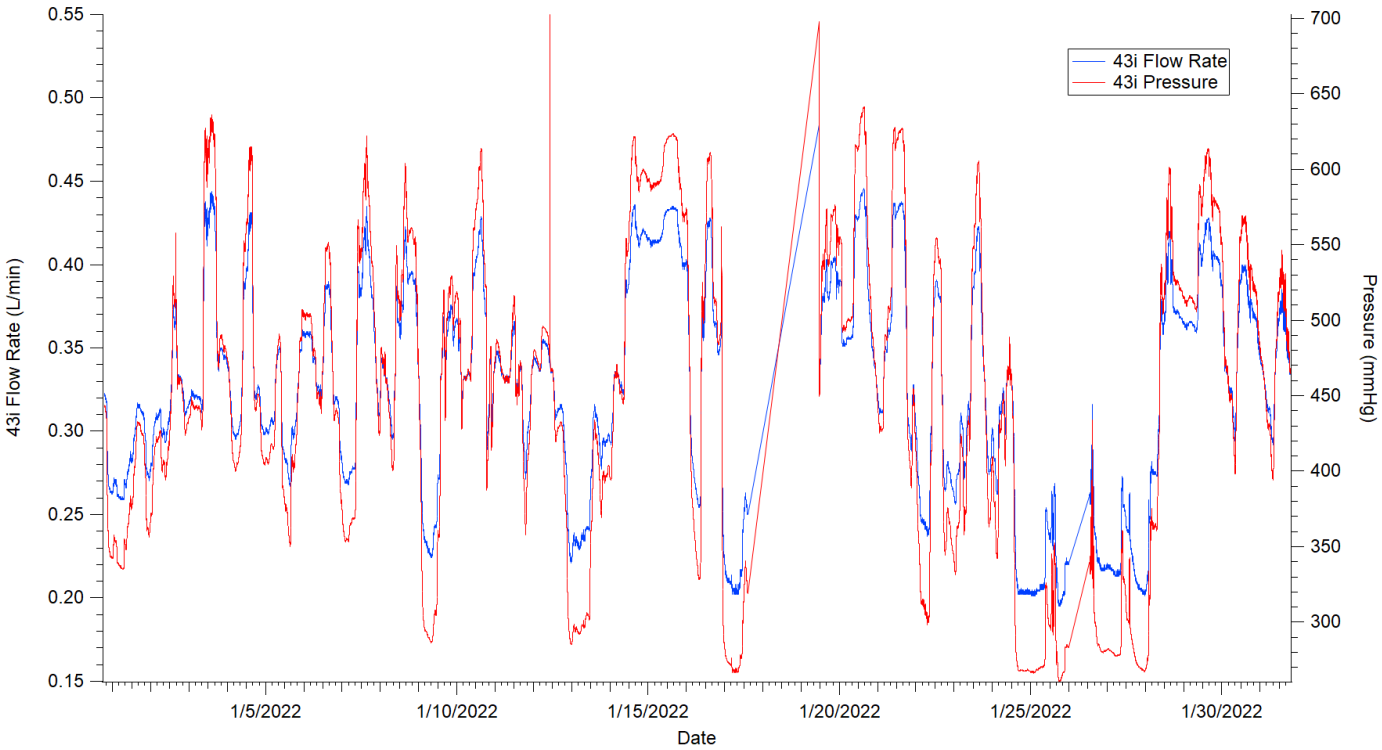

Figure 8. Collected sample flow rate and pressure data for the first 43i instrument during January 2022.

lower flow rate, a low-pressure change in quenching of SO_2 fluorescence with air molecules and with the sides of the reaction cell (altering quantum yield), and some compensation for the low pressure from the instrument itself (Thermo Fisher Scientific uses a proprietary algorithm to correct for low pressure, the details of which were not shared by the company). Despite this algorithm, a significant portion of the data collected over the time period of November 2021 to April 2022 was negative. An attempt was made to manually correct for the negative values in this time period by dynamically adjusting the background correction value.

During the weekly zeroing of the instrument, zero-air was flowed into the instrument from a compressed cylinder at 0.48 L/min, producing an average SO_2 correction mixing ratio value of 1.62 ppb. We expect that our measured SO_2 fluorescence would be proportionally lower for a decreased flow rate, and so this correction value is likely only valid when sampling at the maximum flow rate. To avoid overcorrection during periods of low flow, we retroactively adjust the background correction value using the measured flow rate:

$$[SO_2]_{FlowAd} = [SO_2] + ([SO_2]_{Bg} * \left(\frac{Flow}{0.48\ L/min}\right) \quad (\boldsymbol{Eq.\ 11})$$

Where $[SO_2]_{FlowAd}$ is the flow rate-adjusted mixing ratio of SO_2, $[SO_2]_n$ is the measured mixing ratio of SO_2, $[SO_2]_{Bg}$ is the background correction value of the 43i, and Flow is the flow rate of the 43i. This intentionally does not account for the difference in the actual signal based on flow rate; it was decided that a minor correction of the data was preferred versus an overcorrection that may lead to false conclusions. **Equation 11** has been applied to the collected data from November 1st, 2021, to April 20th, 2022 – as a result, data during this period is likely lower than expected, and may be functionally insignificant.

2.3 Instrumental Setup of the Aerodyne HR-ToF-AMS

The Aerodyne AMS detects aerosols by collecting a sample gas through a particle inlet attached to a high-pressure pump (See **Figure 9** for schematic diagram).[35] The particle beam is separated from the gases by differential pumping. The particle beam passes through a particle sizing region equipped with a rotating chopper disk with an open slit, until it hits a resistively heated block with an electron impact ionizer – any non-refractory species within the sample are

now flash vapourized and ionized and passed into a TOF Mass spectrometer equipped with a single reflectron for high resolution, high sensitivity analysis.[35, 36] The mass concentration and particle sizing data of p-SO4, p -NH_4^+, p-organics, and p-NO_3 are collected in this experiment.

The AMS cycles through several modes over the course of a single 'run.' The setup used here entailed a minute long cycle per run, with a 15-second 'closed' interval, a 15-second 'particle time-of-flight (pTOF)' mode, and a 30 second 'open' interval. The 'closed' interval provided a background for each run, the 'pTOF' interval used a particle beam chopper with a 2% 'open' duty cycle to determine particle sizes, and the 'open' interval collected species' concentrations.

Sampling was performed though 1/8″ steel tubing equipped with a precipitation-blocking "rain hat" cover, affixed to the roof of the Petrie Science and Engineering atmospheric chemistry lab. The data collection period started on August 12th, 2021, and ended prematurely on October 1st, 2021, due to equipment failure. The instrument had been calibrated previously by ECCC, but there was no opportunity to perform a more recent calibration due to COVID-19 restrictions at Environment and Climate Change Canada (ECCC).

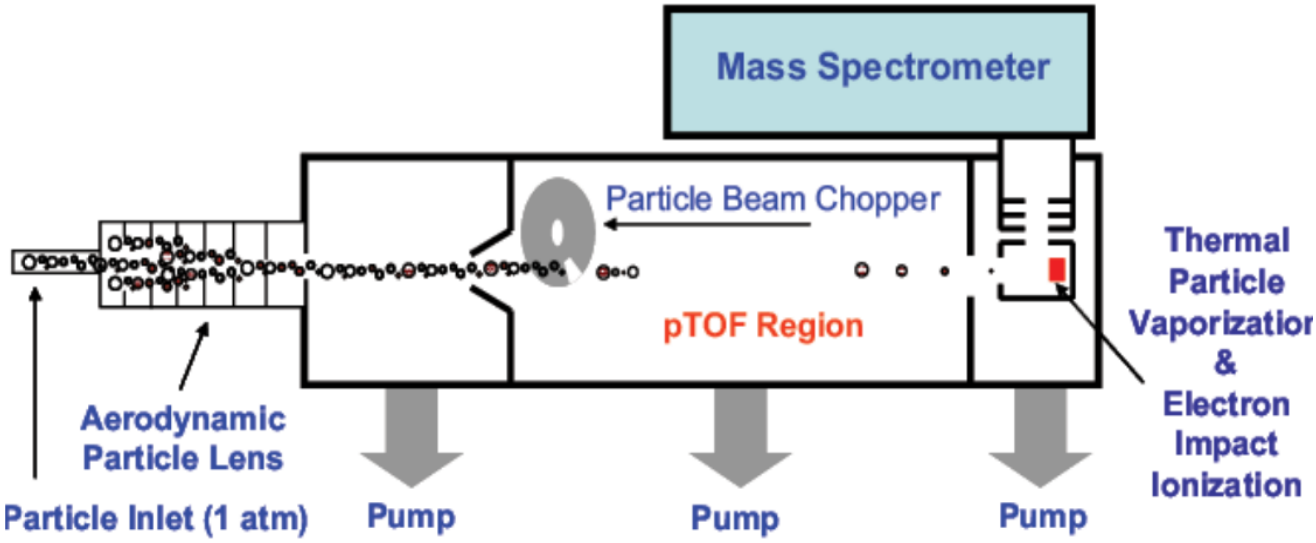

Figure 9. A schematic diagram for an Aerodyne Aerosol Mass Spectrometer.[35]

2.5 Sarnia Field Study

A field study campaign was conducted on July 21-22, 2022, in Sarnia, Ontario. It is known that petroleum refining and chemical manufacturing industries in Sarnia (namely Imperial Oil, Cabot Canada Ltd., Suncor Energy, and Shell Canada Products Ltd.) constitute a significant amount of Ontario's total SO_2 emissions, at roughly 13% of the total emissions in 2020 (according to the NPRI inventory).[12] The individual contributions for the last 20 years for each facility will be provided in **Chapter 3**. Thus, Sarnia is of interest since long range transport of SO_2 and p-SO_4^{-2} to Toronto is possible.

This field study employed a mobile mass-balance method to calculate the quantity of SO_2 emissions originating from the city of Sarnia. This method involves the collection of data from a mobile platform (in this case, a gasoline-powered van) downwind of the emissions sources, including pollutant mixing ratios, meteorological data from a mobile weather station, and GPS data. The weather station was placed at ground level approximately 20 km downwind of the point sources, and measures wind speed and direction at a height of approximately 2 meters.

In this case, based on the prevailing westerly wind conditions on these days, the data was collected in multiple parallel transects east of Sarnia (See **Figures 10 and 11** for the locations, directions, and area covered for each transect on July 21st, 2022, and July 22nd, 2022). Each transect is assumed to be perfectly straight. The data collection period on July 21, 2022, took place from 2:13 PM – 4:27 PM. The data collection period on July 22, 2022, took place from 9:42 AM – 12:49 PM. Each transect was driven in either a south-to-north, or a north-to-south direction. It is not expected that the difference in the south-to-north and north-to-south bearings will make a significant difference in the collected SO_2 data.

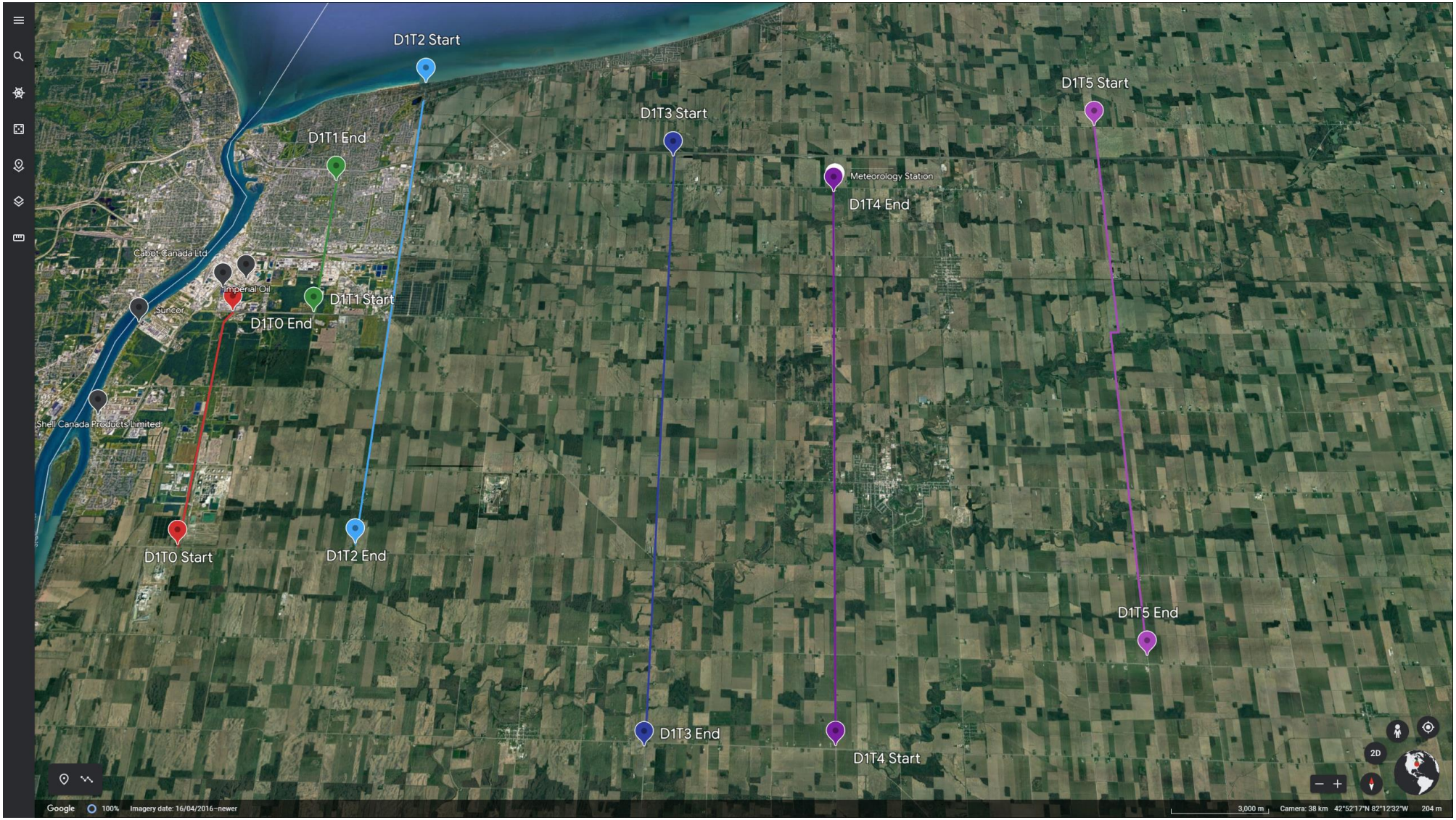

Figure 10. Start and end points for each driven transect on July 21st, 2022, plotted on Google Earth. The number of each transect is noted as "D1T#', where D1 refers to Day 1 of the field study and # refers to the transect number. Point sources (from north to south: Imperial Oil, Cabot Oil Ltd., Suncor Energy, Shell Canada Products Ltd.) are labeled with black markers. The meteorology station is labeled with a white marker.

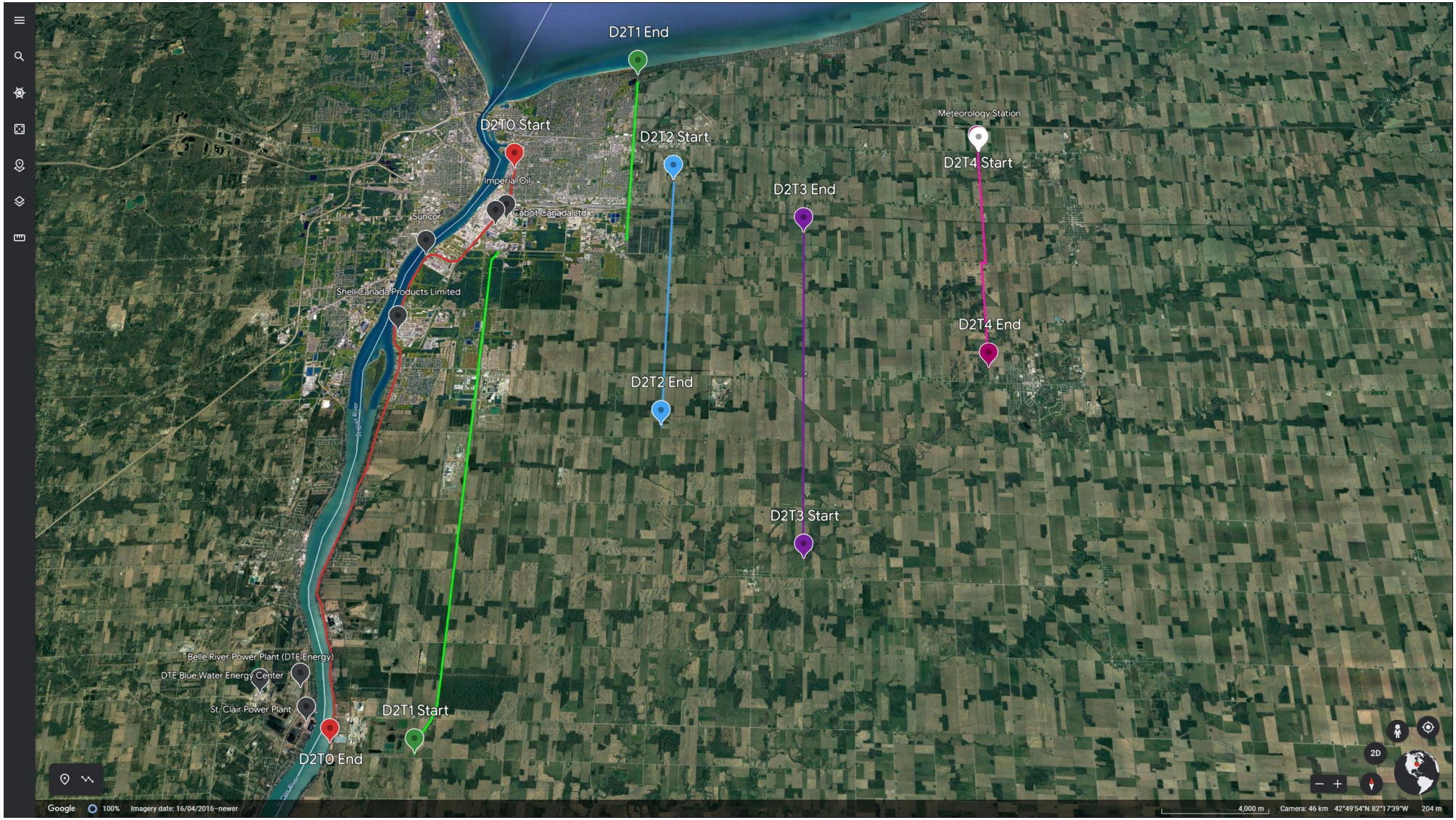

Figure 11. Start and end points for each driven transect on July 22nd, 2022, plotted on Google Earth. Additional point sources from the United States are displayed in the south-most portion of the map.

By integrating the measured mixing ratios for SO_2 across the distance travelled for each transect, it is possible to estimate the total mass emissions of SO_2 from Sarnia, by the following equation:

$$E = \int_{s_{start}}^{s_{end}} \int_{Z_0}^{Z_{PBL}} ([SO_2] - [SO_2]_{Bg}) * U * \cos(\theta) * \frac{P * MW_{SO_2}}{R * T} \, ds \, dz \; (\boldsymbol{Eq.12})$$

Where E is the total emissions rate from the source (in this case, the city of Sarnia, Ontario), s is the distance traveled along the transect, Z is the height above ground level (PBL is the planetary boundary layer), $[SO_2]$ is the combined measured mixing ratio for SO_2, $[SO_2]_{Bg}$ is the background mixing ratio for SO_2 in ppb, U is the average hourly wind speed in Sarnia, θ is the angular offset of the incoming wind direction relative to the plane normal to the transect direction, P is the pressure,[37] MW_{SO2} is the molecular weight of SO_2, R is the ideal gas constant, and T is temperature.[37] See **Chapter 3.5** for the values used for each variable. Note that this equation assumes a homogenously mixed boundary layer, and vertically consistent meteorological conditions and pollutant mixing ratios.

The planetary boundary layer is estimated in two different ways. First, an estimate was calculated from meteorological data using atmospheric modeling. In addition to this estimate, there is also measured ceilometer data from a station in Windsor. We can combine each boundary layer estimate using a weighted average based on their relative uncertainties:

$$\bar{x}_{Weight} = \frac{\sum_{i=1}^{n} (\frac{1}{\sigma_1} * x_1) + \cdots + (\frac{1}{\sigma_n} * x_n)}{\sum_{i=1}^{n} \frac{1}{\sigma_1} + \cdots + \frac{1}{\sigma_n}} \quad (\boldsymbol{Eq.13})$$

Where $\bar{x}_{Weight}$ is the weighted average, and σ is the relative uncertainty on each value x (in this case, the estimate of the boundary layer height Z). **Equation 13** assigns a weight (1/σ) to each boundary layer estimate based on its relative uncertainty, sums the weight-adjusted values [(1/σ)*x] for each estimate, and divides by the sum total weight.

Not all transects will be used to quantify the emissions from Sarnia. There are two types of transects: qualitative and quantitative transects. Qualitative transects are effective for

determining point sources of SO_2 emissions. Quantitative transects are transects that are a far enough distance away for the calculation of the true emission rate.

As the plume of emissions travels away from the point source, it diffuses both horizontally and vertically. Once this plume is well-mixed up to the boundary layer, the calculation of the emissions rate becomes quantitative, and represents the actual emissions from Sarnia. This is due to the mathematical relationship of the distribution of the plume with respect to the distance from the source, as described by G.I. Taylor's statistical theory of plume dispersion.[38] This is a Lagrangian statistical explanation (essentially, the framework description of a mass moving in a system with a constantly changing reference due to movement with air) of the wind-driven movement of an average of tracer particles in the atmosphere, approximated in the vertical direction by the following[38]:

$$\sigma_y{}^2 = 2\sigma_v{}^2 * t_L{}^2 \left[\frac{x}{U*t_L} - 1 + \exp\left(-\frac{x}{U*t_L}\right)\right] \ (\boldsymbol{Eq.14})$$

Where σ_y is the vertical distribution of the tracers, σ_v is the intensity of turbulence, t_L is a Lagrangian time scale (often approximated as 1 minute for boundary layer dispersion), U is the wind speed, and x is the distance downwind from the plume source. It can be seen that the vertical distribution of a plume is directly correlated with its downwind distance from the source.

Taylor also describes the differing relationship between vertical distribution and distance at short distances from the source, and at long differences from the source, through the reduction of **Equation 14**. For a short distance[38]:

$$\sigma_y \approx \sigma_v * \left(\frac{x}{U}\right) \ (\boldsymbol{Eq.15})$$

And for a long distance[38]:

$$\sigma_y \approx \sigma_v * \sqrt{\left(2t_L * \frac{x}{U}\right)} \ (\boldsymbol{Eq.16})$$

It can be seen that, for short distances, the relationship between vertical dispersion and distance from the source is linear. For long distances, this relationship is based on the square

root of the downward distance. Thus, at an adequate distance away, the rate of vertical dispersion of a plume will stop, indicating full mixing up to the boundary layer.

Finally, it can be demonstrated that the source emission rate, and the concentration detected by an instrument are related to the vertical and horizontal distribution of the plume[38]:

$$c = \frac{E}{\pi\sigma_y\sigma_z U} * \exp\left[-0.5 * (\frac{y}{\sigma_y})^2\right] * \exp\left[-0.5 * \left(\frac{z_c}{\sigma_z}\right)^2\right] \ (\boldsymbol{Eq.\ 17})$$

Where c is the concentration of a pollutant detected by an instrument, E is the source emission rate in g/s, σ_z is the vertical dispersion of the plume, y is the lateral distance of the detector from the center of the plume, and z_c is the height of the centre of the plume from ground level (assuming a detector height of 0 m).

Per **Equation 17**, detected concentrations are inversely proportional to the dispersion of the plume. Thus, plume concentration is indirectly inversely correlated with downwind distance, and at a far enough distance from the source, the rate of the reduction in concentration will decrease to the point of near stabilization in measurements. This can be seen with successive transect measurements. During the qualitative transects, the measured peak concentrations of a pollutant will drop rapidly from one transect to the next. At a critical downwind distance from the source, it can be observed that peak concentrations for each transect will converge, and while they are still decreasing, the transects further from the source will be more similar to each other than the transects closer to the source. When this is observed, the plume can be thought to be well-mixed up to the boundary layer and transects taken at this distance (or farther) are included in calculations using **Equation 12**.

Assuming a constant wind speed and stable boundary layer, the required downward distance for adequate vertical plume dispersion can be quantified according to the relationship between the time required for pollutants to mix up to the boundary layer and the mean wind speed, by the following equations[39]:

$$t_m = \frac{z_{PBL}}{w^*} \ (\boldsymbol{Eq.\ 18})$$

$$x_q = 3t_m * U \ (\boldsymbol{Eq.\ 19})$$

Where t_m is the mean mixing time in seconds (the time it takes for a tracer to mix up to the boundary layer, typically between 5-15 minutes[40]), w* is the convective velocity scale, and x_q is the minimum distance required to define a quantitative transect (the distance traveled by a plume over one t_m). The convective velocity scale requires measurements of kinematic heat flux[40]; in the absence of these measurements, a conservative estimate of 15 minutes will be used to approximate x_q for this field study (See **Chapter 3.5** for calculation). We use a factor of 3 mean mixing times; with each mean mixing time, the plume disperses up to the boundary layer, but is only fractionally mixed. It is assumed that, for the purposes of this study, that 3 repetitions of mixing are adequate to assume plume homogeneity up to the boundary layer.

During the course of the field study the 43i instrument was set up in the back of the van and was powered with a portable battery (See **Figure 12**). A T-junction manifold was installed to allow the 43i and CDRS simultaneous access to a single 1/8″ Teflon sampling line affixed to front of the vehicle. Through this study, the 43i instrument was used to collect SO_2 data, using the same operational parameters outlined in **Chapter 2.2**, with the exception of the averaging time, which was switched from 300-second averaging to 2-second averaging to increase the spatial- and time-resolution of the measurements (supplemented by manual recording during peak concentration periods every 10 seconds). The CDRS used the same instrumental setup that will be described in **Chapter 2.7**, and collected CO, CH_4, and CO_2 data. A model 100 WS-25 mobile weather station was setup at 5783 Camlachie Road, Wyoming, Ontario, along the path of July 21st's Transect 4 to collect wind speed and direction data (note that this station collects data at a height of roughly 2 m). GPS data was collected through the "Gaia GPS" smartphone app.

Figure 12. Setup of the Picarro CDRS and Thermo Fisher 43i in the van used for the Sarnia field study.

2.6 Data Processing & Analysis Software

Data was analyzed using Microsoft Excel and Wavemetrics Igor Pro Version 9. Microsoft Excel was used to organize raw data outputted by the instruments. Igor Pro is an analysis toolset used to process large quantities of complex scientific data packaged together as "waves". Raw AMS data specifically is processed into a usable form through an Igor data package called "PIKA and Squirrel."[40] Data processing, statistical analysis, and figure generation for the other instruments is performed through the base Igor software. Particularly, Igor will be used for ANOVA analysis, which compares multiple means to determine if there are any statistically significant differences within the set. ANOVA results are posted in the following format: (F(degrees of freedom between groups, degrees of freedom within groups) = [F-value],

p = [p-value). Full statistical results are recorded for specific important data only. Post-hoc testing is used to identify the exact comparisons identified as significant by ANOVA. Igor will be used to perform Neuman-Keuls tests, which are a higher-statistically-powered variant of Tukey's Test, which successively checks the statistical significance of each possible comparison in the set.

High pollution air quality events and Sarnia point source emissions are tracked through the use of the NOAA HYSPLIT atmospheric transport and dispersion trajectory model.[42] HYSPLIT is a combined Lagrangian and Eulerian methodology model that makes use of a moving frame of reference to track dispersing air plumes.[42] For the purposes of tracking high pollution air quality events, HYSPLIT is used to generate backwards trajectories for times of high detected pollutant concentrations to determine where the air mass originated from. Trajectory start points for the model were selected at a height of 20 m centered on the Petrie Science and Engineering rooftop lab. During the Sarnia Field Study, HYSPLIT was used in the 'forecast trajectory' configuration, where known point sources were selected at the start time of the field study, and plume trajectories were simulated from these point sources. Meteorology is simulated using the Global Forecast System (GFS) quarter-degree resolution archive. Back trajectories are supported by NOAA's Hazard Mapping System for Smoke and Fire Products (HMS Smoke) to determine the influence of forest fires on particulate matter formation.

2.7 Description of Collaborative Data Instruments

Data provided by Yeuhyun Kim was collected via Picarro CRDS. The operating principle of the Picarro CRDS is cavity ring-down spectroscopy, by which a sample of air is contained within a cavity in the instrument, surrounded by a triangular configuration of three mirrors, and excited with the laser.[43] The cavity fills with the emitted light, reflecting repeatedly in a cycle by the mirrors; upon reaching a certain photodetector signal threshold, the laser shuts off, and the light slowly and steadily decays from the cavity in a process known as ring-down.[43] A gas species that can absorb the light from the laser will accelerate the loss of light, and the difference between empty cavity and sample cavity ring down time is characteristic of species concentration.[43] Tuning the laser allows for species differentiation. Sampling for this instrument

was performed through the same 1/8" Teflon tube as the 43i, at 0.5 L/min. Calibrations were performed and no corrections were needed

Data provided by Dr. Joudan was collected via AIM-IC-MS. The operating principle of this technique is online ion-chromatography mass spectrometry of water-soluble gas and fine particulate components.[44] A parallel plate wet denuder system separates gas-phase compounds from the sample via diffusion, while particles are collected in a particle supersaturation chamber.[44] Samples collected via AIM were injected by syringe into anion and cation channels in an ion chromatography system, with a Dionex IonPac AS24 250 mm column and NaOH eluent.[44] Separated species were introduced to the ThermoFisher Scientific mass spectrometer via electrospray and quantified by a single quadrupole operating in selected ion mode.[44] Calibrations were performed offline using analytical standards of the species of interest, diluted appropriately to create a calibration curve.[44] The data used spans from November 16th-25th, 2021, which encompasses three high pollution air quality events not captured in the AMS dataset.

Meteorology data was provided the York University Earth and Space Science Meteorological Observation Station (EMOS) station, which is a tower located at surface level slightly northwest of the Petrie Science and Engineering rooftop lab.[45] To collect wind data, the EMOS station employs an R. M. Young wind monitor at the top of the tower (approximately 10 meters above ground level), and samples data every second, with 5-minute averaged data points recorded.[45]

Chapter 3 – Data & Results

3.1 Historic Data

NAPS data for the Toronto, Windsor, and Simcoe monitoring stations have been collated, summarized, and displayed graphically here, in addition to testing the statistical significance of any comparisons made. The functional significance of selected comparisons will be discussed in **Chapter 4.1**. In particular, 4 main metrics have been targeted: SO_2 mixing ratios, p-SO_4^{-2} concentrations, SO_x concentrations, and the ratio of p-SO_4^{-2}/SO_x, for each site.

This data was collated from 2003 - 2020. The advantage to this data collection period is twofold: first, there is enough data here to form proper trends, which is important for contextualizing the changing nature of sulfur in Ontario over time. Given that the stated research objective of this thesis is to evaluate the current state of sulfur in Ontario (in particular, around Toronto) and determine how this has changed in recent years, this context is critical for substantiating any analysis of the data collected by the 43i instrument over the course of this thesis project. The second advantage is that this 2003-2020 analysis window should demonstrate the effects of several periods of successively increased environmental regulations, from the 1980s to more recent sets of regulations including emissions limits enacted in 2015 and 2019.

SO_2 mixing ratio means, 95% confidence intervals of the means, 95th percentiles of the annual data set, as well as the annual hourly maximum for each NAPS site have been tabulated in **Table 5**. In addition, box plots have been generated for the annual SO_2 means for each NAPS site in **Figure 13**. In these box plots, the filled boxes represent the 25th to 75th percentile interquartile range, per the Tukey method. The whiskers extended upwards to the 95th percentile, and down to the 5th percentile. Outlier data has been omitted to preserve visual clarity. The annual mean data has been displayed with a white marker for each year, and the median is displayed with a white line. Note that median values were often equivalent to the lowest value of 0 in these data sets, and so the median line is not readily visible. In addition, a side-by-side trend plot of annual SO_2 means for all three NAPS sites is also shown in **Figure 13**, to allow for direct intercomparison of the differences in SO_2 based on location.

Table 5. NAPS sites summarized annual means, confidence intervals of the means, 95th percentiles, and max hourly values for SO_2. Data spans from 2003 to 2020 for Toronto and Windsor, and from 2007 to 2020 for Simcoe. All values are in ppb. Missing data is denoted with "-".

	Toronto				Windsor				Simcoe			
Year	**Mean ($\bar{x}$)**	**95% CI (± $\bar{x}$)**	**95th %tile**	**Max**	**Mean ($\bar{x}$)**	**95% CI (± $\bar{x}$)**	**95th %tile**	**Max**	**Mean ($\bar{x}$)**	**95% CI (± $\bar{x}$)**	**95th %tile**	**Max**
2003	2.9	0.09	9.0	107	6.3	0.20	22	110	-	-	-	-
2004	2.7	0.08	8.0	82	4.5	0.14	18	72	-	-	-	-
2005	2.3	0.06	7.0	54	5.1	0.16	21	98	-	-	-	-
2006	2.0	0.04	6.0	27	4.9	0.15	19	96	-	-	-	-
2007	1.5	0.05	6.0	26	5.2	0.15	20	67	1.8	0.06	7.0	43
2008	1.4	0.04	5.0	24	4.7	0.13	19	65	1.2	0.04	5.0	27
2009	1.2	0.04	4.0	18	3.6	0.12	15	59	0.9	0.03	3.0	17
2010	0.9	0.03	3.0	27	3.2	0.13	16	74	0.6	0.03	3.0	38
2011	1.5	0.02	4.0	17	3.4	0.11	14	75	0.5	0.03	2.0	25
2012	0.6	0.02	3.0	18	2.8	0.11	13	69	0.6	0.03	2.0	36
2013	0.5	0.02	2.0	15	2.6	0.10	13	52	0.5	0.02	2.0	16
2014	0.7	0.02	2.0	21	2.7	0.11	14	59	0.5	0.02	2.0	21
2015	1.0	0.02	3.0	15	1.9	0.08	10	43	0.4	0.02	2.0	16
2016	0.6	0.02	2.0	10	1.4	0.06	7.0	33	0.1	0.01	1.0	12
2017	0.5	0.01	1.3	11	0.9	0.04	4.3	28	0.6	0.01	1.0	10
2018	0.3	0.01	1.0	10	0.6	0.03	3.0	27	0.5	0.02	1.0	12
2019	0.3	0.01	0.9	12	0.8	0.04	3.8	32	0.3	0.01	0.8	14
2020	0.2	0.01	0.7	10	0.3	0.02	1.5	20	0.8	0.01	1.4	5.8

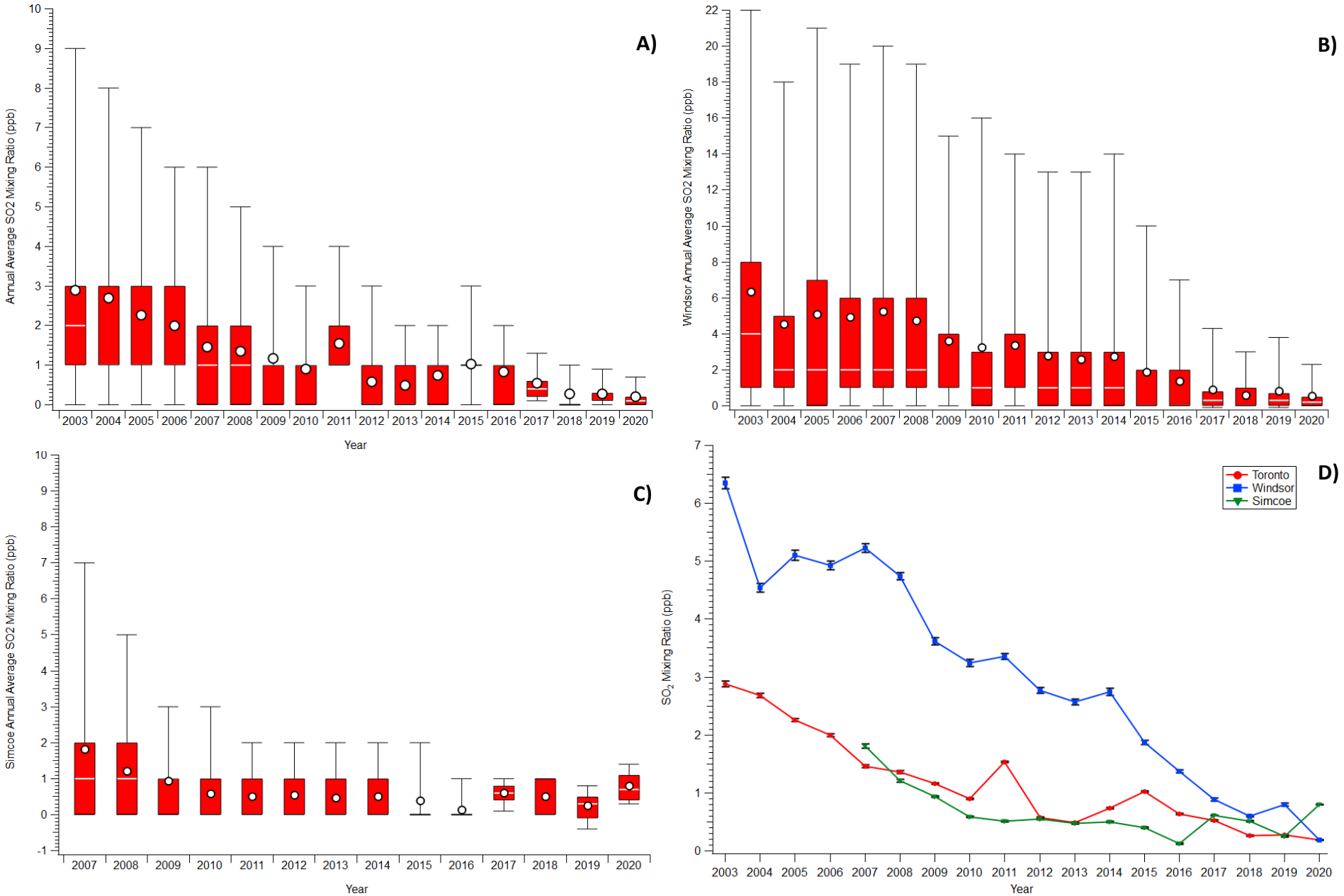

Figure 13. Annual SO_2 box plots for each NAPS site, where A) is Toronto, B) is Windsor, C) is Simcoe, and D) is a year-over-year comparison of the average annual SO_2 mixing ratios for all 3 sites. Whiskers are up to 95th- and down to 5th-percentile. Mean is displayed as a white marker. Median is displayed as a white line when not the same as the minimum. Y-error bars are displayed on graph D) that are equivalent to the calculated standard error of the mean.

One-way ANOVA ($\alpha = 0.05$) was performed in Igor to determine the effect of time on Toronto's annual SO_2 mean. ANOVA analysis revealed that there was a significant difference between at least two annual SO_2 means for the Toronto NAPS site ($F(17, 153401) = [1540.15]$, $p = 0$). Given the high number of intercompared categories, post-hoc testing is needed to determine where the significant differences are. A Newman-Keuls test ($\alpha = 0.05$) was performed in Igor to successively compare each annual SO_2 mean in Toronto. It was revealed that every annual SO_2 mean in Toronto was significantly different from one another, with the following exceptions: 2012 versus 2017, 2013 versus 2017, and 2018 versus 2019.

One-way ANOVA ($\alpha = 0.05$) was performed in Igor to determine the effect of location on annual SO_2 mean for 3 years. The years selected were 2007 (the earliest recorded year of data common to all sites), 2015 (the year of a recent instatement of sulfur-limiting Environmental Protection Act regulations) and 2020 (the most recent recorded year of data). ANOVA analysis revealed that there was a significant difference between annual SO_2 mean between at least 2 locations in 2007 ($F(2, 25798) = [1744.50]$, $p = 0$), in 2015 ($F(2, 25984) = [903.17]$, $p = 0$), and 2020 ($F(2, 34263) = [846.97]$, $p = 0$). A Newman-Keuls test ($\alpha = 0.05$) was performed in Igor to successively compare each location's annual SO_2 mean per year. It was revealed that each location's SO_2 mean was significantly different from one another in every tested year.

For all 3 NAPS sites, p-SO_4^{-2} concentration means, 95% confidence intervals of the means, 95th percentiles, as well as the annual hourly maximums have been tabulated in **Table 6.** Box plots have again been generated for the annual p-SO_4^{-2} concentrations for each NAPS site, with the parameters remaining identical from the SO_2 box plots (see **Figure 14**). A year-over-year comparison of the plotted trends for each NAPS site is also included in **Figure 14.** Note that data for Windsor was not available for 2011. The completeness of the datasets used for this p-SO_4^{-2} was inconsistent. Several years for each site were missing several data points; in some cases, entire months and seasons were not available for analysis. Additionally, the calculated standard errors of the mean for sulfate are much higher than SO_2 owing to the low number of data points (the average number of data points for one year at one NAPS site was N=8760 for SO_2, and N = 95 for p-SO_4^{-2}.

Table 6. NAPS sites summarized annual means, confidence intervals of the means, 95th percentiles, and max hourly values for p-SO_4^{-2}. Data spans from 2003 to 2019 for Toronto, from 2004-2010 and 2012-2019 for Windsor, and from 2007 to 2019 for Simcoe. All values are in µg/m^3. Missing data is denoted with "-".

	Toronto				Windsor				Simcoe			
Year	**Mean ($\bar{x}$)**	**95% CI (± of $\bar{x}$)**	**95th %tile**	**Max**	**Mean ($\bar{x}$)**	**95% CI (± of $\bar{x}$)**	**95th %tile**	**Max**	**Mean ($\bar{x}$)**	**95% CI (± of $\bar{x}$)**	**95th %tile**	**Max**
2003	3.2	1.7	17	27	-	-	-	-	-	-	-	-
2004	2.6	0.6	11	16	4.0	0.9	13	14	-	-	-	-
2005	2.9	0.7	11	22	3.4	1.2	13	13	-	-	-	-
2006	2.2	0.5	8.9	14	3.2	0.7	9.5	11	-	-	-	-
2007	2.7	0.6	10	17	3.7	0.7	11	18	2.6	0.7	9.8	17
2008	2.1	0.4	7.4	11	3.3	1.0	11	12	2.8	0.7	8.1	11
2009	1.5	0.2	4.0	12	2.1	0.4	5.7	10	2.0	0.4	4.6	12
2010	1.9	0.6	8.5	11	2.0	0.4	6.3	11	1.2	0.4	4.5	11
2011	1.6	0.4	4.8	6	-	-	-	-	1.3	0.4	3.7	6.5
2012	1.9	0.4	4.8	9	2.3	0.4	5.3	9.1	1.8	0.3	4.7	9.0
2013	1.9	0.4	6.2	7	2.1	0.3	5.1	7.4	1.6	0.2	4.6	6.7
2014	1.5	0.3	3.7	6	1.9	0.2	4.3	7.7	1.6	0.2	4.2	6.4
2015	1.5	0.3	4.1	4	1.8	0.2	4.0	5.3	1.5	0.2	4.1	4.4
2016	1.0	0.2	2.4	3	1.3	0.1	2.8	3.3	1.1	0.1	2.6	3.0
2017	1.2	0.2	3.2	4	1.2	0.1	2.4	3.4	1.0	0.1	2.6	4.3
2018	1.1	0.2	1.7	2	1.3	0.2	2.7	5.1	1.1	0.1	2.7	1.7
2019	0.9	0.2	2.3	3	1.1	0.1	2.1	2.5	1.0	0.2	2.4	2.6

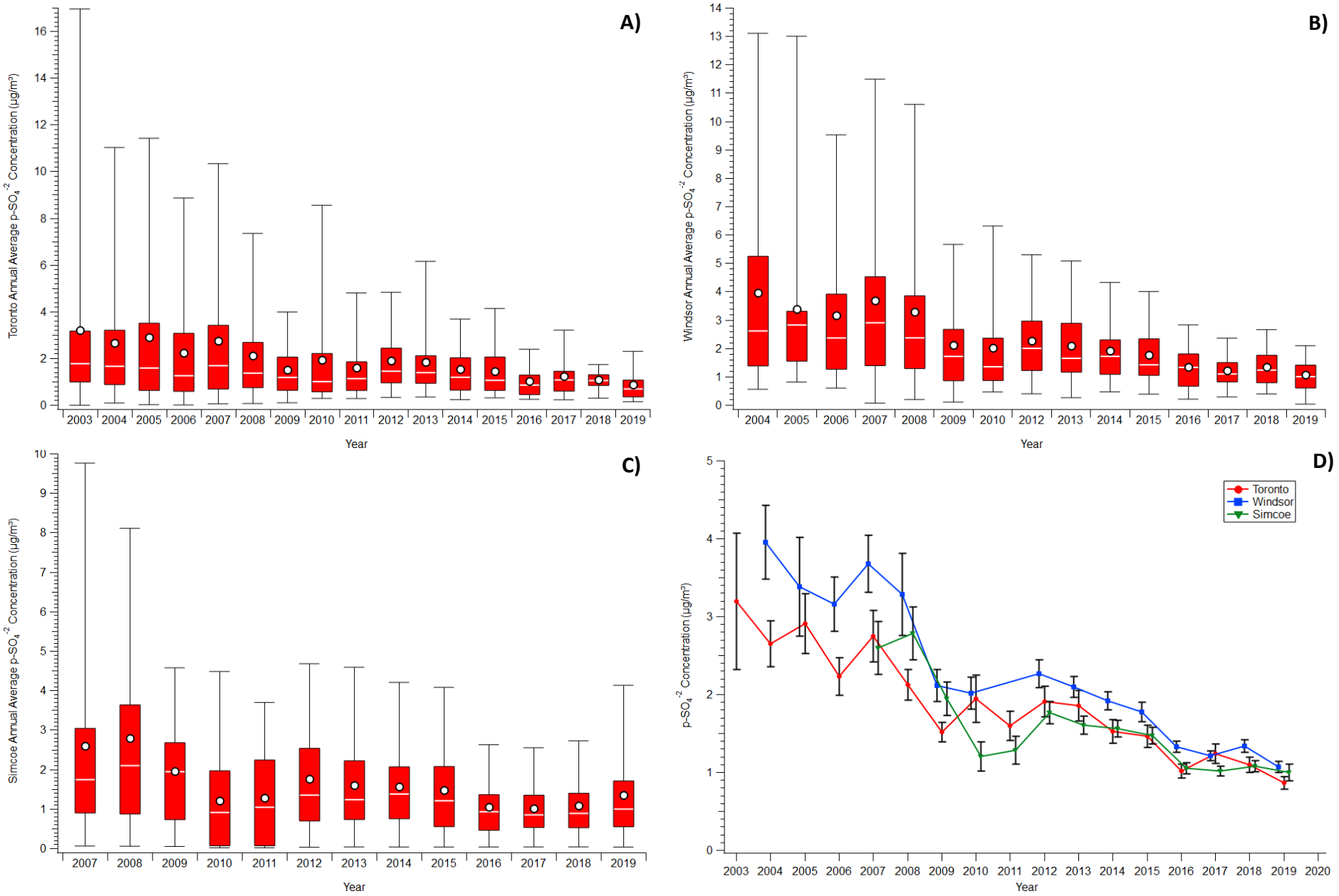

Figure 14. Annual p-SO_4^{-2} box plots for each NAPS site, where A) is Toronto, B) is Windsor, C) is Simcoe, and D) is a year-over-year comparison of the average annual p-SO_4^{-2} concentrations for all 3 sites. Whiskers are up to 95th- and down to 5th-percentile. Mean is displayed as a white marker. Median is displayed as a white line. Error bars are displayed on graph D) that are equivalent to the calculated standard error of the mean. Note that a slight horizontal offset has been applied to the Windsor and Simcoe plots on graph D) to improve clarity of the error bars.

ANOVA analysis revealed that there was a significant difference between at least two annual p-SO_4^{-2} means for the Toronto NAPS site ($F(16, 1228) = [5.61]$, $p = 8.6x10^{-6}$). Post-hoc testing revealed that every annual p-SO_4^{-2} mean after 2008 in Toronto was not significantly different from one another. The majority of significant differences occurred with comparisons of 2003, 2004, and 2005 versus years later than 2008.

ANOVA analysis revealed that there was not a significant difference between annual p-SO_4^{-2} means in 2007 ($F(2, 253) = [2.77]$, $p = 0.064$) and in 2015 ($F(2, 260) = [2.04]$, $p = 0.13$), and that there was a significant difference between the annual p-SO_4^{-2} means of at least 2 locations in 2019 ($F(2, 256) = [5.93]$, $p = 0.003$). Post-hoc testing for 2019 showed that the only statistically different comparison for 2019 was between Toronto and Simcoe.

For all 3 NAPS sites, SO_x concentration means and 95% confidence intervals of the means have been tabulated in **Table 7.** Since SO_x is an addition of the average SO_2 and p-SO_4^{-2} values for the year, there are no complete datasets to calculate 95^{th} percentiles or determine annual max values. Confidence intervals were calculated from the propagated standard error of the mean from SO_2 and p-SO_4^{-2}. Year-over-year SO_x trends for all 3 NAPS sites have been plotted in **Figure 15**. In addition, for each site, the yearly p-SO_4^{-2}/SO_x ratio (X_{pSO4}) has been plotted, demonstrating the proportion of total sulfur that is made up of particle sulfate. A linear correlation factor between SO_2 and SO_x from 2003 to 2019 was calculated in Igor Pro, where the strength of correlation for historic SO_2 and SO_x is $r = 0.99$.

Table 7. NAPS sites calculated and summarized annual means, and confidence intervals of the means for SO_x, as well as X_{pSO4} and the confidence interval of X_{pSO4}. the Data spans from 2003 to 2019 for Toronto, from 2004-2010 and 2012-2019 for Windsor, and from 2007 to 2019 for Simcoe. All values are in µg/m^3. Missing data is denoted with "-".

	Toronto				Windsor				Simcoe			
Year	**Mean ($\bar{x}$)**	**95% CI (± of $\bar{x}$)**	**X_{pSO4}**	**95% CI (± of X_{pSO4})**	**Mean ($\bar{x}$)**	**95% CI (± of $\bar{x}$)**	**X_{pSO4}**	**95% CI (± of X_{pSO4})**	**Mean ($\bar{x}$)**	**95% CI (± of $\bar{x}$)**	**X_{pSO4}**	**95% CI (± of X_{pSO4})**
2003	11	1.7	0.29	0.14	-	-	-	-	-	-	-	-
2004	9.9	0.6	0.27	0.10	16	1.0	0.24	0.12	-	-	-	-
2005	9.0	0.8	0.32	0.14	17	1.3	0.20	0.13	-	-	-	-
2006	7.6	0.5	0.29	0.09	17	0.8	0.19	0.08	-	-	-	-
2007	6.7	0.7	0.41	0.16	18	0.8	0.21	0.08	7.5	0.7	0.35	0.23
2008	5.8	0.4	0.37	0.10	16	1.1	0.20	0.12	6.1	0.7	0.46	0.26
2009	4.7	0.3	0.33	0.07	12	0.5	0.18	0.05	4.5	0.4	0.43	0.15
2010	4.4	0.6	0.44	0.19	11	0.5	0.19	0.06	2.8	0.4	0.43	0.16
2011	5.8	0.4	0.28	0.08	-	-	-	-	2.7	0.4	0.48	0.23
2012	3.5	0.4	0.55	0.15	9.8	0.4	0.23	0.06	3.3	0.3	0.54	0.10
2013	3.2	0.4	0.59	0.17	9.1	0.4	0.23	0.05	2.9	0.2	0.56	0.11
2014	3.5	0.3	0.43	0.11	9.4	0.4	0.21	0.04	2.9	0.2	0.54	0.12
2015	4.2	0.3	0.35	0.08	6.9	0.3	0.26	0.05	2.5	0.2	0.58	0.10
2016	2.8	0.2	0.37	0.06	5.1	0.2	0.26	0.04	1.4	0.1	0.75	0.08
2017	2.7	0.2	0.46	0.10	3.6	0.2	0.34	0.04	2.7	0.1	0.38	0.10
2018	1.8	0.2	0.60	0.11	3.0	0.2	0.45	0.07	2.5	0.1	0.44	0.08
2019	1.6	0.2	0.54	0.09	3.3	0.2	0.33	0.05	1.7	0.2	0.59	0.08

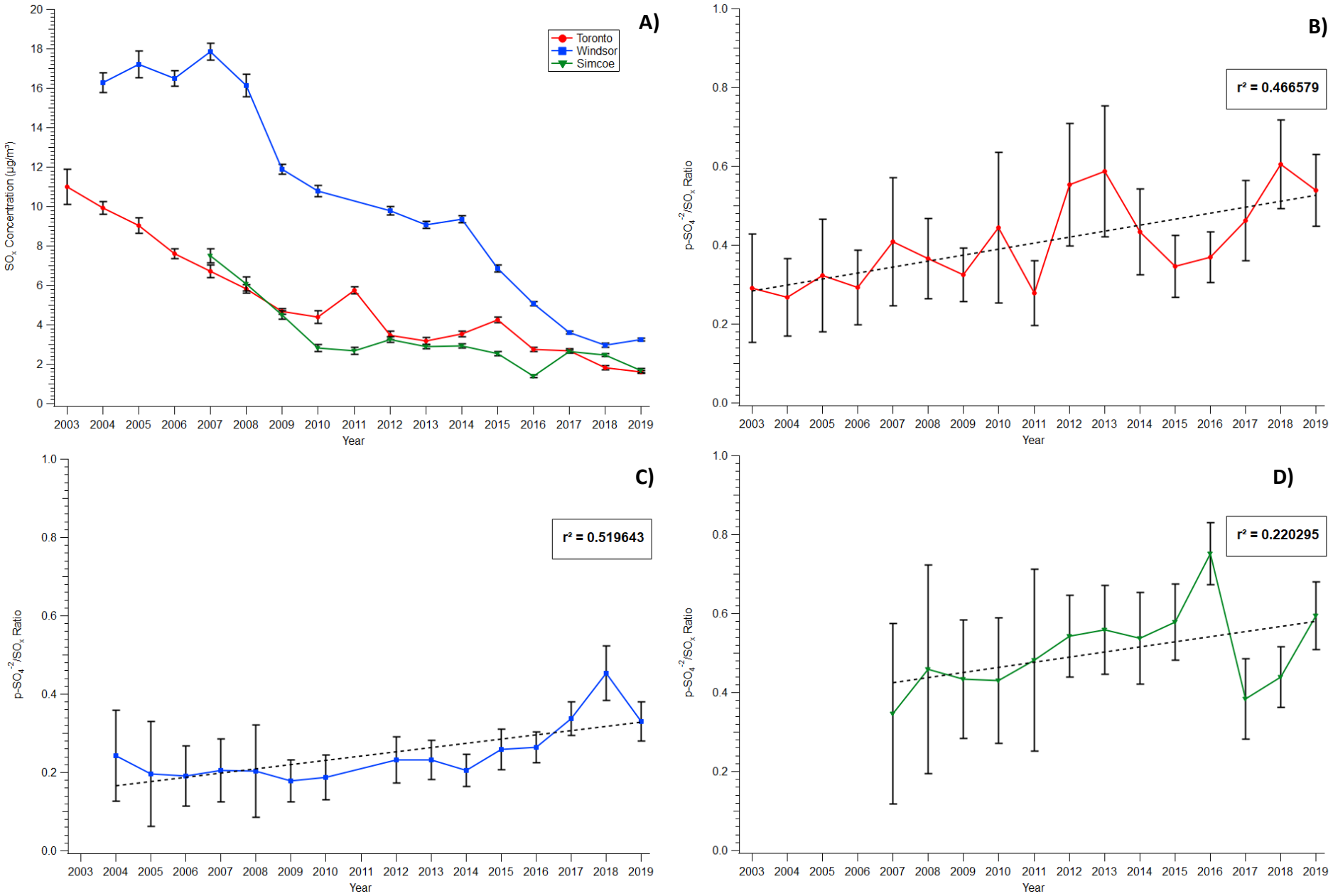

Figure 15. Annual SO_x concentrations and X_{pSO4} for each NAPS site, where A) is a year-over-year comparison of the average SO_x concentration for each site, B) is Toronto X_{pSO4}, C) is Windsor X_{pSO4}, and D) is Simcoe X_{pSO4}. Error bars are displayed on graph A) that are equivalent to the calculated standard error of the mean. Error bars are displayed on graphs B), C), and D) that are equivalent to the 95% confidence intervals. Linear trendlines have been added to graphs B), C), and D) as dashed lines, with the displayed corresponding r^2 values.

We can compare the effect of time on X_{pSO4} for starting, middle, and endpoints for each region (full statistical results posted for effects of time in Toronto only). For Toronto, there was no significant difference between 2003 and 2015 [Δ_{XpSO4} = 0.06 (-0.08, 0.20)], though there was a significant difference between 2003 and 2019 [Δ_{XpSO4} = 0.25 (0.11, 0.39)] and 2015 and 2019 [Δ_{XpSO4} = 0.19 (0.10, 0.28)]. For Windsor, there was no significant difference between 2004 and 2015, and 2004 and 2019, and there was a significant difference between 2015 and 2019. For Simcoe, there was no significant difference between 2007 and 2015, and 2015 and 2019, though there was a significant difference between 2007 and 2019. Between the NAPS sites for these years, there was a difference between Toronto and Windsor in 2007, 2015 and in 2019, and a difference between Simcoe and Windsor in and in 2019. The only difference between Toronto and Simcoe was in 2015.

Seasonal SO_2 and p-SO_4^{-2} means have been displayed as box plots in **Figure 16** and **Figure 17**, respectively. Box plot parameters are identical to previous box plots. To constrain the analysis to a single relevant parameter, only the Toronto NAPS site's seasonal differences will be investigated. In addition, the effect of time on sulfur means has already been determined, and it is expected that the trend within a given season over the years will follow the trend of the annual mean over the years.

For the effect of season on Toronto's annual SO_2 means, ANOVA revealed that there was a statistically significant difference between at least 2 seasons in 2007, and in 2020. For every tested year, every seasonal mean was significantly different from one another, with one exception: in 2020, the SO_2 mean of Spring and Winter were not significantly different.

For the effect of season on Toronto's annual p-$SO4^{-2}$ means, we selected a wider sample of years to compensate for the high uncertainty in p-SO_4^{-2} means relative to the low uncertainty in SO_2 means (2004, 2005, 2006, 2007, 2015, and 2019). There was no statistically significant difference between any season in 2004, 2006, 2007, 2015, and in 2019. The only notable differences were in 2005, between Summer and Spring, and between Summer and Winter.

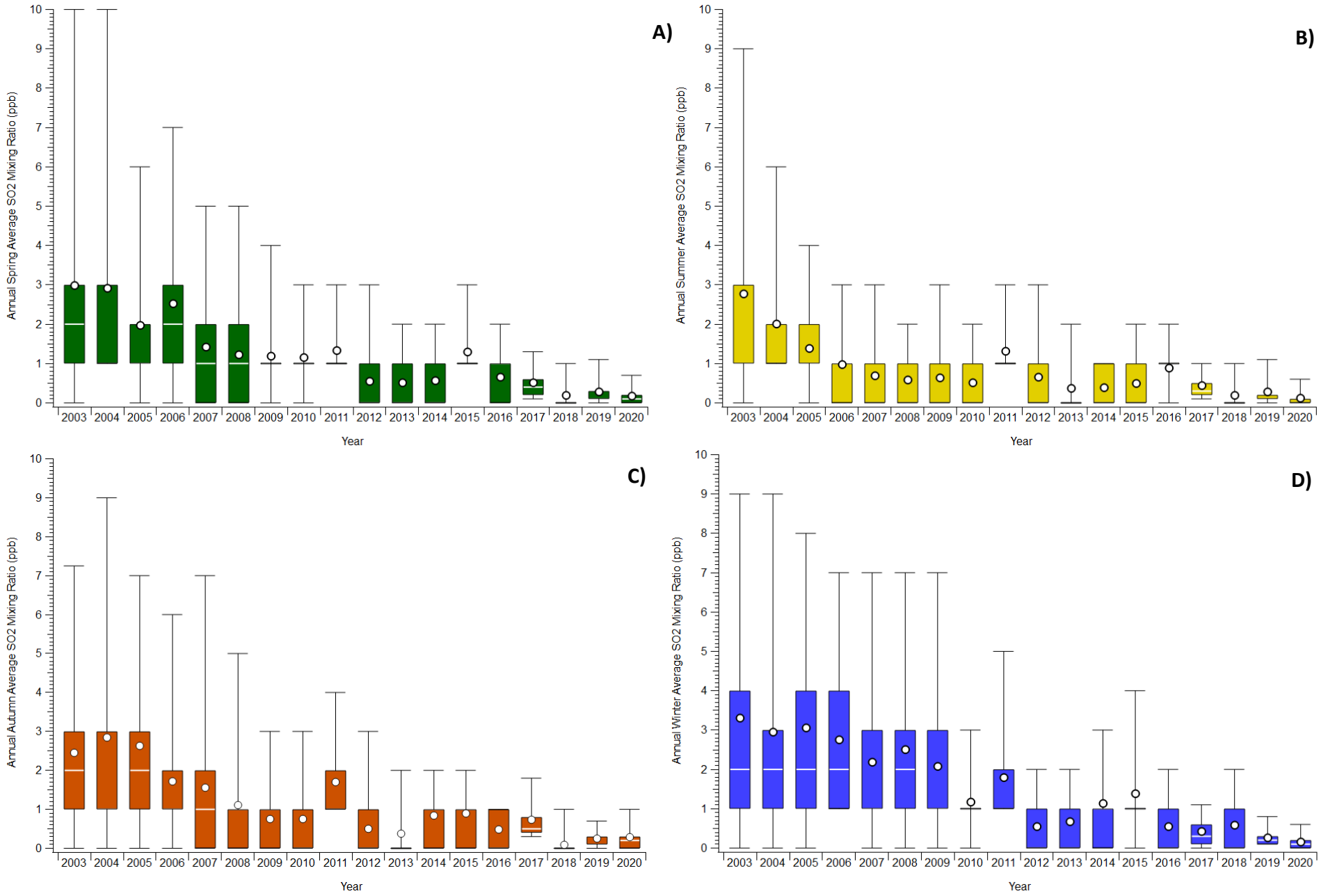

Figure 16. Annual Toronto SO_2 box plots divided by season, where A) is Spring, B) is Summer, C) is Autumn, and D) is Winter. Whiskers are up to 95th- and down to 5th-percentile. Mean is displayed as a white marker. Median is displayed as a white line.

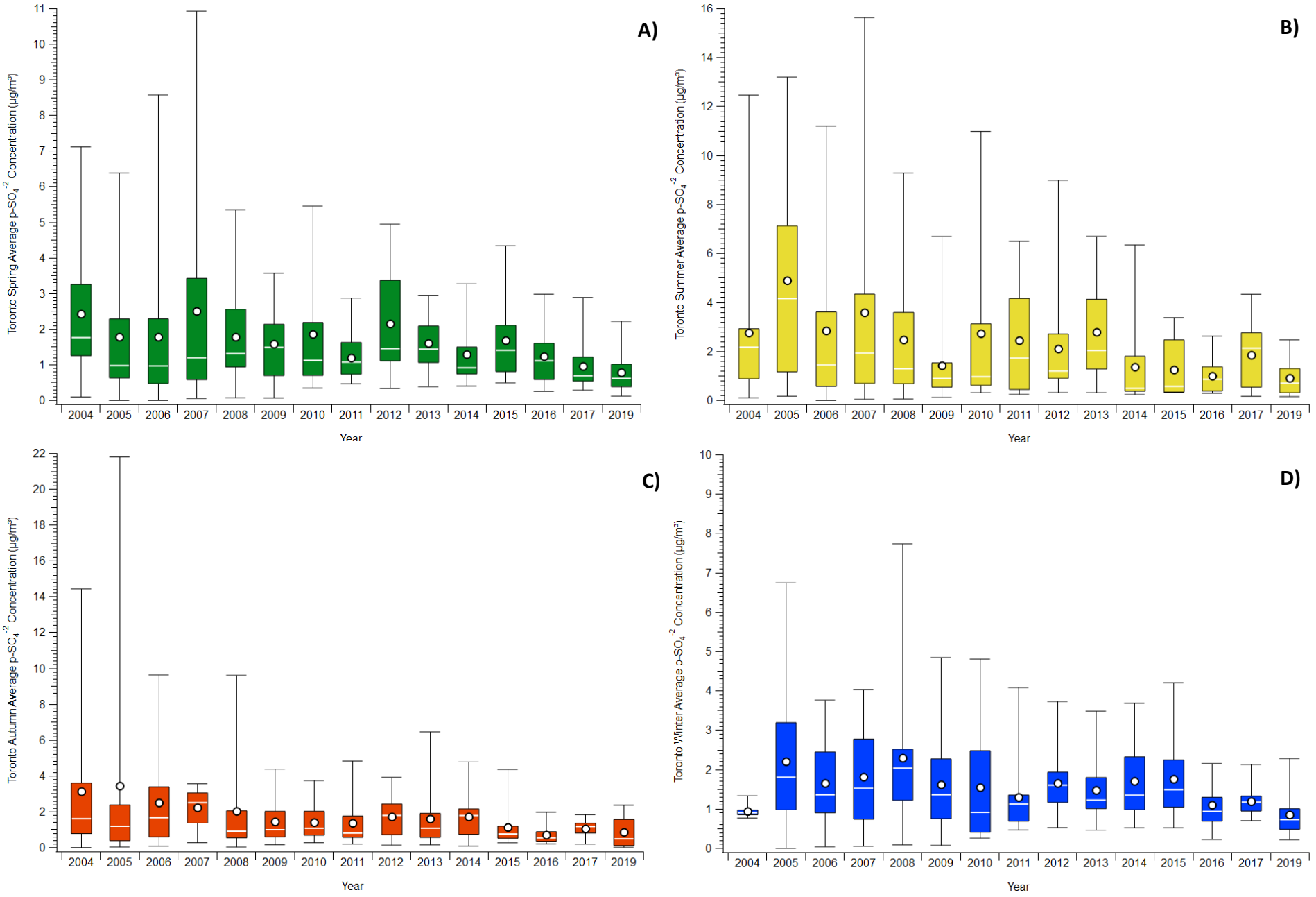

Figure 17. Annual Toronto p-SO_4^{-2} box plots divided by season, where A) is Spring, B) is Summer, C) is Autumn, and D) is Winter. Whiskers are up to 95th- and down to 5th-percentile. Mean is displayed as a white marker. Median is displayed as a white line.

Daytime and nighttime SO_2 means have been displayed as box plots in **Figure 18**. Box plot parameters are identical to previous box plots. To constrain the analysis to a single relevant parameter, only the Toronto NAPS site's day/night differences will be investigated. Note that due to the data collection interval for p-SO_4^{-2} spanning days, not hours, it is not possible to compare the daytime and nighttime intervals for p-SO_4^{-2} and SO_x. To compare between daytime and nighttime, 3 relevant years will again be selected to represent the time period pre-, during, and post-environmental regulation (2007, 2015, and 2020, respectively). Much like the seasonal analysis, it will be assumed that both daytime and nighttime interval annual averages will be affected similarly by time as the 24-hour annual averages.

Successive two sample t-tests ($\alpha = 0.05$) were performed in Igor to determine the effect of daytime/nighttime intervals on Toronto's annual SO_2 means for specific pairs of years (2007, 2015, and 2020 selected as test years). The t-test revealed that there was a statistically significant difference between daytime and nighttime in 2007, 2015, and 2020.

Note that pollutant data is typically not distributed normally. Notable events in atmospheric pollutant data are characterized by peaks caused by discrete plumes passing the detector, resulting in a skew in the frequency of the data from normal. The majority of the data will distribute around the mean, with a long, narrow tail representing the peak data (see **Figure 19**). ANOVA analysis, post-hoc testing, and two-sample t-tests rely on an assumption of normality of data with low variation; thus, the non-normal distribution of atmospheric pollutant data would theoretically reduce the statistical power of these tests. In reality, however, the data sets used here have a high number of points (e.g., average yearly Toronto SO_2 $N \approx 8760$), which increases the power of the test, and the majority of these points are largely distributed normally (see **Figure 19**). The main problems arise with the p-SO_4^{-2} data sets, where there were often only a few points for an individual year, resulting in high variation. The result of this is that the statistical tests used for any p-SO_4^{-2} analysis may not properly detect significant differences between two samples and may result in a conservative analysis of the data.

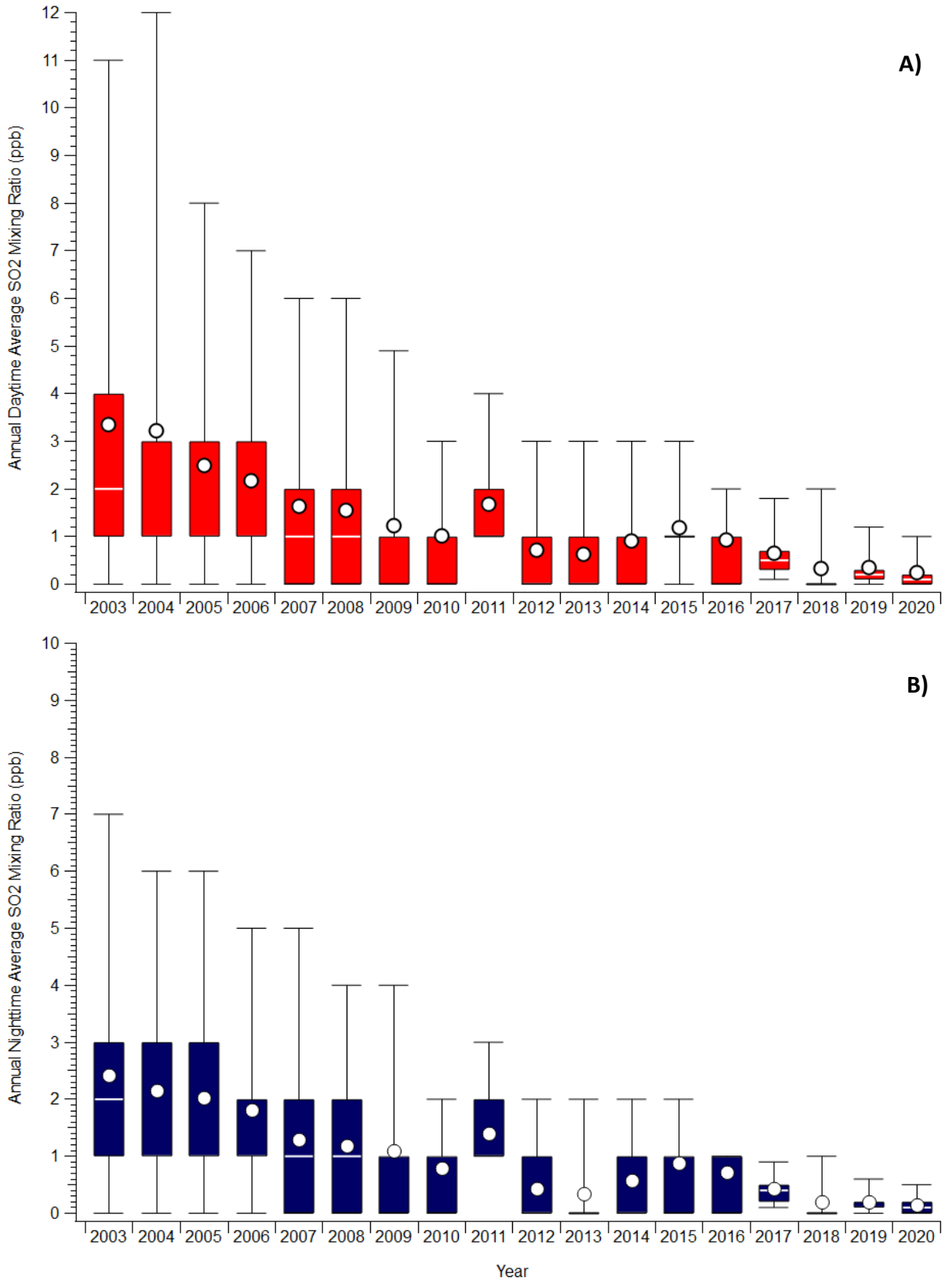

Figure 18. Annual Toronto SO_2 box plots divided by day- and nighttime, where A) is Daytime, and B) is Nighttime. Whiskers are up to 95th- and down to 5th-percentile. Mean is displayed as a white marker. Median is displayed as a white line.

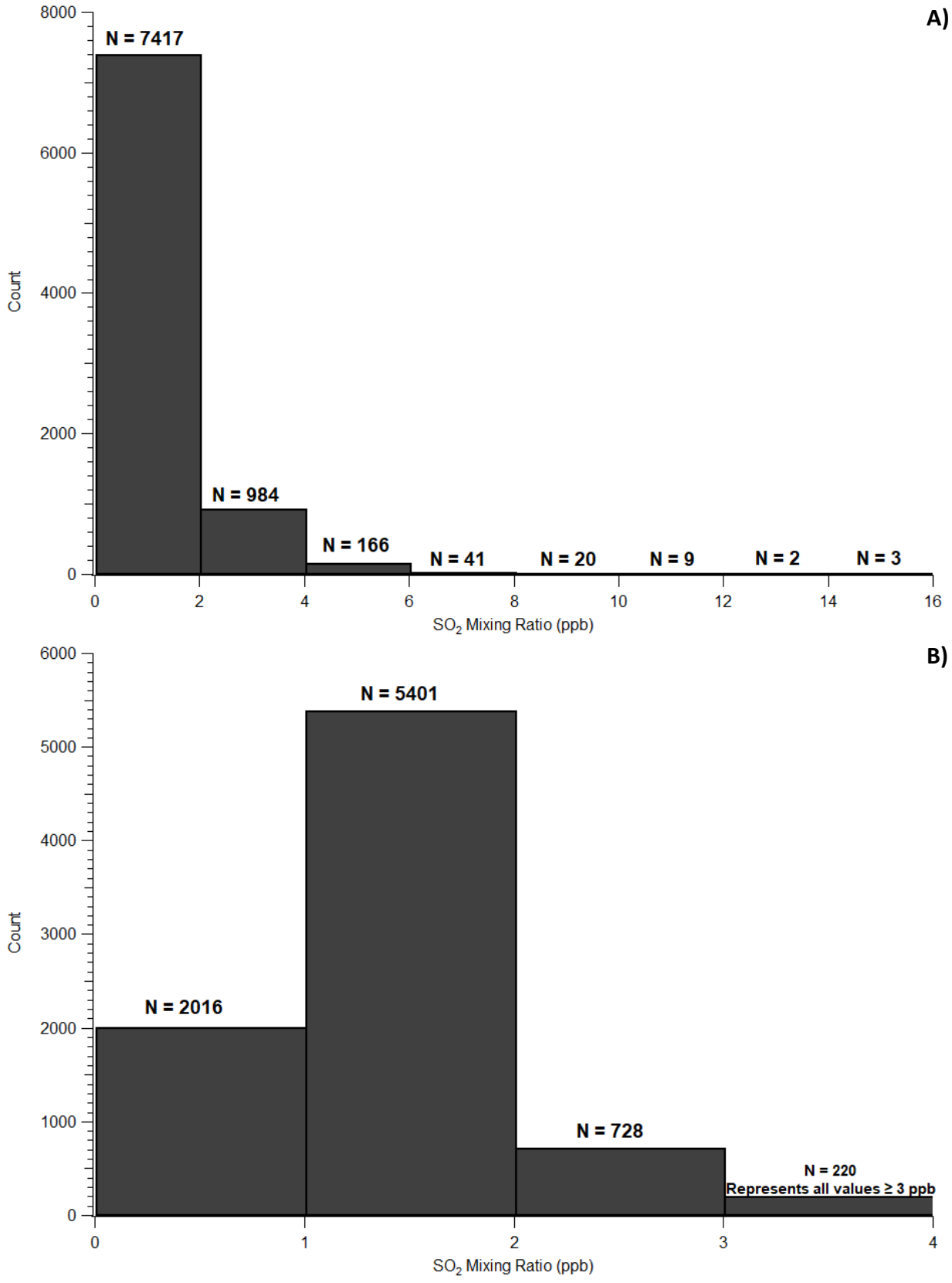

Figure 19. Frequency histograms for the annual SO_2 data set for Toronto in 2015 (N = 8642, M = 1.02, SD = 1.03) to demonstrate sample distribution. Histogram A) shows the data separated out in 2 ppb wide bins all the way to the max of 16 ppb, and histogram B) shows the data separated in 1 ppb bins to better illustrate the distribution of the data (with all data ≥ 3 ppb in the last bin).

3.2 Trends in Ontario's Sulfur Dioxide

SO_2 data was collected from the roof of the Petrie Science and Engineering Building at York University in Toronto, Ontario, from August 12th, 2021, to October 18th, 2022. A data point was collected near-continuously every 10 seconds over this interval. Both the raw data plot (See **Figure 20**) and summarized descriptive statistics for the entire time period will be displayed here (See **Table 8**), as well as data plots for each month, season, and daytime/nighttime interval. In addition, meteorological data will be integrated into this section, to demonstrate the relationship between wind direction frequency and SO_2. In this section, the data collected during this thesis project provides a current and comprehensive view of SO_2, its trends, and the effects of its seasonal and temporal variations. Presentation of any high pollution events will occur in **Chapter 3.4**. Any comparisons will be displayed graphically, and the most important comparisons will be discussed in **Chapter 4.2**.

Table 8. Descriptive statistics for the entire collected SO_2 data set from August 12th, 2021, to October 18th, 2022, computed via Igor Pro.

Statistic	Mixing Ratio (ppb)
Mean ($\bar{x}$)	0.37
Standard Deviation (σ)	0.82
Standard Error (±)	0.0004
95% CI (± $\bar{x}$)	0.0008
Median	0.19
Maximum	27
5th Percentile	-0.14
95th Percentile	1.4

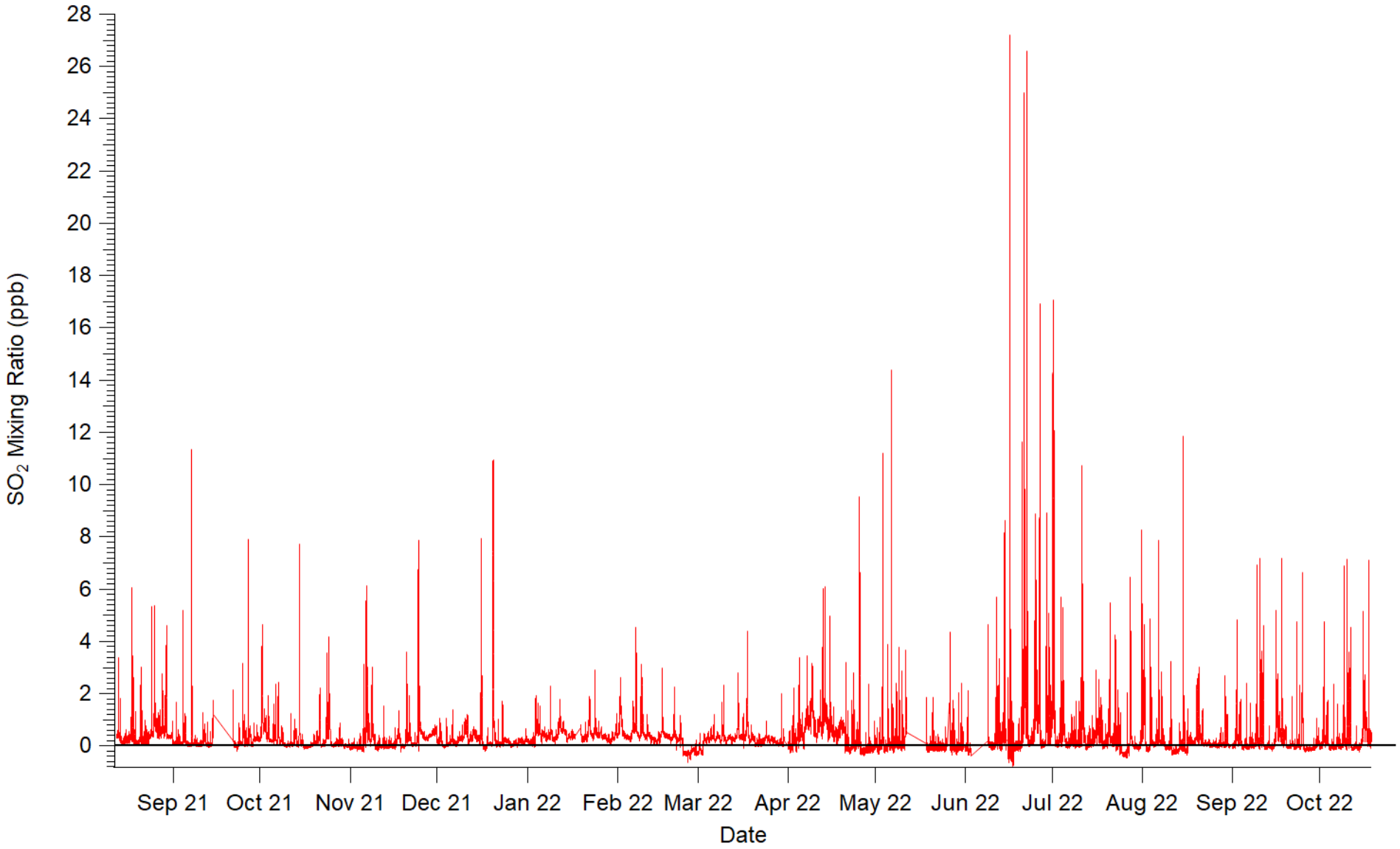

Figure 20. Complete SO_2 data (N = 3,490,740) collected from the 43i instrument from August 12th, 2021, to October 18th, 2022. Note that values below 0.07 ppb are considered to be below the lower detectable limit for this method. Values below the lower detectable limit are still included for calculations of summary statistics.

A notable portion of the data is below zero; realistically, atmospheric pollutant mixing ratios physically cannot be a negative number, but in the interest of analytical consistency, these values have not been removed from any calculations or statistical analysis. Per **Chapter 2.2**, we note that a significant portion of the data collection period (November 1st, 2021 – July 18th, 2022) was affected by flow rate issues, hardware failure, or both; conclusions made on data within this range will be caveated with a large degree of uncertainty.

To establish the statistical difference between the historic data and currently collected data, one-way ANOVA and post-hoc analysis was used to compare the effect of time on annual SO_2 mean across 2019, 2020, and the current data, which revealed a significant difference between all three time intervals.

Box and whisker plots have been generated for each month of collected SO_2 data, as well as the trend of the monthly means (see **Figures 21 and 22**). The setup and methodology of these box plots have been described previously in **Chapter 3.1**. ANOVA and post-hoc testing revealed that there was a statistically significant difference between every month, with the exception of August 2022 and September 2022.

The collected data was split into seasonal intervals (Autumn: September – November 2021, Winter: December 2021 - February 2022, Spring: March – May 2022, Summer: June - August 2022). Note that the months of August 2021, September 2022, and October 2022 have been omitted to create even, 3-month intervals for a full year. Seasonal box plots were generated (see **Figure 23**). ANOVA and post-hoc testing was discovered that every seasonal SO_2 mean was significantly different from one another.

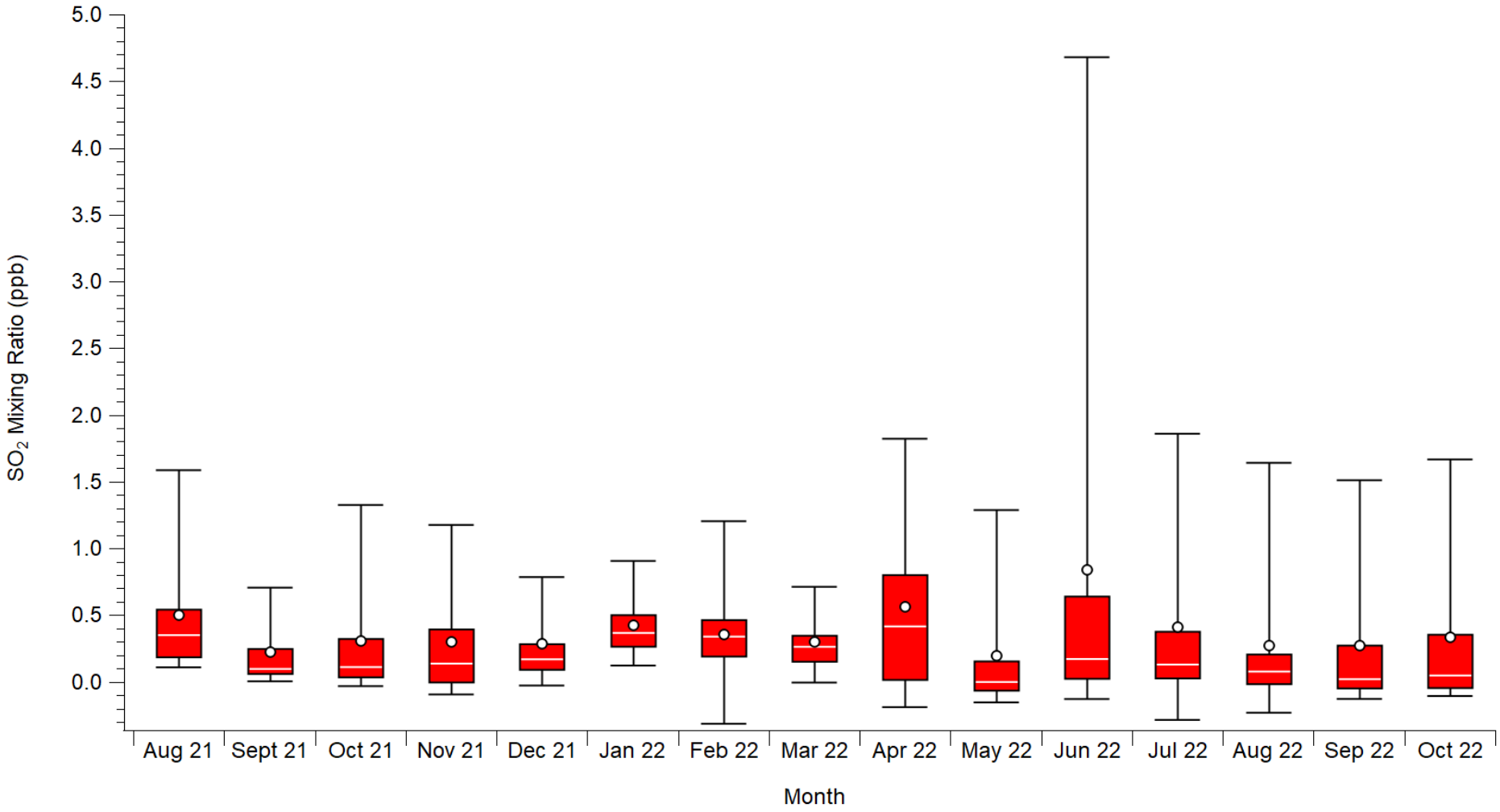

Figure 21. Chronologically ordered monthly SO_2 box plots for the collected data from the 43i instrument at York University, from August 12th, 2021, to October 18th, 2022. Whiskers are up to 95th- and down to 5th-percentile. Mean is displayed as a white marker. Median is displayed as a white line.

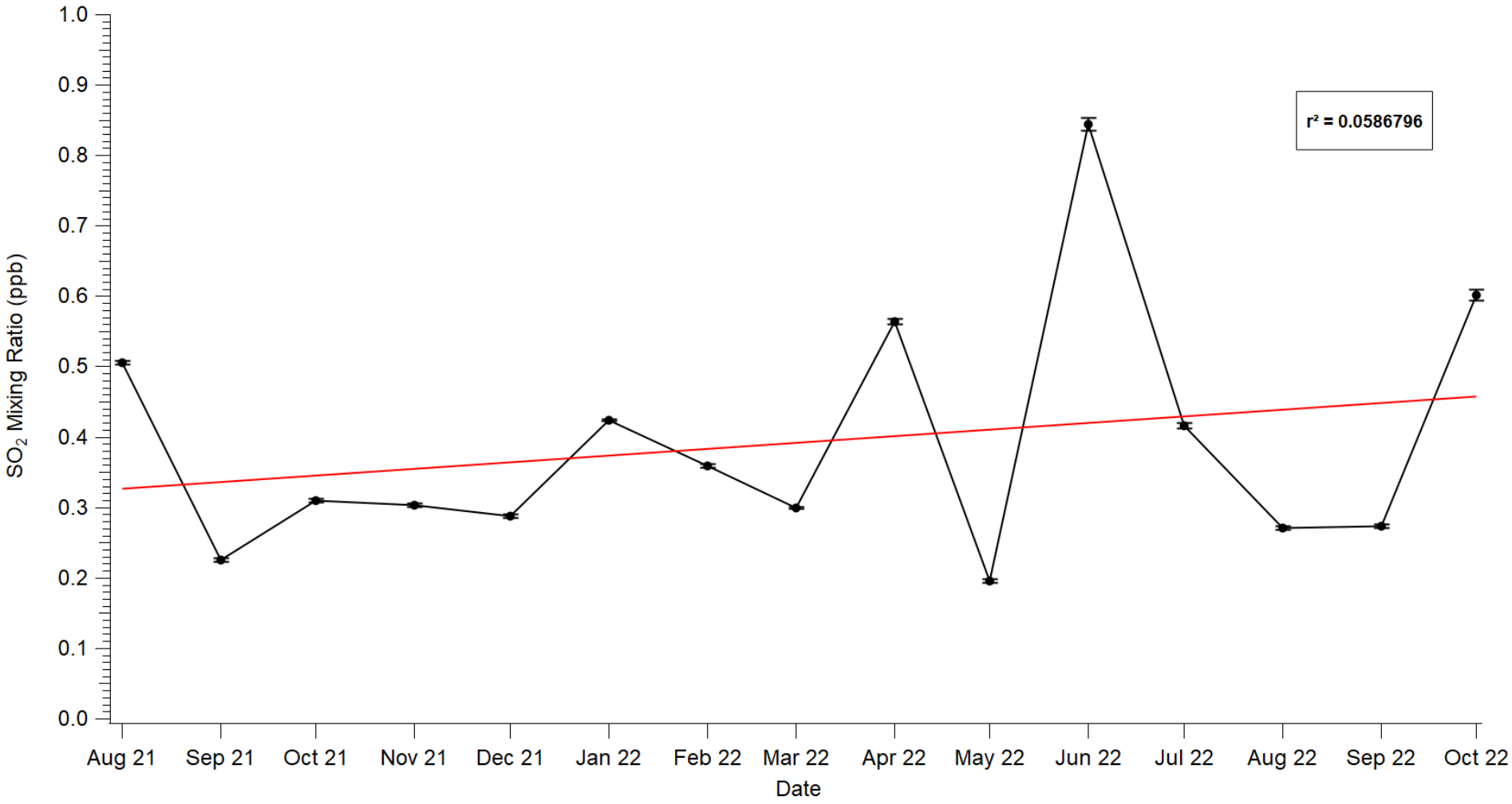

Figure 22. Plotted monthly SO_2 means over time for the collected data from the 43i instrument at York University, from August 12th, 2021, to October 18th, 2022. Y-error bars have been added to each point, representing the 95% confidence intervals. A line-of-best-fit has been added to the plot by Igor Pro, and the corresponding r^2 value was calculated by linear regression.

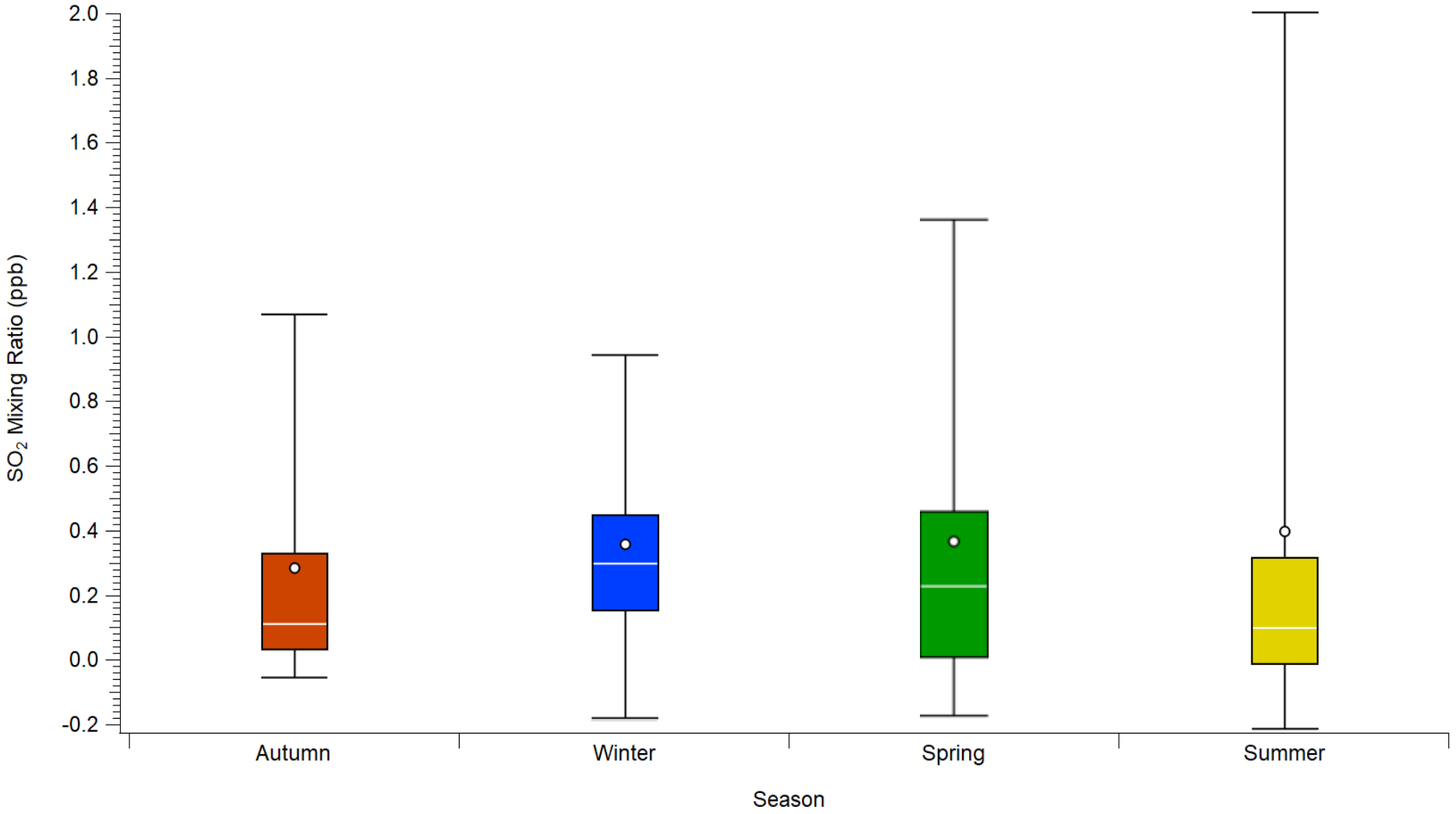

Figure 23. Seasonal SO_2 box plots for the collected data from the 43i instrument at York University, from August 12th, 2021, to October 18th, 2022. Whiskers are up to 95th- and down to 5th-percentile. Mean is displayed as a white marker. Median is displayed as a white line.

The daytime and nighttime 12-hour intervals were also investigated. Once again, the daytime interval was defined as the time period from 8:00 AM to 8:00 PM, and the nighttime interval spanned from 8:00 PM to 8:00 AM. Monthly box plots have been generated for each interval, using the previously described parameters (see **Figure 24**). A two-sample t-test revealed that there was a statistically significant difference between daytime and nighttime for the collected data set.

Polar plots of SO_2 versus wind direction were generated in Igor Pro from the York University EMOS Station meteorology data (see **Figure 25**). The first polar plot is a wind rose that demonstrates the frequency of the air mass origin versus the direction. Radial distance from the centre indicates the proportion of the SO_2 data points that originated from a specific 15° sector. Each concentric ring, starting from zero in the origin, represents 0.01 (or 1%) of the total data. The origin represents the relative location of the meteorological tower just outside of the Petrie Science and Engineering Building at York University, in Toronto, Ontario. Note that the data is not separated out by pollutant mixing ratio; this polar plot merely represents the frequency of the entire dataset, regardless of how high the mixing ratio is. This is because separating the data by mixing ratio on a frequency plot can be misleading, as sectors with very few points (but high mixing ratios) can be visually underrepresented. In addition, the vast majority of the data points were under 5 ppb; attempts to create categories to visually display the highest SO_2 mixing ratio data did not work, as the proportions of each sector above 5 ppb were too small to be visualized.

To address these issues, a pollution rose was generated. For this plot, the SO_2 mixing ratios were plotted against wind direction. Instead of grouping each 15° sector into a single frequency bar, each individual point was plotted. Each concentric ring, starting from 0 in the origin, represents an increase of 5 ppb, up to 30 ppb. While it is difficult to visually resolve data below 5 ppb, due to the density of points, the highest peak data and their associated direction of origin can be seen from this plot. Note that, while the shape of each pollution rose is similar, the frequency of data and the peak mixing ratios are not necessarily correlated.

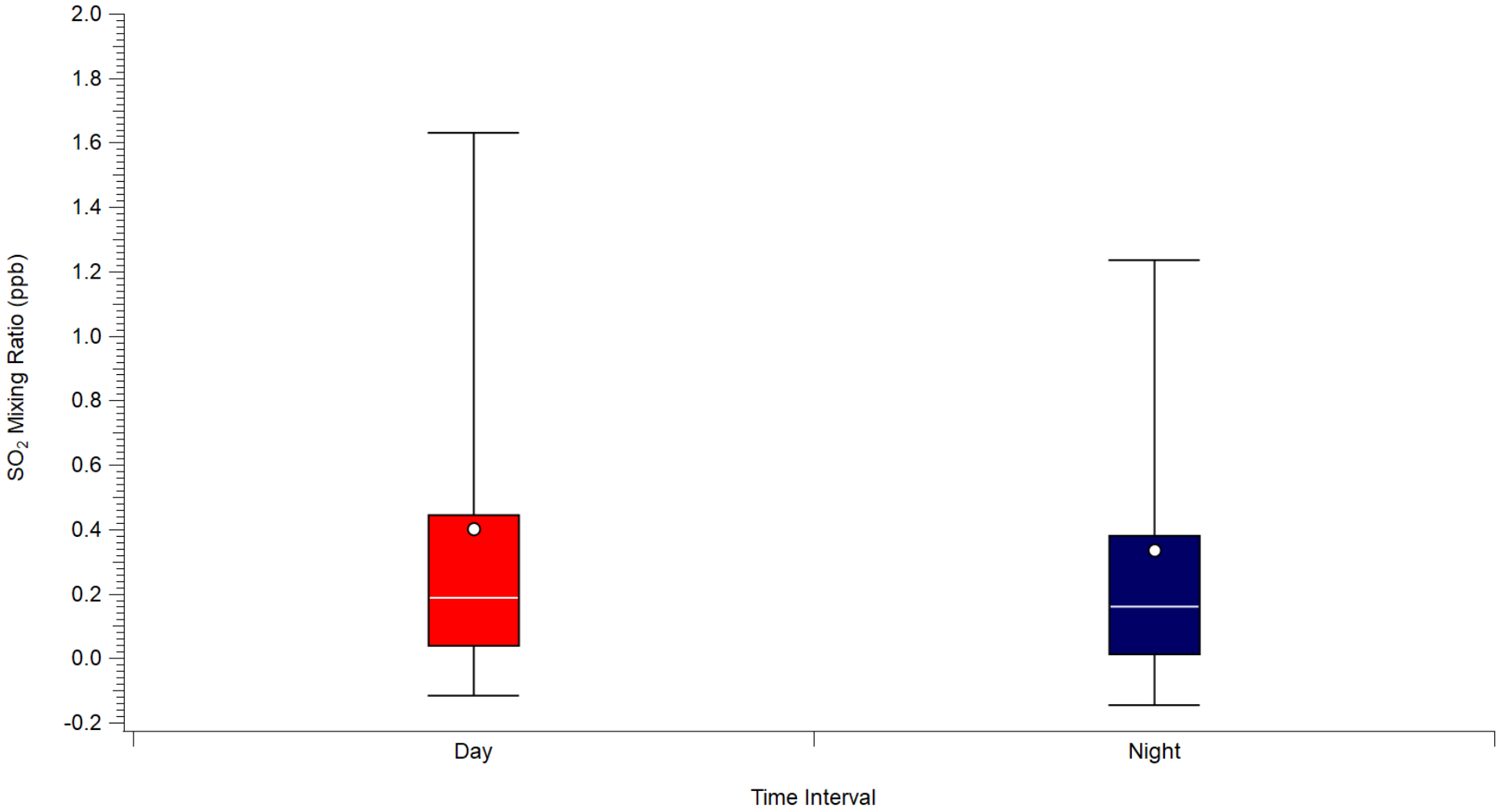

Figure 24. Daytime and nighttime SO_2 box plots for the collected data from the 43i instrument at York University, from August 12th, 2021, to October 18th, 2022. Whiskers are up to 95th- and down to 5th-percentile. Mean is displayed as a white marker. Median is displayed as a white line.

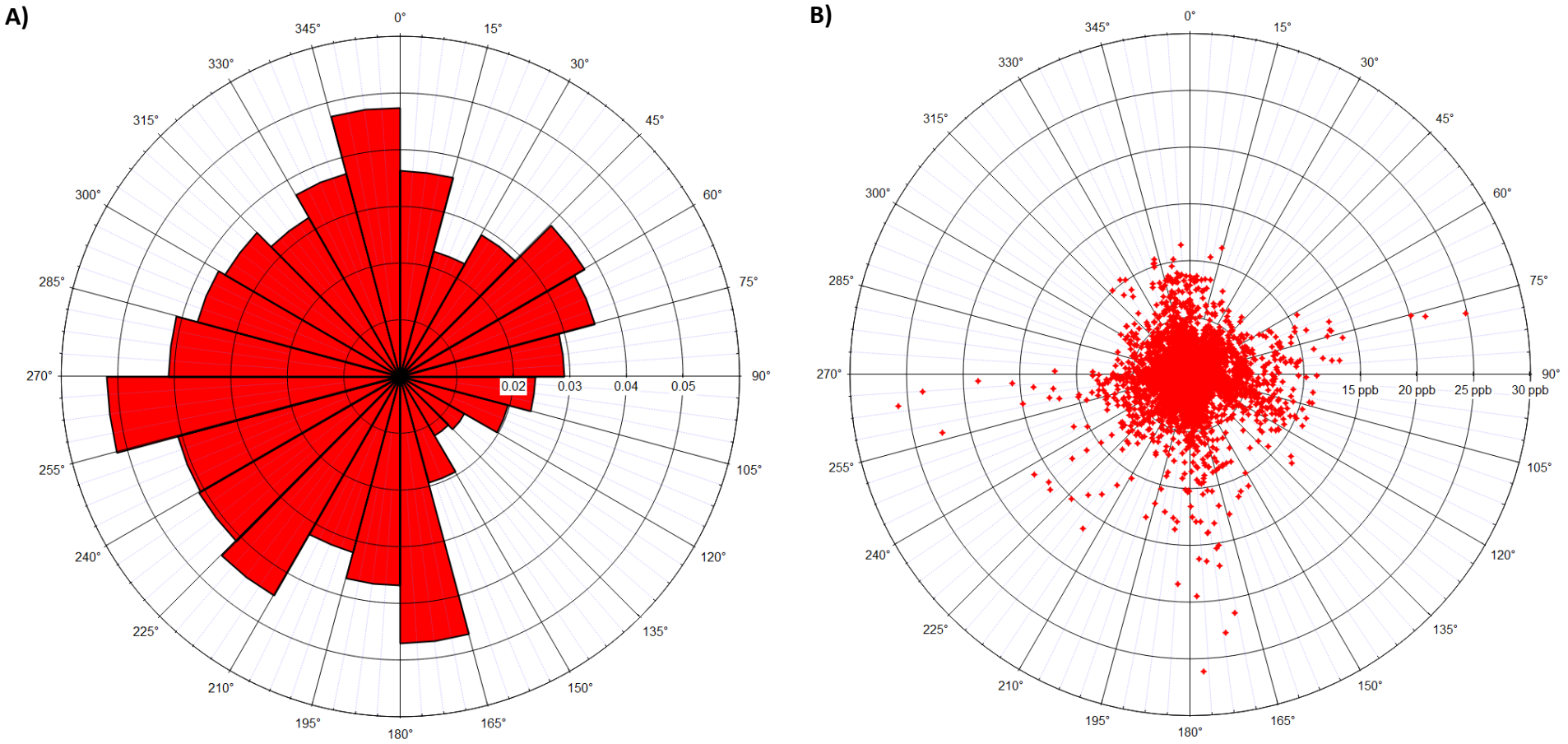

Figure 25. Polar plots for the collected SO_2 data from the 43i instrument at York University, from August 12th, 2021, to October 18th, 2022. Polar plot A) is an SO_2 frequency by wind direction origin wind rose with 15° sectors (units are proportions up to 1.00). Polar plot B) is an SO_2 mixing ratio by wind direction origin pollution rose. Note that the first radial label from the origin for plot A), and the first and second radial labels from the origin for plot B) are not included to improve visual clarity of the data.

3.3 Trends in Local Particulate Matter

Particulate matter data was collected from August 12th, 2021, to October 1st, 2021. This data was collected using the Aerodyne AMS and consists of p-SO_4^{-2}, p-NH_4^+, p-NO_3, and p-organic. The AMS collected a data point every minute over this time interval. Both a plot of the raw data (see **Figure 26**) and a table summarizing the descriptive statistics for p-SO_4^{-2} (**Table 9**) are provided below. In addition, plots of all of the other particulate matter species are provided for comparison (see **Figure 27**). Finally, we sum and plot $PM_{2.5}$ as the addition of all the particulate matter species (see **Figure 27**).

Note that an experimental lower detectable limit for the Aerodyne AMS was never established, since there was no opportunity to perform an on-site calibration. An experimental determination from the literature demonstrates that the lower detectable limit for an HR-ToF-AMS is below 0.04 $\mu g/m^3$ when operating in the single reflectron high-sensitivity mode.[46] Note that values below this limit are still included for calculations of summary statistics. After August 25th, 2021, the performance of the AMS became unreliable, likely due an error with the flow rate related to an unknown failure in the instrument, and any data after this date was discarded from the analysis. For p-SO_4^{-2}, the descriptive statistics from the August 12th to 25th, 2021 "AMS" dataset, and the November 16th to 25th, 2021 "AIM-IC-MS" dataset will be summarized below. Summary statistics for non-p-SO_4^{-2} particulate species detected by the AMS are also included below, in **Table 10**.

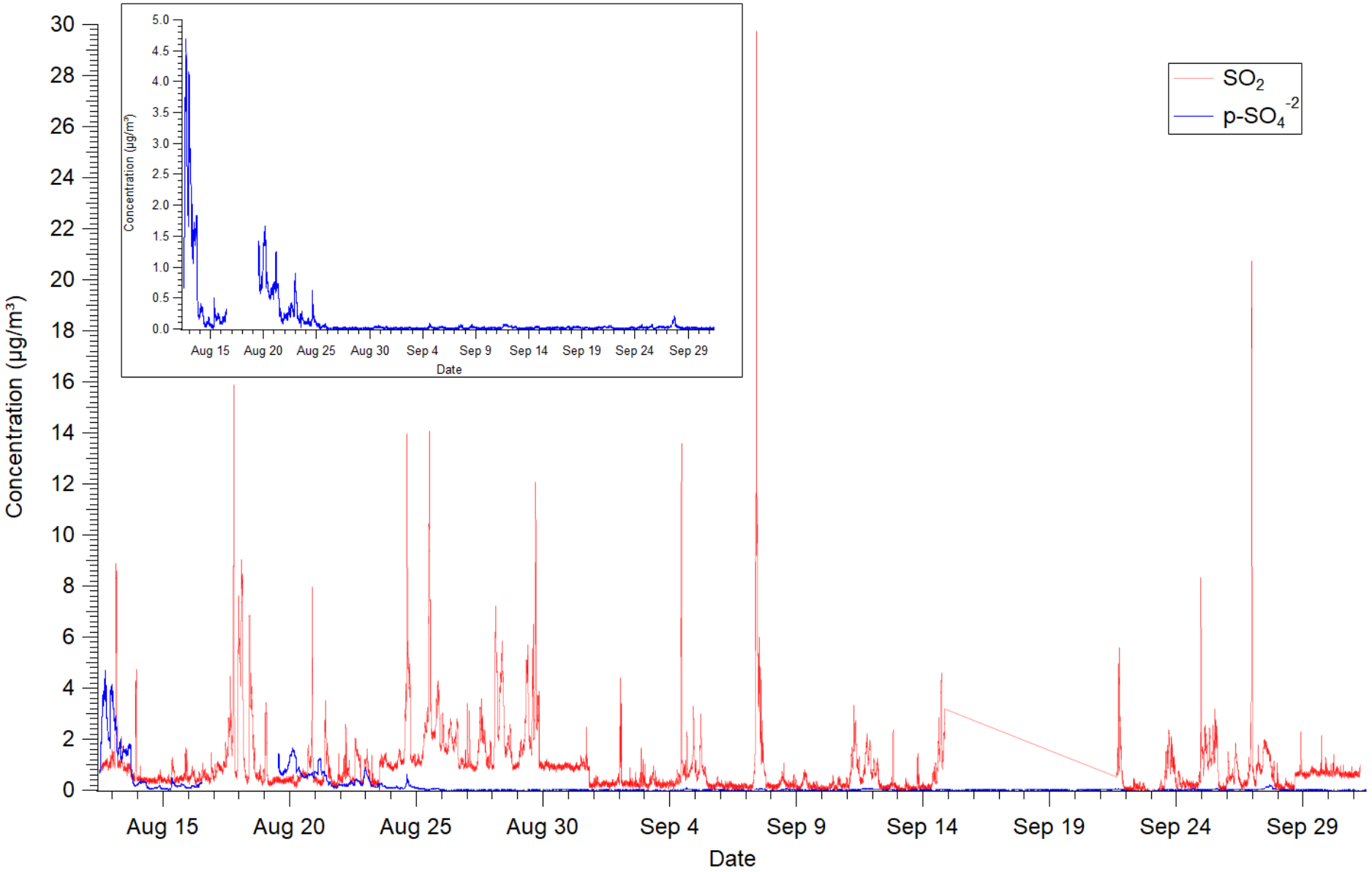

Figure 26. Complete p-SO_4^{-2} data (N = 60,217) collected from the AMS instrument from August 12th, 2021, to October 1st, 2022. A 5-point median smoothing has been applied to reduce noise. SO_2 data from the 43i instrument has been converted to µg/m^3 and plotted alongside p-SO_4^{-2} to provide a visualization of the relationship between the species. An isolated plot of p-SO_4^{-2} has been provided in a sub-window in the top left.

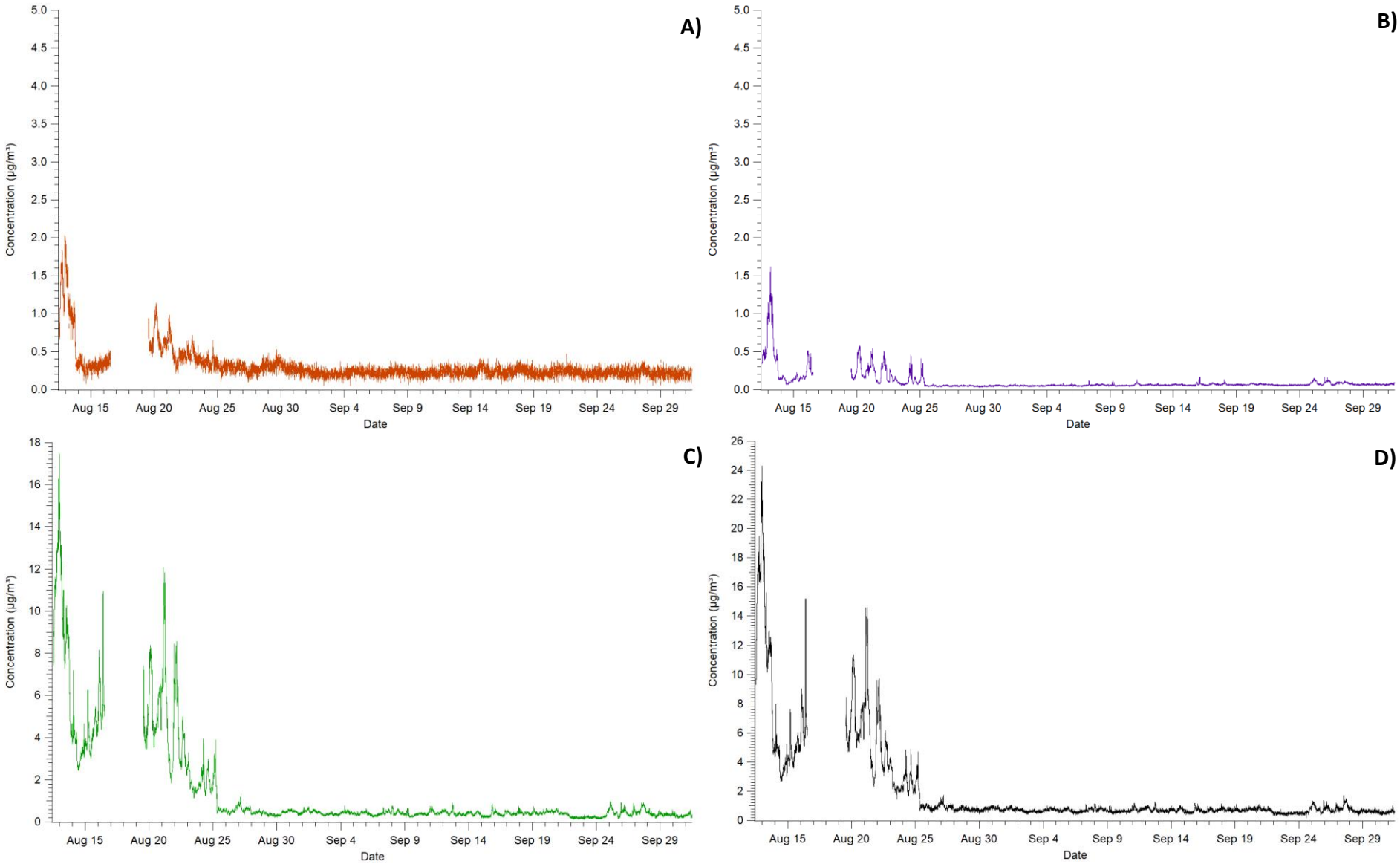

Figure 27. Complete particulate species data (N = 60,217 each) collected from the AMS instrument from August 12th, 2021, to October 1st, 2022, where A) is p-NH_4^+, B) is p-NO_3^-, C) is p-organics, and D) is the summed total $PM_{2.5}$. A 10-point median smoothing has been applied to each plot to reduce noise.

Table 9. Summary statistics for p-SO_4^{-2} ("AMS" and "AIM-IC-MS" datasets)

	Concentration (μg/m$^{3)}$	
Statistic	**AMS**	**AIM-IC-MS**
Mean ($\bar{x}$)	0.60	0.38
Standard Deviation (σ)	0.80	0.51
Standard Error (±)	0.008	0.03
95% CI (± $\bar{x}$)	0.015	0.07
Median	0.25	0.17
Maximum	4.7	2.6
5th Percentile	0.06	0
95th Percentile	2.4	1.5

Table 10. Summary statistics for non-sulfate species for the "AMS" dataset.

	Concentration (μg/m$^{3)}$			
Statistic	**p-NH_4^+**	**p-NO_3^-**	**p-Organics**	**$PM_{2.5}$**
Mean ($\bar{x}$)	0.55	0.25	4.9	6.3
Standard Deviation (σ)	0.35	0.23	3.0	4.2
Standard Error (±)	0.003	0.002	0.03	0.04
95% CI (± $\bar{x}$)	0.007	0.004	0.05	0.08
Median	0.42	0.16	4.2	5.0
Maximum	2.0	1.6	17	24
5th Percentile	0.25	0.07	1.5	2.1
95th Percentile	1.4	0.67	11	16

As previously stated, the data collected by the AMS is speculated to be unreliable past August 25th. It is theorized that a suboptimal flow rate was responsible for reducing instrument performance past this time, though this was not able to be determined, since the instrument was sent away for repairs following acute hardware failure on October 1st, 2021 (see **Figure 28**). From the plot of the collected flow rate data, it does appear that some sort of notable event occurs on August 22nd that immediately decreased the flowrate below 1 cc/s; soon after this, another notable event on August 25th caused a momentary decrease in the flow rate below 0.6 cc/s. Note that the AMS used a separate sampling manifold from the 43i, and the two instruments' low flow rate issues are unrelated. Since this same pattern is observed in all of the collected species' data, we expect that this is a systematic error, and not an observable variation in the behaviour of atmospheric p-SO_4^{-2}.

In addition, the data collection period for the AMS was aborted before the intended time; as a result, the dimensions of the analysis will have to be constrained (i.e., there is not enough data to perform meaningful seasonal and daytime/nighttime analysis). Within the collected data, there is also a notable gap. From August 17th – August 19th, 2021, the AMS data collection was halted; during this time, the flow rate was suboptimal (< 1.0 cc/s), and so the atmospheric sampling inlet was closed to avoid damaging the instrument while awaiting support from a technical expert.

The AMS collection period only provided 2 weeks of data in 2021, and so the AMS data does not necessarily represent the annual p-SO_4^{-2} trend; additionally, there is not enough data to make a meaningful statistical comparison with the historic data.

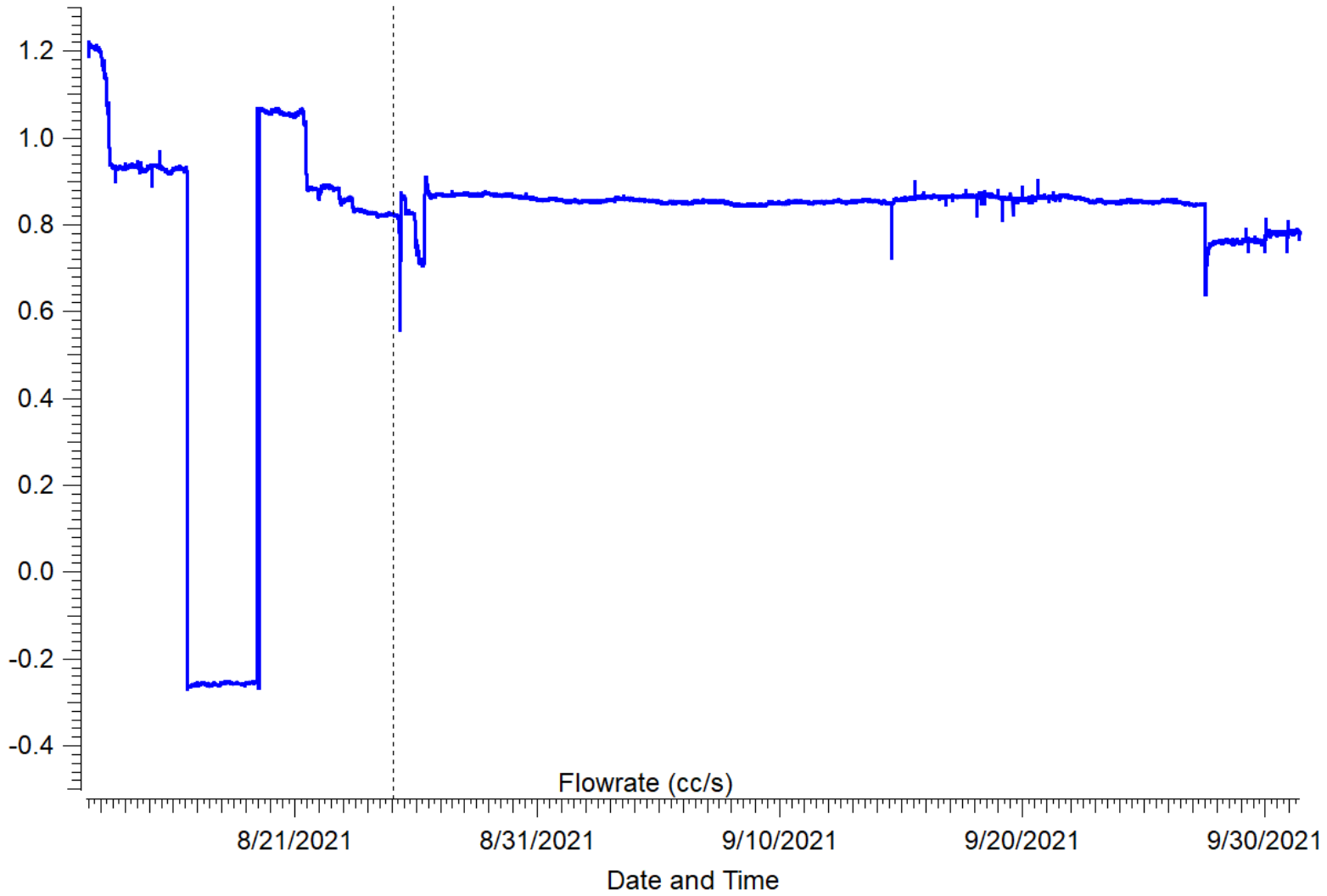

Figure 28. Flow rate data for the AMS from August 12th, 2021, to October 1st, 2021. A vertical dashed line has been added on August 25th, 2021, to indicate the beginning of the period of unreliable data. The negative flow rate period was the result of an intentional closing of the sampling inlet.

Polar plots were created from the wind direction data to determine the origin directions of particle sulfate (see **Figure 29**). The first polar plot created is a frequency of p-SO_4^{-2} versus wind direction wind rose. Once again, the frequency plot can be misleading, and underrepresents high concentration peaks from low frequency sectors, and so a second polar plot was generated to address these issues. The second polar plot created was a p-SO_4^{-2} concentration versus wind direction pollution rose. The setup of both of these polar plots was similar to the polar plots created for SO_2 in **Chapter 3.2**, though the radial concentration axis will be increments of 1 μg/m^3 (instead of 5 ppb) in the pollution rose.

In addition to the data collected by the AMS, there is a 10-day p-SO_4^{-2} dataset, from November 16th – 25th, 2021, captured via AIM-IC-MS **(See Figure 30**). This data is used for comparison with the AMS data period, as well as high pollution event analysis (summary statistics are provided in **Table 9**).

Finally, we can calculate the SO_x and X_{pSO4} values from the AMS and 43i data (see **Table 11**). SO_x will be calculated as the mean SO_2 (converted to μg/m^3) added to the mean p-SO_4^{-2}. X_{pSO4} will be calculated as the mean p-SO_4^{-2} concentration over the calculated mean SO_x concentration. In addition, the uncertainty and 95% confidence intervals of SO_x and X_{pSO4} can be propagated from the standard errors of the mean for SO_2 and p-SO_4^{-2}, as shown previously in **Chapter 3.1**. We can also calculate the linear correlation factors of SO_2 and p-SO_4^{-2} for SO_x and X_{pSO4} in Igor, including historic and current data. For SO_x, the correlation is r = 0.99 with SO_2 and r = 0.91 with p-SO_4^{-2}. For X_{pSO4}, the correlation is r = -0.76 with SO_2 and r = -0.40 with p-SO_4^{-2}. Between SO_x and X_{pSO4}, we note a linear correlation of r = -0.69.

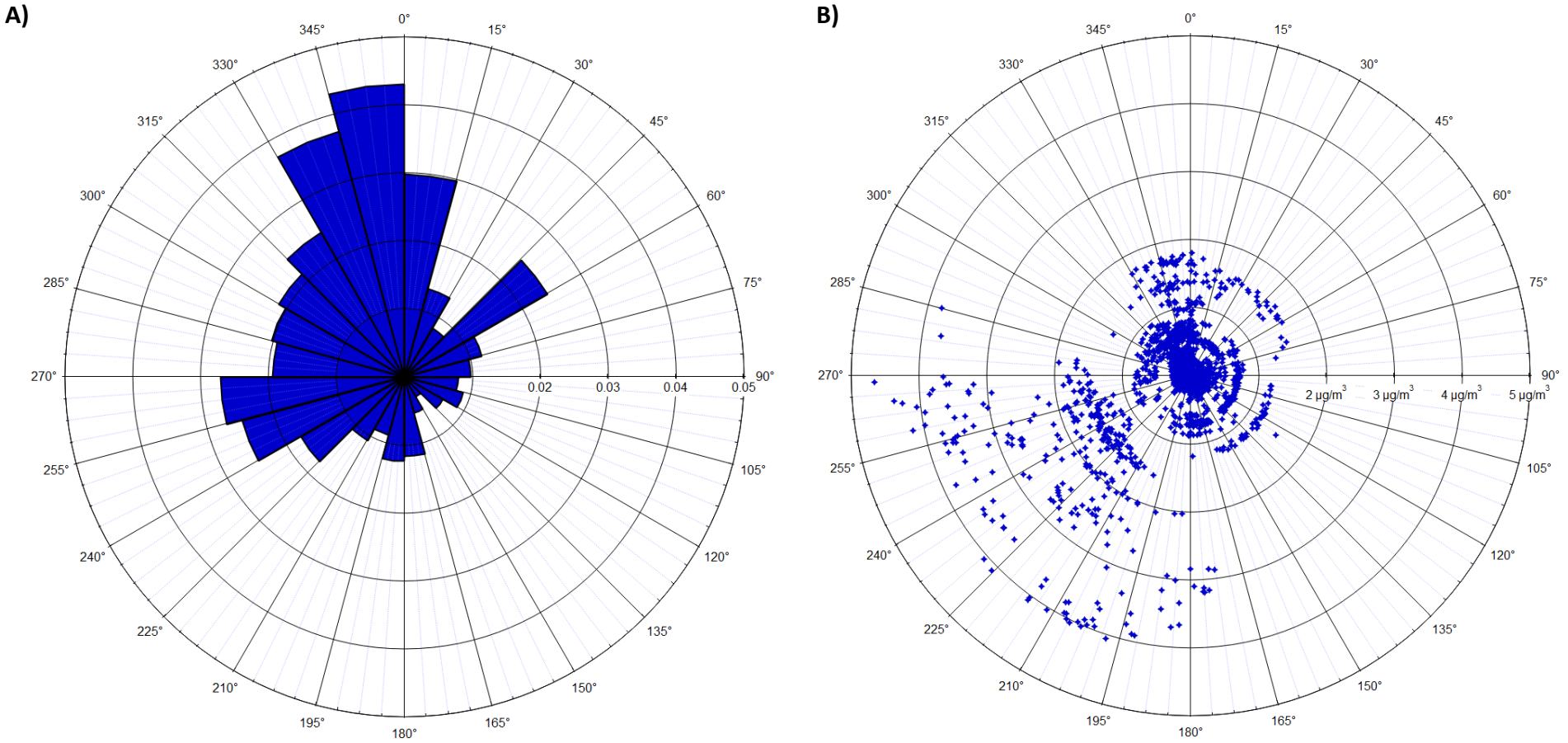

Figure 29. Polar plots for the collected p-SO_4^{-2} data from the Aerodyne AMS at York University, from August 12th, 2021, to October 1st, 2021. Plot A) is a wind rose plot with 15° sectors, while plot B) is an p-SO_4^{-2} concentration by wind direction origin pollution rose. Note that the first radial label from the origin for plot A) and B) are not included to improve visual clarity of the data.

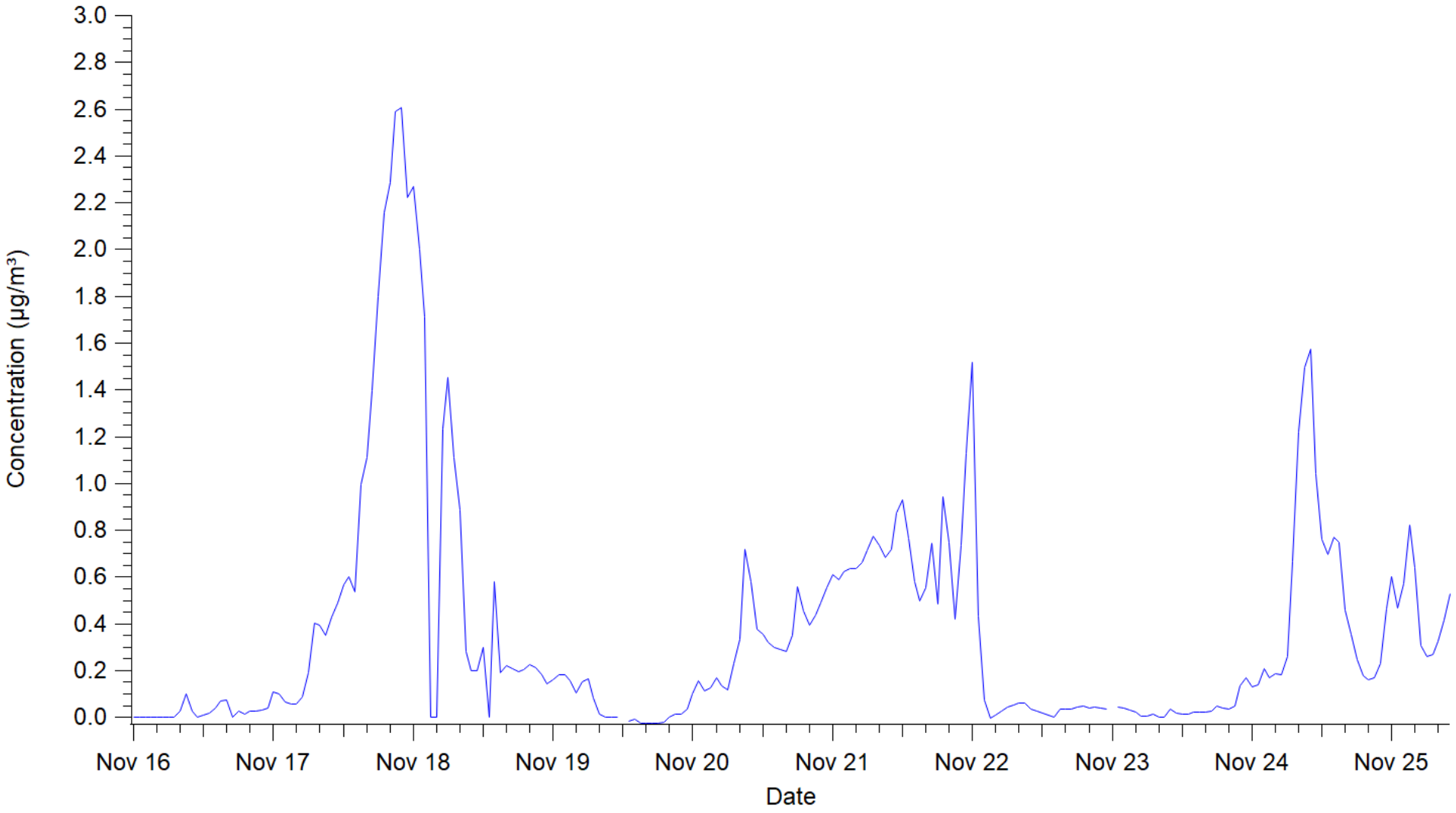

Figure 30. Complete p-SO_4^{-2} data (N = 234) collected from the AIM-IC-MS instrument at York University from November 16th to 25th, 2021.

Table 11. Calculated SO_x, X_{pSO4}, and their calculated uncertainties for the AMS and AIM-IC-MS datasets.

	Concentration (µg/m$^{3)}$	
Parameter	**Detectable**	**AIM-IC-MS**
Mean SO_x ($\bar{x}$)	1.6	1.4
Standard Error (±)	0.009	0.04
95% CI (± $\bar{x}$)	0.02	0.07
X_{pSO4} ($\bar{x}$)	0.38	0.28
Standard Error (±)	0.006	0.03
95% CI (± $\bar{x}$)	0.01	0.05

3.4 High Pollution Events in Local Sulfur

The original intention of this research project was to collect both gas-phase SO_2 and particle sulfate data over the same time period, compare the trends of the two species, and perform high pollution event origin tracking and analysis for both. Due to the AMS malfunction, however, the time periods cannot be directly compared past August 25th, 2021. The high pollution event analysis will therefore be split into two sections: the first being analysis of any high pollution p-SO_4^{-2} events over the AMS time period, with comparison to the collected SO_2 and meteorology data. This will include calculations of SO_x and X_{pSO4} for each high pollution event, as well as the wind sectors of origin. The second section is the analysis of all the SO_2 high pollution events, including origin wind sectors.

To properly analyze the origin of any high pollution event, we must visualize the relevant point sources that significantly contribute to SO_2 emissions in Ontario (see **Figure 31**). Likely point sources in 2022 are assumed to be the same as the highest emitting facilities from the NPRI 2020 inventory, summarized in **Table 1**. While the total emissions and relative

contributions of each facility may change from 2020 to 2022, it is not expected that, in general, significant point sources will be different. Point sources from the surrounding U.S. states (Michigan, Ohio, New York, Pennsylvania, and Indiana) are also included in this map, listed by state in **Table 12**. Data is derived from the Environmental Protection Agency's (EPA) 2017 National Emissions Inventory (NEI).[48] Note that this is the most recent dataset available from the EPA at the time of this writing.

For the purposes of this analysis, high pollution emissions will be defined as times with pollutant concentrations equal to or greater than 1σ above the mean for the AMS (periods ≥ 1.4 $\mu g/m^3$), and 2σ above the mean for the AIM-IC-MS (also ≥ 1.4 $\mu g/m^3$). Adjacent peaks may be added together and treated as one high pollutant event. These periods have all been plotted on Google Earth using NOAA HYSPLIT outputs (See **Figure 32**). Back trajectories can be organized into 4 broad categories, based on the direction of air plume origin: North (315-45°), East (45-135°), South (135-225°), and West (225-315°). Average SO_2, p-SO_4^{-2}, SO_x, p-SO_4^{-2}/SO_x ratio, and event count can be calculated for each origin sector. Back trajectories were run for 24 hours. Note that lake breeze effects, as well as the lower resolution meteorology data, reduce the accuracy of back trajectories. Given that the sampling site is surrounded by the Great Lakes, high lake breeze effects are expected; therefore, the influence of point sources will be generalized and not exactly traced by the back trajectory.

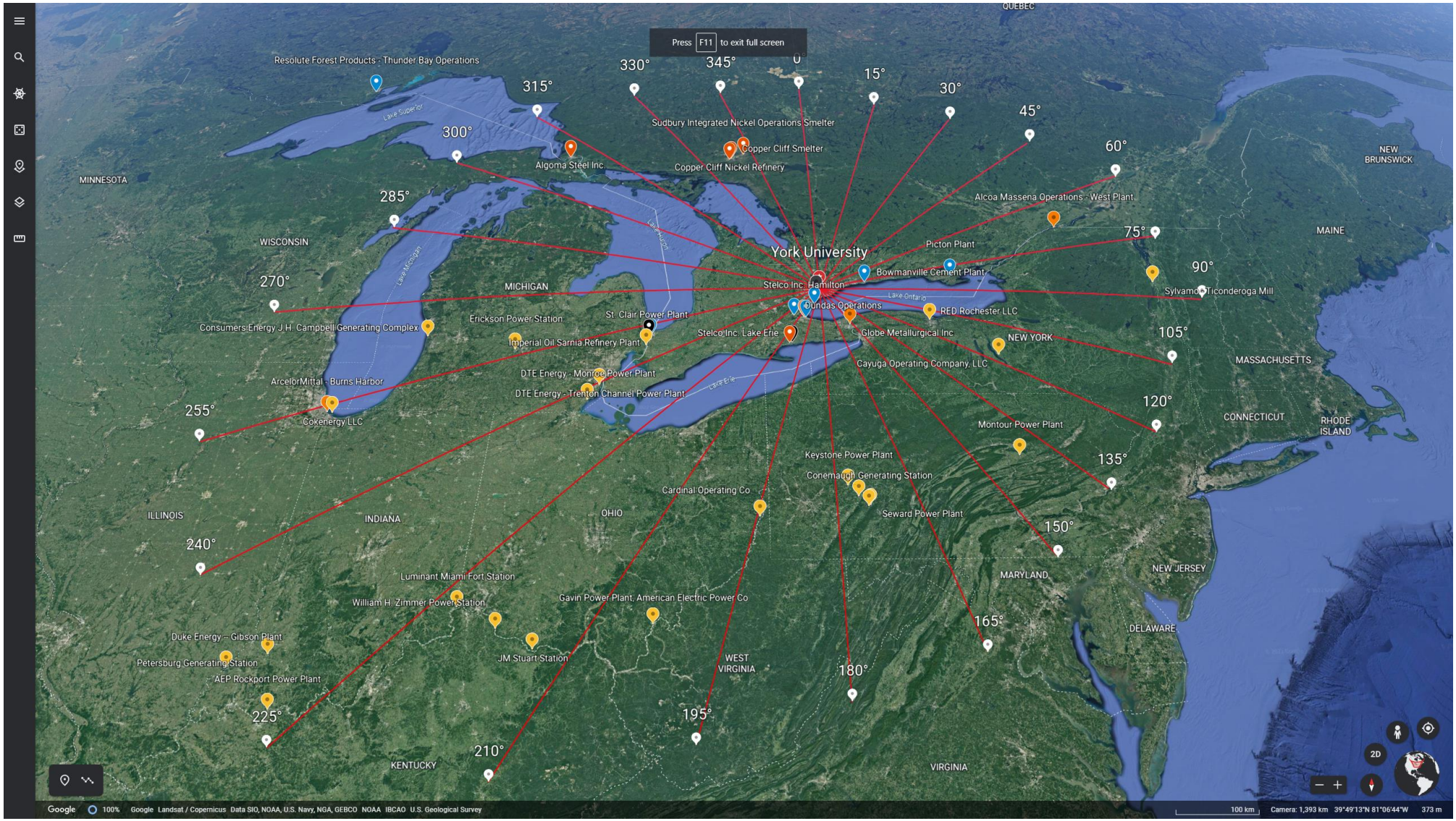

Figure 31. Map of significant SO_2 point sources from the 2020 NPRI inventory and 2017 EPA NEI plotted on Google Earth, as described in **Tables 1 and 13**. Metal refineries are marked with orange, petroleum refineries are marked with black, chemical production facilities are marked with blue, and power generation is marked with yellow. Radial lines have been added to denote every 15° sector

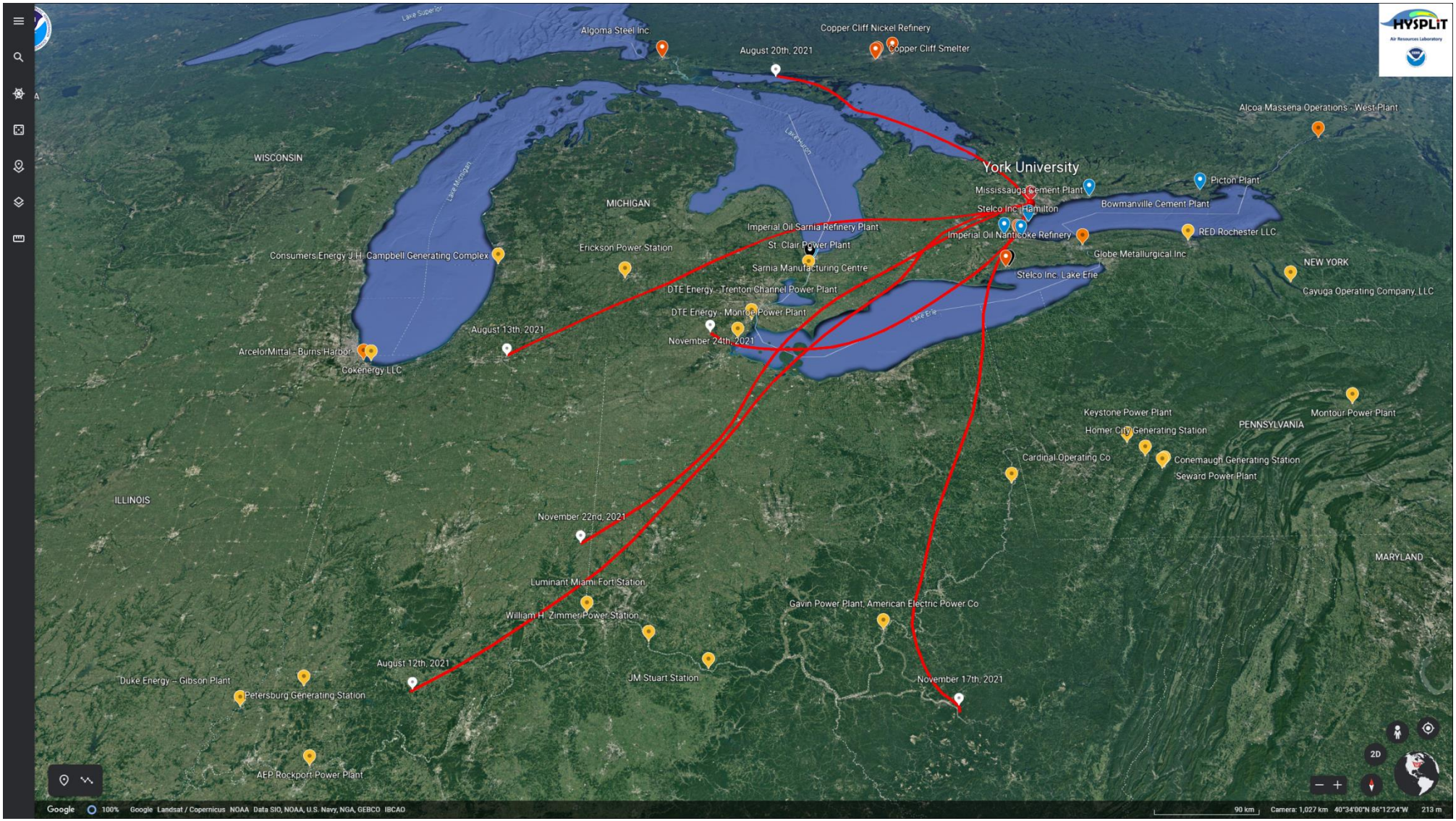

Figure 32. HYSPLIT 24-hour back trajectories (in red) for all 6 p-SO_4^{-2} high pollution events plotted on Google Earth. Each line is labeled at the trajectory origin (capped at 24-hours, not necessarily at a specific point source) with the date of detection at York University.

Table 12. Top 5 SO_2 point sources for each U.S. state surrounding Ontario, Canada in 2017. Sources organized in state by descending quantity of SO_2 emissions.

State	Sources	SO_2 Emissions (tonnes)
Michigan	St. Clair Power Plant	36,920
	DTE Trenton Channel Power Plant	6,180
	J.H. Campbell Power Plant	4,905
	DTE Monroe Power Plant	3,076
	Erikson Power Station	3,033
Ohio	Gavin Power Plant	25,421
	William H. Zimmer Power Station	14,070
	Cardinal Power Plant	11,259
	Luminant Miami Fort Power Station	10,514
	JM Stuart Power Station	6,675
Pennsylvania	Keystone Power Station	23,248
	Seward Generating Plant	7,265
	Homer City Generating Station	5,748
	Montour Power Plant	5,263
	Conemaugh Station	4,619
New York	RED Rochester LLC.	8,231
	Alcoa USA Corp.	2,405
	Sylvamo Paper - Ticonderoga Mill	626
	Globe Metallurgical Inc.	517
	Cayuga Operating Company Power Station LLC	505
Indiana	Rockport Generating Station	20,783
	Duke Energy – Gibson Plant	13,648
	ArcelorMittal – Burns Harbor	12,959
	Petersburg Generating Station	7,967
	Cokenergy LLC.	5,681

The date and time (approximated to the closet hour due to HYSPLIT's hourly time resolution of its meteorological data), average p-SO_4^{-2}, average SO_2, average SO_x, X_{pSO4}, average wind direction, and HYSPLIT sectors are tabulated below (see **Table 13**). Carbon monoxide mixing ratios are also included. Note that the wind direction data is the averaged wind direction from the meteorology station at York University, while the HYSPLIT sector direction is based on the modeled path of an air plume, with the origin sector defined as the trajectory start point. Since the origin from the meteorology station wind direction is a linear extrapolation from York University, while the HYSPLIT origin will vary based on its path over time, the two directions may disagree on the origin of the air plume. In addition, since the wind direction is averaged over the entire time period, fluctuations in meteorological conditions over time may skew the apparent origin wind direction from the 'true' arrival direction of the air plume as indicated by HYSPLIT.

The average carbon monoxide mixing ratio is included for each high pollution event. Carbon monoxide is a byproduct of hydrocarbon combustion, and thus, is an effective tracer gas for vehicular emissions. This metric is used to approximate the relative contribution of very-near SO_2 emissions to the total detected SO_2. The average CO from August 12th to November 25th, 2021, (the p-SO_4^{-2} measurement period) was 0.21 ppm. The average CO from August 12th, 2021, to October 18th, 2022, (the SO_2 measurement period) was also 0.21 ppm.

The summarized statistics for each HYSPLIT sector will be tabulated below (see **Table 14**), including the average SO_2, p-SO_4^{-2}, SO_x, and X_{pSO4} for the North, South, and West sectors, calculated from **Table 13**. Standard error of the mean (SEM) and 95% confidence intervals are also included. Note that there were no high pollution p-SO_4^{-2} events originating from the east, and thus, it will be excluded from this analysis. The North and West sectors are only represented by 1 event for p-SO_4^{-2} and are therefore the same as in **Table 13** (but are included here for comparison). Standard error is calculated from the average of the high pollution events for the South sector; since there is only one event each, the standard error is calculated by Igor for the North and West events. There is not enough data from the North and West sectors to perform meaningful statistical analysis across sectors.

Table 13. Summarized p-SO_4^{-2} high pollution event times and concentrations, and their corresponding mean SO_2, SO_x, calculated X_{pSO4}, HYSPLIT sector, wind direction, and mean CO.

Event Number	Timestamp (Local)	SO_2 ($\mu g/m^3$)	p-SO_4^{-2} ($\mu g/m^3$)	SO_x ($\mu g/m^3$)	X_{pSO4}	Sector	Wind Direction (°)	CO (ppm)
1	8/12 13:00 – 8/13 04:00	1.6	4.7	6.3	0.75	South	230	0.21
2	8/13 6:00 – 18:00	1.0	1.6	2.6	0.62	West	240	0.19
3	8/20 00:00 – 05:00	0.39	1.5	1.9	0.79	North	330	0.20
4	11/17 17:00 – 11/18 06:00	1.3	1.7	3.0	0.57	South	230	0.20
5	11/22 00:00	0.81	1.5	2.3	0.65	South	240	0.17
6	11/24 09:00 – 10:00	5.4	1.5	6.9	0.22	South	195	0.36

Table 14. Sector analysis for each NOAA HYSPLIT origin direction category of high pollutant emission events, from August 12th to November 24th, 2021. Units are μg/m^3, excepting X_{pSO4}.

Parameter	North	South	West	Total
Mean SO_2 ($\bar{x}$)	0.39	2.3	1.0	1.8
Standard Error (±)	0.0008	1.1	0.002	0.75
95% CI (± $\bar{x}$)	0.002	2.1	0.004	1.5
Mean p-SO_4^{-2} ($\bar{x}$)	1.5	2.4	1.6	2.1
Standard Error (±)	0.005	0.78	0.007	0.52
95% CI (± $\bar{x}$)	0.01	1.5	0.01	1.0
Mean SO_x ($\bar{x}$)	1.9	4.7	2.6	3.8
Standard Error (±)	0.005	1.2	0.007	0.89
95% CI (± $\bar{x}$)	0.01	2.3	0.01	1.7
X_{pSO4} ($\bar{x}$)	0.79	0.55	0.62	0.60
Standard Error (±)	0.004	0.12	0.005	0.08
95% CI (± $\bar{x}$)	0.009	0.23	0.01	0.16
Event Count	1	4	1	6

For SO_2, each high pollution event is again plotted on Google Earth via NOAA HYSPLIT (see **Figure 33**). Given the high amount of data collected by the 43i relative to the AMS, we constrain the high pollution event analysis to any peak above 5 ppb. Since the mean of the data is 0.37 and the standard deviation of the data is 0.82, we can see that 5 ppb is greater than 5σ above the mean and represents only the most extreme outliers. All of the high pollution SO_2 events are summarized in **Table 15**. Every SO_2 mean value presented is an average of the corresponding time, with the HYSPLIT trajectory set at the middle of the time range.

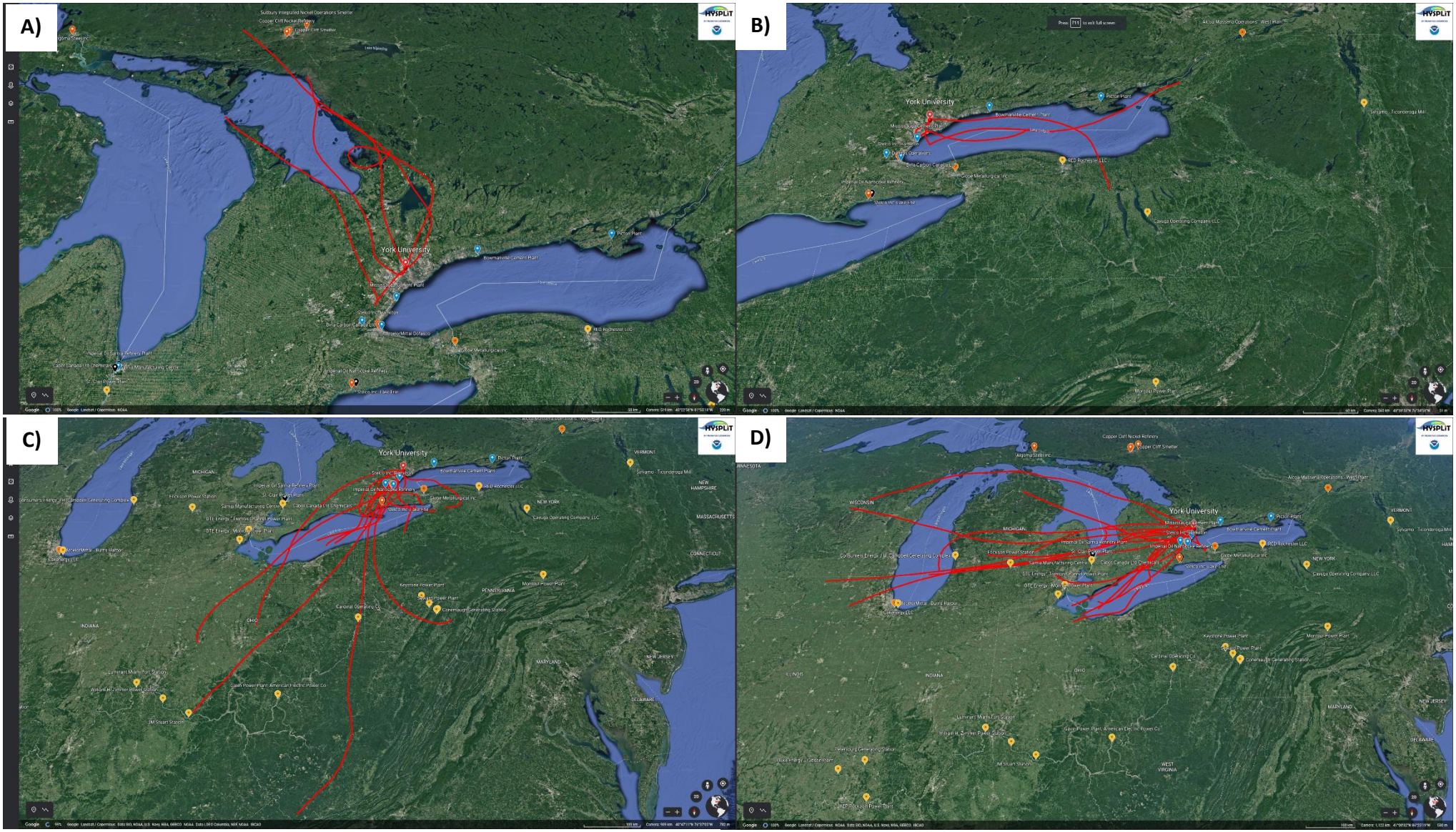

Figure 33. HYSPLIT 24-hour back trajectories (in red) for all 39 SO_2 high pollution events plotted on Google Earth. Each map contains the trajectories from one HYSPLIT sector, where A) is North, B) is East, C) is South, and D) is West. Date labels have been omitted for visual clarity due to the high number of trajectories. Refer to **Figures 32 and 33** for a better view of SO_2 point sources depicted here.

Table 15. Summarized SO_2 event times, means, HYSPLIT sectors, wind direction, and mean CO. Missing data denoted with "-".

Event Number	Timestamp	SO_2 (ppb)	Sector	Wind Direction (°)	CO (ppm)
1	8/12/2021 19:00 - 20:00	5.6	West	265	0.18
2	8/24/2021 15:00 - 16:00	5.2	West	180	-
3	8/25/2021 12:00 - 13:00	5.2	West	170	0.30
4	9/04/2021 11:00 – 12:00	5.0	North	200	0.24
5	9/07/2021 10:00 – 11:00	8.4	West	185	0.20
6	9/26/2021 23:00 – 24:00	6.6	West	215	0.28
7	10/14/2021 10:00 – 11:00	6.5	West	170	-
8	10/14/2021 15:00 – 16:00	5.9	South	170	-
9	11/06/2021 11:00 – 12:00	5.3	South	220	0.27
10	11/06/2021 19:00 – 20:00	5.7	South	190	0.24
11	11/24/2021 09:00 – 10:00	5.9	West	200	0.37
12	12/16/2021 02:00 – 03:00	6.6	South	185	0.21
13	12/21/2021 06:00 – 07:00	7.6	West	345	0.18
14	4/12/2022 23:00 – 24:00	5.5	West	330	0.19
15	4/25/2022 08:00 - 11:00	7.2	East	170	0.22
16	5/03/2022 08:00 – 09:00	8.0	West	155	0.27
17	5/06/2022 06:00 – 07:00	9.9	North	50	0.25
18	6/14/2022 08:00 - 10:00	5.9	North	75	0.12
19	6/16/2022 05:00 - 09:00	9.1	West	180	0.21
20	6/20/2022 11:00 – 14:00	7.6	North	180	0.20
21	6/21/2022 03:00 – 06:00	10	West	150	0.16
22	6/21/2022 11:00 – 14:00	7.1	South	170	0.20
23	6/22/2022 03:00 – 04:00	13	West	190	0.31
24	6/25/2022 01:00 – 05:00	7.2	West	210	0.17

Table 15. (Continued)

Event Number	Timestamp	SO_2 (ppb)	Sector	Wind Direction (°)	CO (ppm)
25	6/26/2022 08:00 – 15:00	6.8	South	175	0.21
26	6/26/2022 21:00 – 23:00	7.7	West	255	0.15
27	6/30/2022 23:00 – 7/01/2022 03:00	11	South	195	0.22
28	7/01/2022 14:00	8.7	South	190	-
29	7/11/2022 00:00 – 02:00	8.4	South	235	-
30	7/20/2022 18:00 – 19:00	5.2	South	185	0.16
31	7/31/2022 12:00 – 13:00	6.8	West	170	0.15
32	8/06/2022 09:00 – 11:00	6.1	East	215	0.23
33	8/14/2022 23:00 – 24:00	8.2	East	55	-
34	9/09/2022 10:00 – 11:00	6.0	South	160	0.27
35	9/10/2022 10:00 – 11:00	6.1	South	185	0.21
36	9/17/2022 23:00 – 24:00	6.4	South	195	0.22
37	9/24/2022 23:00 – 24:00	6.1	South	175	0.16
38	10/09/2022 10:00 – 11:00	6.0	West	280	0.15
39	10/10/2022 10:00 – 11:00	6.1	North	325	0.14

Similar to p-SO_4, we can summarize the SO_2 mean results by HYSPLIT sector to determine the relative contribution of each direction of pollutant origin to total SO_2 high pollution events in Ontario. The summarized statistics for each HYSPLIT sector will be tabulated below (see **Table 16**), including SO_2 and CO means (averaged over entire listed time periods), standard error of the means, and 95% confidence intervals for the North, South, and West sectors, calculated from **Table 15.**

Table 16. Sector analysis for each NOAA HYSPLIT origin direction category of high pollutant emission events, from August 12th, 2021, to October 10th, 2022. SO_2 units are in ppb, while CO units are in ppm. Note that 6 events are missing for CO.

Parameter	North	East	South	West	Total
SO_2 ($\bar{x}$)	6.9	7.2	6.8	7.3	7.1
Standard Error (±)	0.86	0.61	0.42	0.49	0.28
95% CI (± $\bar{x}$)	1.7	1.2	0.8	1.0	0.55
CO ($\bar{x}$)	0.24	0.24	0.22	0.20	0.21
Standard Error (±)	0.02	0.06	0.02	0.01	0.01
95% CI (± $\bar{x}$)	0.12	0.05	0.03	0.03	0.02
Event Count	5	3	14	17	39

Since the collected SO_2 data time span is greater than a year, we can also examine the high pollution events from a seasonal perspective (see **Table 17**). From September 2021 to August 2022, we split the high pollution events into their 4 corresponding seasons. As before, the Autumn period will be from September to November 2021, the Winter period will be from December 2021 to February 2022, the Spring period will be from March to May 2022, and the Summer period will be from June to August 2022. Again, "SO_2" is an average of the entire time periods of high pollution SO_2.

ANOVA analysis revealed that there was no significant difference in high pollution event SO_2 or CO mean between any HYSPLIT origin sector, and no significant difference in high pollution event SO_2 mean between any season.

Table 17. Seasonal analysis for the high SO_2 pollutant emission events, from August 12th, 2021, to October 10th, 2022. SO_2 units are in ppb.

Parameter	Autumn	Winter	Spring	Summer
SO_2 ($\bar{x}$)	6.2	7.1	7.7	8.1
Standard Error (±)	0.37	0.50	0.91	0.50
95% CI (± $\bar{x}$)	0.73	0.98	1.8	0.98
North Event Count	1	0	1	2
East Event Count	0	0	1	2
South Event Count	3	1	0	6
West Event Count	4	1	2	6
Event Count	8	2	4	16

3.5 Sarnia Field Study Results

In this section, we present the results of the Sarnia field study. Before discussing our findings, it is important to establish the parameters of the mass balance equation used to determine the Sarnia emissions rate for SO_2. The constants and associated uncertainties used in the mass balance equation are summarized in **Table 18**. Note that wind measurements were performed at a height of roughly 2 meters; it is known that wind speed correlates with height, and thus, the measurements listed here likely underrepresent the actual wind speed at the boundary layer.[49] As a result, the mass-balance calculation performed here will likely be somewhat conservative. The background SO_2 values for each transect (defined as the mean SO_2 away from emission plumes) is listed in **Table 19.** The boundary layer height, as previously established, is estimated by the National Centers for Environmental Protection North American Regional Reanalysis Product (NCEP NAARP) model as well as Windsor ceilometer data from the ECCC MOOSE (Michigan – Ozone Ontario Study Experiment) campaign. For July 21st, 2022, the NCEP NAARP model estimates the boundary layer height as 1750 ± 1000 m, while the average ceilometer-derived height is 578 ± 58 m. For July 22nd, 2022, the model estimate is 1000 ± 500 m, while the ceilometer-derived height is 452 ± 30 m. Using **Equation 13**, we can derive a weighted average of the model and ceilometer boundary layer height estimates for each day (see **Table 18**).

For the first day, the SO_2 background was given as an average of the measured background for each transect. For the second day, meteorological conditions were inconsistent, and so the variation in the measured SO_2 background was high. As such, each day 2 transect will use its own measured background value.

Table 18. Summary of constants for the mass balance equation for Days 1 and 2.

	Day	
Constants	**July 21st, 2022**	**July 22nd, 2022**
Wind Speed (m/s)	4.3 ± 0.2	3.1 ± 0.25
WD (°)	284 ± 1	269 ± 3
θ (°)	-12.40 ± 1	2.13 ± 3
Pressure (Pa)	99,000 ± 10	99,040 ±
Temperature (K)	304.3 ± 0.3	302.7 ± 0.6
Boundary Layer Height (m)	750 ± 180	520 ± 94

Table 19. Summary of measured background SO_2 means for each transect.

July 21st, 2022		**July 22nd, 2022**	
Transect	**Background (ppb)**	**Transect**	**Background (ppb)**
0	0.6	0	0.47
1	0.64	1	0.41
2	0.51	2	0.20
3	0.65	3	0.16
4	0.74	4	0.10
5	0.5		
Average	0.49	**Average**	0.27

The mass balance equation was applied to collected SO_2 data across multiple transects. On July 21st, 2022, a total of 6 transects were driven, starting at Transect 0 (T0) and ending at Transect 5 (T5) (see **Figure 34**). On July 22nd, 2022, a total of 5 transects were driven, starting at Transect 0 (T0) and ending at Transect 4 (T4) (see **Figure 35**). Note that 'T0' on July 22nd is not a true Transect, as it is upwind of the sources. SO_2 data for every transect is plotted against distance to illustrate the magnitude and relative location of each pollutant plume (see **Figures 36 and 37**). For each of these transects, the SO_2 data was integrated vertically (to the boundary

layer height) and horizontally (across the length of the transect) and multiplied by a factor of the meteorological constants as shown in **Equation 12** (see **Table 20**).

To visualize the relationship between plume downwind distance and calculated integral sum, we plot each transects' summed integral for each day (see **Figure 38**). The average of the mass balance equation results for the quantitative transects is an estimate of the Sarnia emissions rate. Using a conservative 15 minutes for the mean mixing time (multiplied by 3 for a total of 45 minutes), and the wind speed of each day (see **Table 18**), we calculate the minimum distance to classify a transect as quantitative as 12 km for July 21st, and 8.4 km for July 22nd. Therefore, for July 21st, the quantitative transects are 3, 4, and 5, and for July 22nd, the quantitative transects are 3 and 4.

Table 20. Mass balance equation results in tonnes/hr for each transect driven in Sarnia, Ontario, from July 21st, 2022, to July 22nd, 2022, and the distance from the source.

	July 21st, 2022		**July 22nd, 2022**	
Transect	**Mass Balance Result ± SEM**	**Distance (km)**	**Mass Balance Result ± SEM**	**Distance (km)**
0	0.11 ± 0.03	1	0.09 ± 0.02	-0.2
1	0.74 ± 0.18	3	1.31 ± 0.29	5
2	0.30 ± 0.07	5	0.32 ± 0.07	7
3	0.14 ± 0.03	15	0.15 ± 0.03	12
4	0.14 ± 0.04	20	0.22 ± 0.05	20
5	0.27 ± 0.07	30		

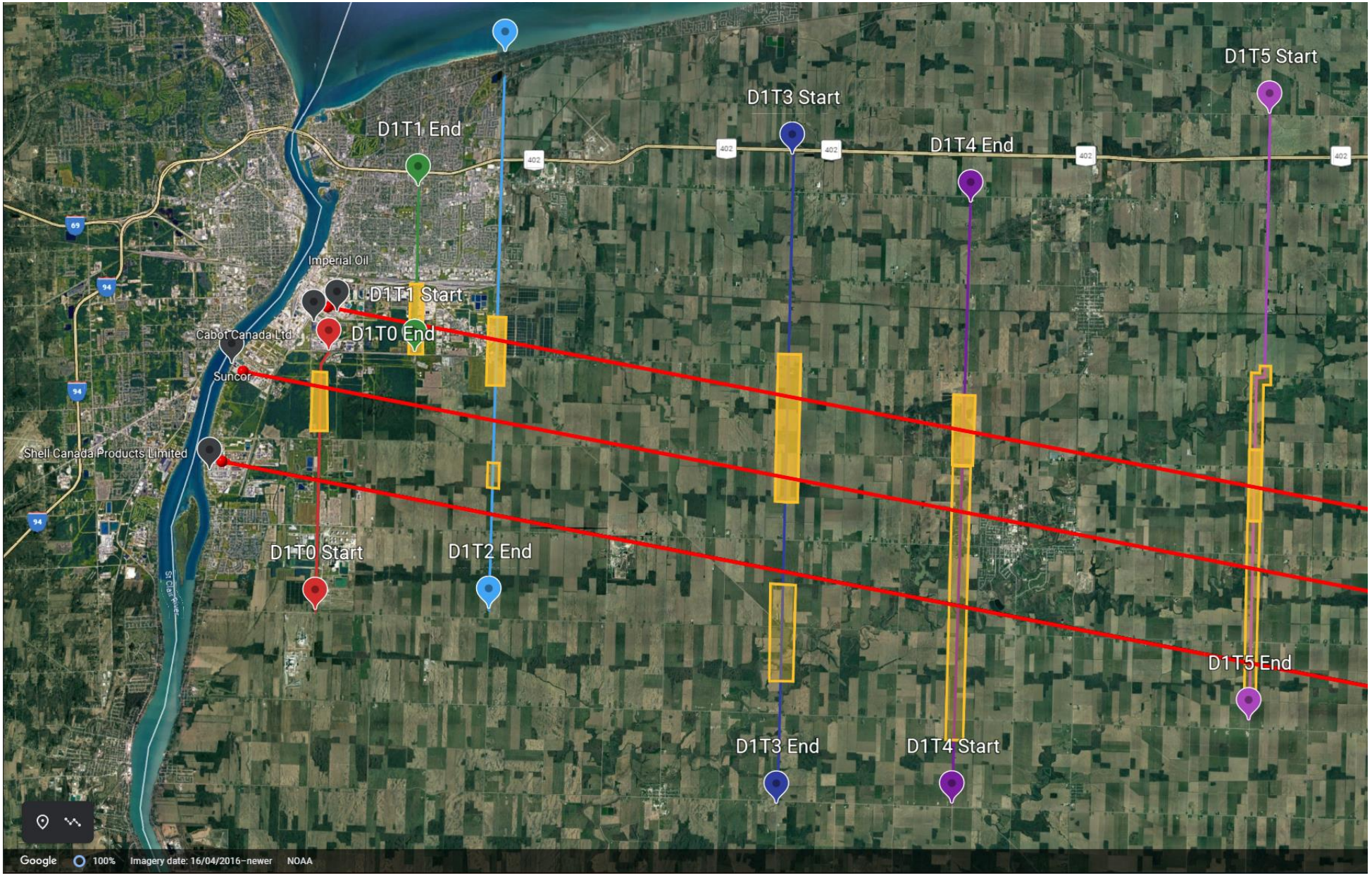

Figure 34. Transects driven on July 21st, 2022, plotted on Google Earth. HYSPLIT trajectories are overlaid on the map from east to west in red originating from the point sources listed (note that Imperial Oil and Cabot Canada Ltd. are too close to be distinguished and are represented by the same trajectory). Periods of high SO_2 elevation are abstractly highlighted; the highest peak of SO_2 is highlighted in opaque yellow, while any periods of lower, secondary elevation are highlighted in transparent yellow.

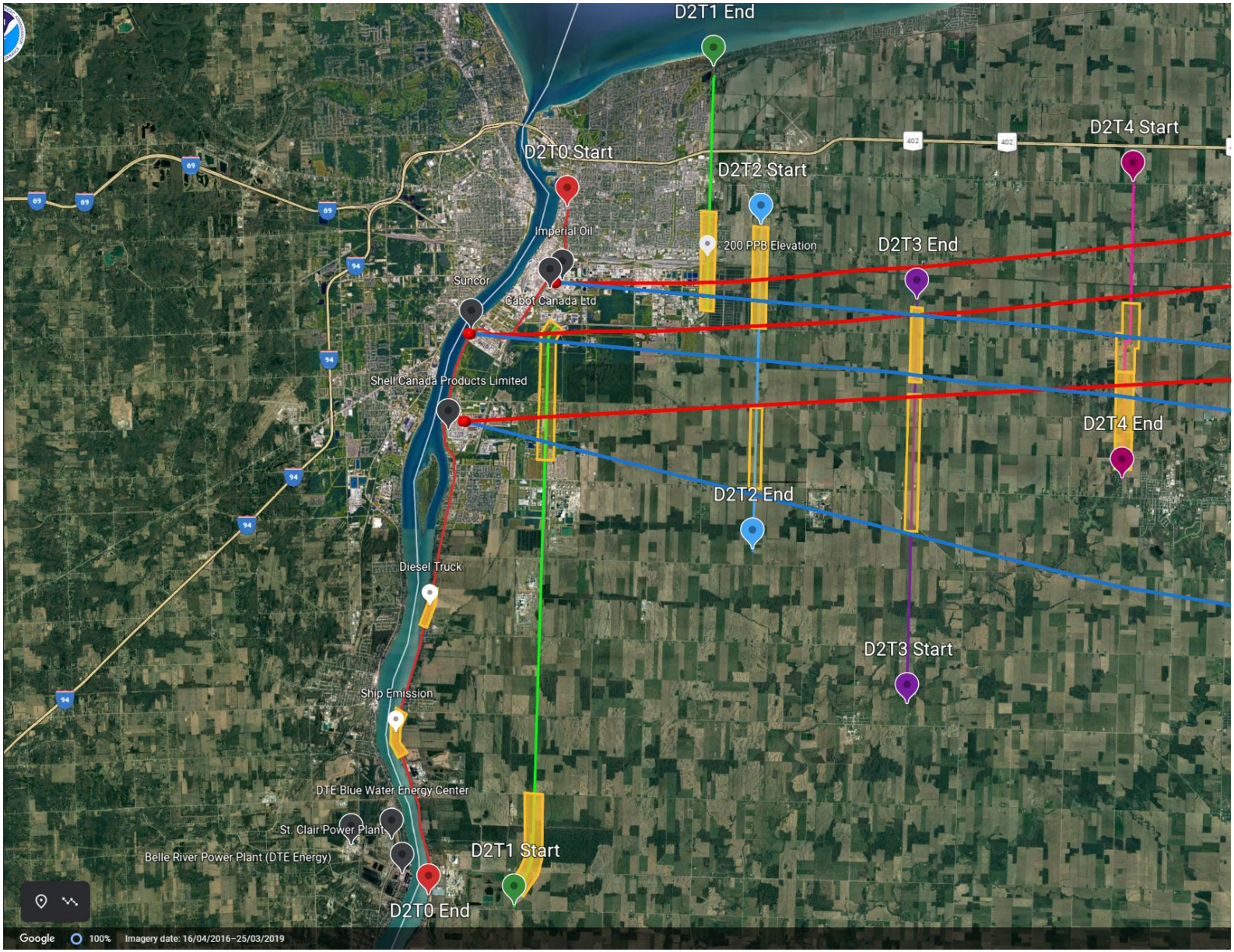

Figure 35. Transects driven on July 22nd, 2022, plotted on Google Earth. HYSPLIT trajectories are overlaid on the map from east to west in red and blue. Note that the meteorology for July 22nd shifted significantly through the day, and so 2 HYSPLIT trajectories are displayed here. The first one (red) is based on the 9 AM meteorology dataset, while the second one (blue) is based on the 12 PM meteorology dataset. White markers have been added to denote special events.

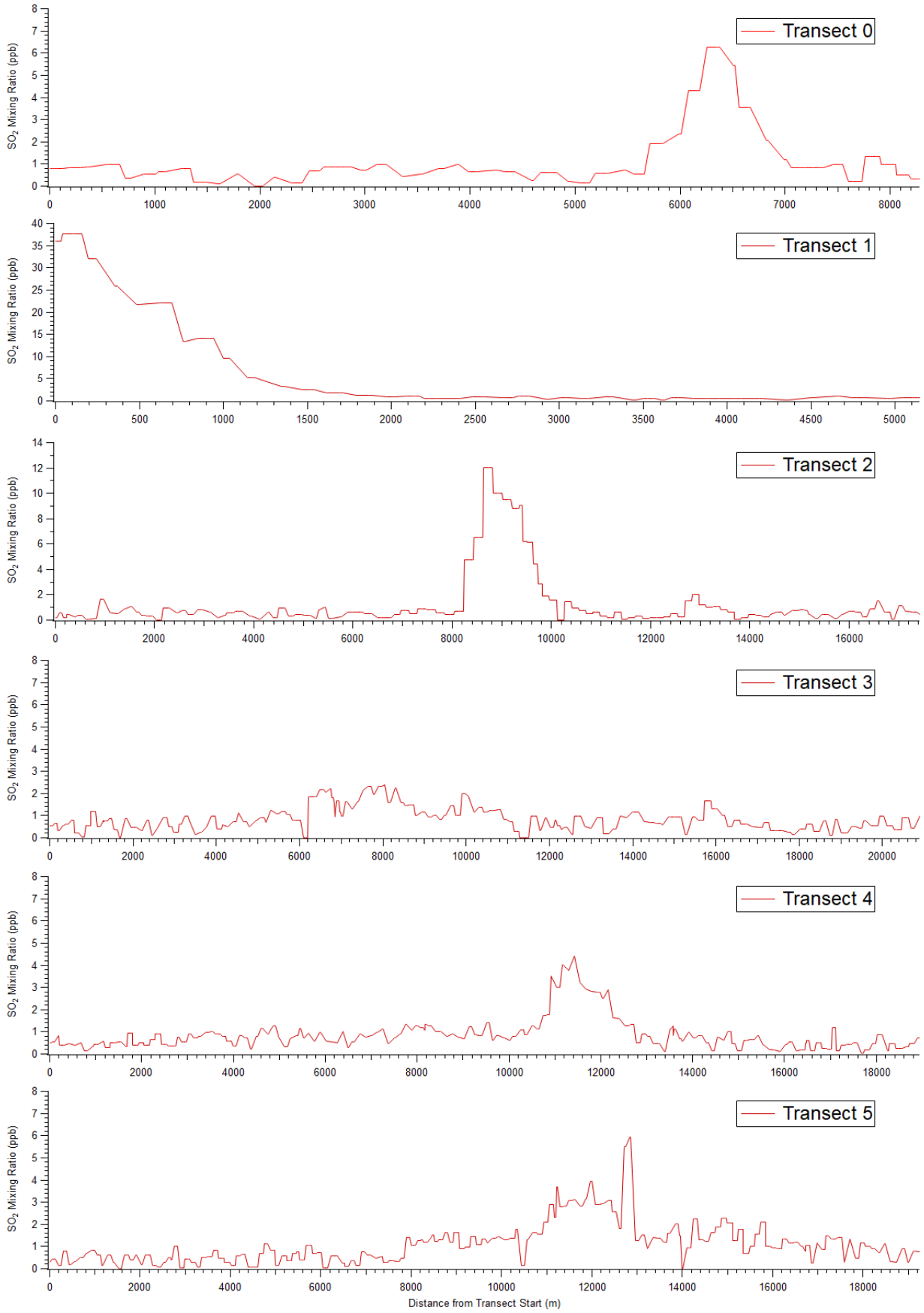

Figure 36. SO_2 mixing ratio data versus driven distance for each transect on July 21st, 2022.

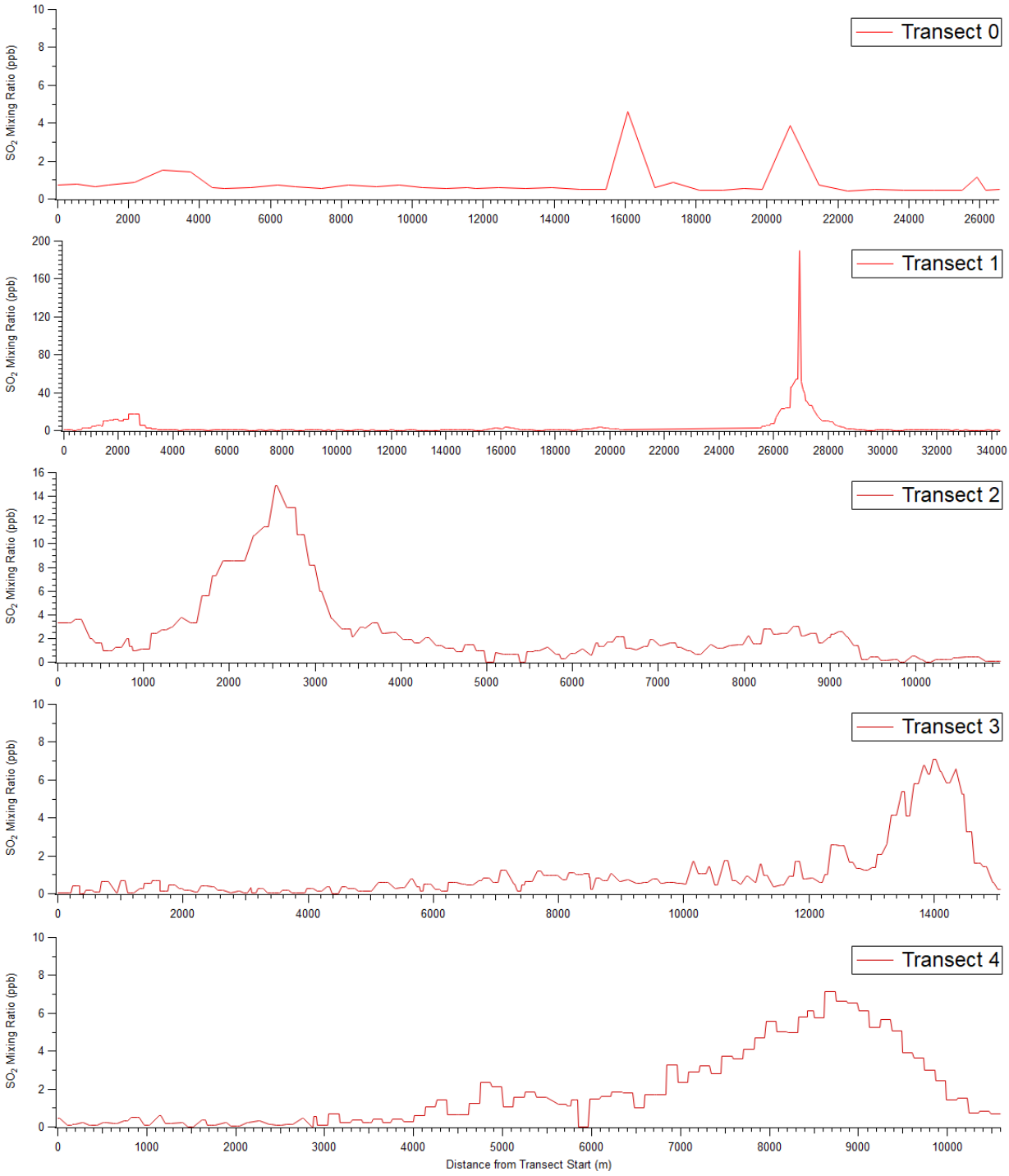

Figure 37. SO_2 mixing ratio data versus driven distance for each transect on July 22nd, 2022.

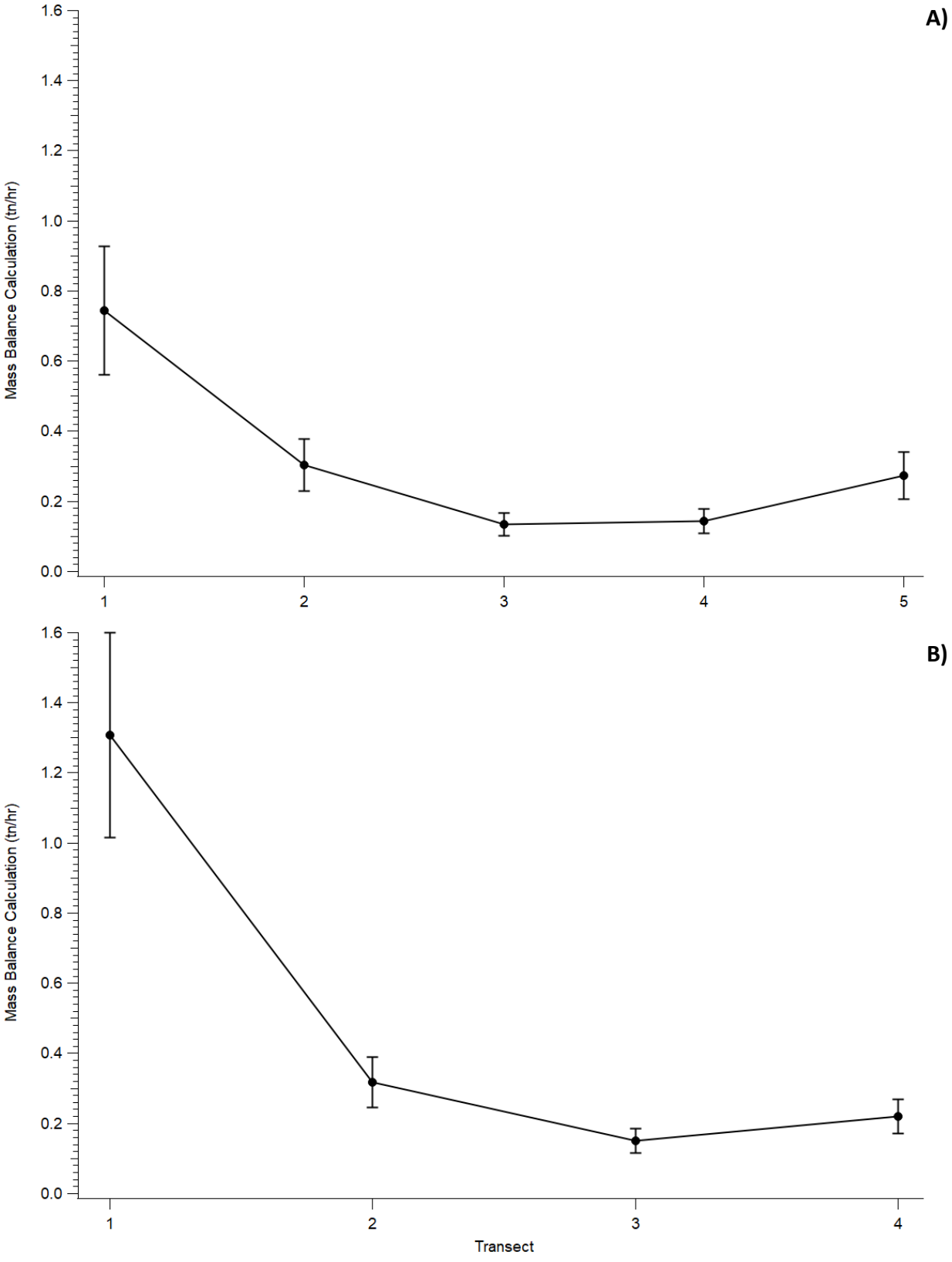

Figure 38. SO_2 mass-balance calculations in Sarnia, Ontario for each transect on A) July 21st, 2022, and B) July 22nd, 2022. Y-error bars are equal to the propagated error of each transects' mass balance calculation.

The average of the quantitative transects together, across both days, represents our estimate of the SO_2 emissions rate of Sarnia, which is equal to 0.18 tn/hr (95% CI [0.14, 0.22]), or roughly 4300 kg/day. Across both days, the standard deviation of the 5 quantitative transects is $\sigma = 0.052$. It is important to emphasize that this calculated emission rate cannot be used to extrapolate across an entire year to estimate the total emissions of SO_2 from Sarnia in 2022, as it only represents a small, two-day period of emissions. We can, however, take the emissions inventory for an entire year, and approximate its hourly emission rate to compare to the results of this field study.

The NPRI emissions inventory for Sarnia from 2002 – 2021 will be plotted against time to visualize the trend over the years (see **Figure 39**).[12] Emissions estimates from the inventory are based on 4 facilities: Imperial Oil, Cabot Chemicals Ltd., Suncor Energy, and Shell Canada. Note that Shell Canada is technically based in the town of Corunna, Ontario, but will be approximated as part of the general Sarnia region as it is captured by our transects. The nearby St. Clair Power Plant in Michigan (see **Figure 35**) could theoretically have influence on the approximation of Sarnia's SO_2 emissions, but, based on the wind direction for both days, has been excluded from consideration for this study.

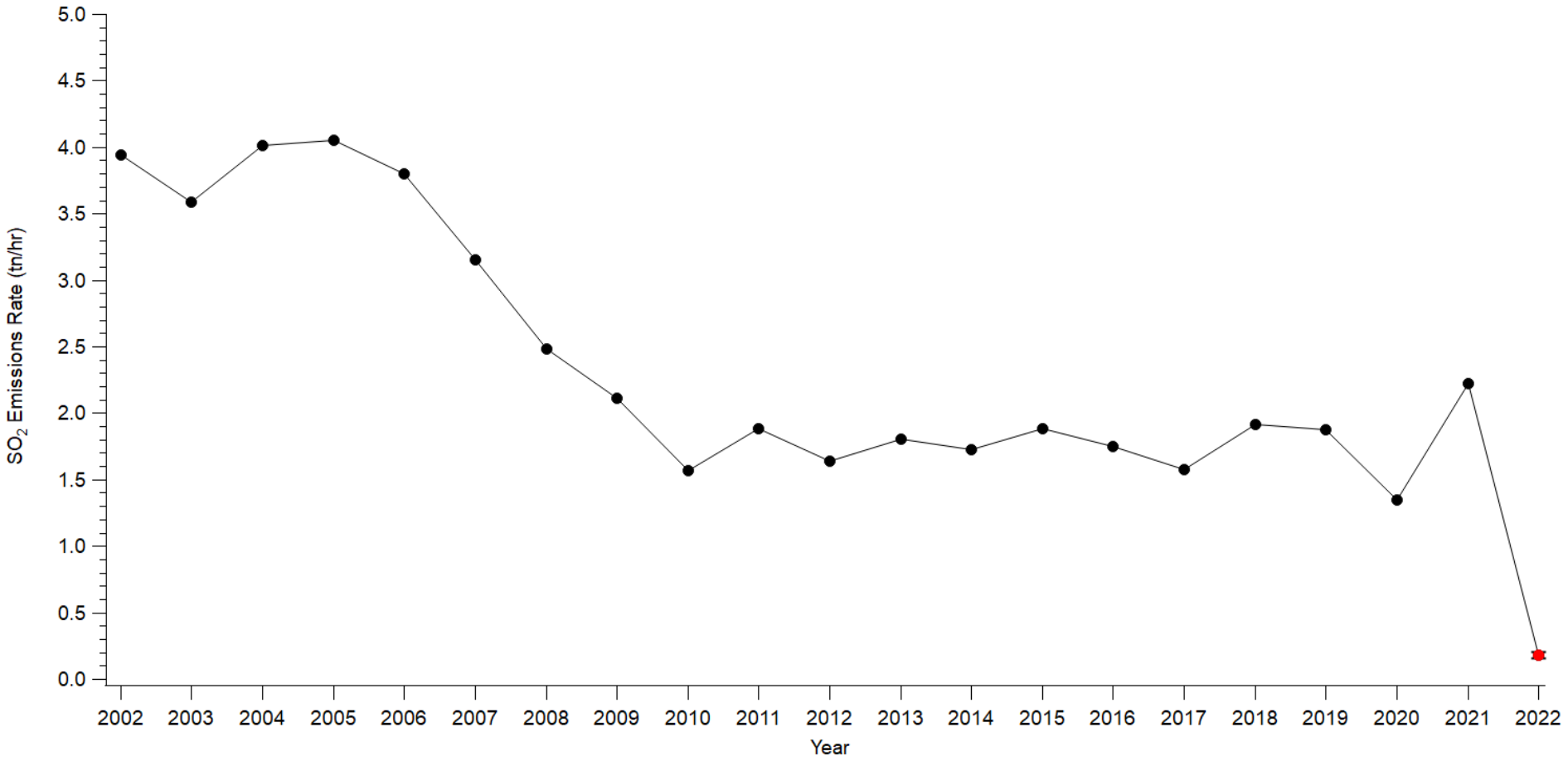

Figure 39. Estimated hourly average SO_2 emissions rate for the Sarnia region based on the 2002 to 2021 NPRI inventory. Included for comparison in red is the mass-balance derived hourly average SO_2 emissions rate from the July 21st to July 22nd field study. Y-error bars have been included for the 2022 data point equal to the propagated uncertainty on the mass balance equation but may be too small to see.

Chapter 4 - Discussion

4.1 Trends in Historic Data

One important delineation we need to make is the distinction between a statistically significant difference and a functionally significant difference. In **Chapter 3,** the results and plots of the data were provided without analysis; in addition, the determination of statistical significance of each dimension of the data was included. Statistical significance is a mathematical determination that indicates there is a difference between multiple values that is likely unrelated to chance. However, a statistically significant difference does not necessarily indicate the presence of a short or long term trend. For example, the annual mean mixing ratio of SO_2 decreasing by 0.01 ppb from one year to the next may be statistically significant if there are enough data points to reduce the variance of both datasets. Realistically speaking, however, this minor decrease in SO_2 mixing ratio will not have any significant consequences with respect to health or environmental impact. Given that the Ontario AAQC (by the annual parameter) is 4 ppb, a change in mixing ratio by a fraction of a single ppb will likely not have an impact on the overall air quality in Ontario. With this in mind, a key focus of this chapter will be distinguishing between statistical differences, and functionally significant differences, which will be evaluated by health and environmental metrics.

SO_2 is the first metric of interest for this historic data analysis. There are two important factors to consider: first, as previously established, the majority of atmospheric sulfur is emitted as SO_2 gas versus particle sulfate. Second, SO_2 oxidizes over time to p-SO_4^{-2}. This means that gas-phase SO_2 emissions are the most accurate metric of local sulfur emissions, as particle sulfate concentrations are likely to be influenced by long-range transport.

When analyzing the historic SO_2 data for the three sites, there were a few apparent trends. First, over the entire time period from 2003 to 2020, the annual mean SO_2 for Toronto decreased 93% from 2.9 ppb to 0.2 ppb and decreased 95% from 6.3 ppb to 0.3 ppb for Windsor (see **Table 5**). From 2007 to 2020, the annual mean SO2 for Simcoe decreased 55% from 1.8 to 0.8 ppb (see **Table 5**). All of these changes are statistically significant and show a

generally linear decrease over time (see **Figure 13**), following consistent environmental regulations targeting sulfur emissions over time.

We can also specifically examine the difference in mean SO_2 from the enforcement of the most recent set of new environmental regulations enacted in 2015. From 2015 to 2020, we see an 80% decrease in mean SO_2 for Toronto from 1.0 to 0.2 ppb, and an 84% in Windsor from 1.9 to 0.3 ppb. Simcoe, on the other hand, increased 100% from 0.4 to 0.8 ppb (see **Table 5**). The trend line for these three sites again generally follow a linear trend downwards, excepting Simcoe which trended upwards. (see **Figure 13**).

Max hourly SO_2 values also decreased; Toronto's max SO_2 hourly mixing ratio in 2003 was 107 ppb, while the highest value in 2020 was 10 ppb (see **Table 5**). In Windsor, the max value decreased from 110 to 20 ppb from 2003 to 2020 (see **Table 5**). In Simcoe (from 2007 to 2020), the value decreased from 43 to 5.8 ppb (see **Table 5**).

The differences over time for SO_2 at these 3 NAPS sites from their starting years to 2020 are both statistically (see **Chapter 3.1**) and functionally significant. From the expected dose-response relationship (1.4% all-cause deaths decrease per 1.0 $\mu g/m^3$), reductions in SO_2 over this time period represent a potential decrease in all-cause deaths of 0.41% for Toronto, 0.9% for Windsor, and 0.15% for Simcoe.[2] SO_2 in both urban areas (Toronto and Windsor) had decreased by over 90%, while rural SO_2 (Simcoe) had decreased by over half of its original value. SO_2 mixing ratios would have exceeded the current annual AAQC criteria (≥ 4 ppb) for Windsor in 2003. In addition, all 3 NAPS sites would have exceeded the currently hourly AAQC criteria (≥ 40 ppb) at some point during the year. In 2020, there were no hourly exceedances contained within the NAPS data sets, and the annual means are below half of the AARC for all 3 NAPS sites.

While the differences in SO_2 means are statistically significant from 2015 to 2020, it is unclear if these differences are functionally significant. Toronto and Windsor both demonstrated decreases of over 80%, likely as a direct consequence of recent environmental regulations enacted in 2015. For Windsor, the difference is clear – a decrease from roughly 2 ppb to 0.3 ppb, coupled with a downward trend, shows that SO_2 annual means were

significantly affected in heavily industrialized areas, especially in a region proximally affected by petroleum refining and chemical production facilities in Sarnia. For Toronto and Simcoe, although the trends seem significant from 2015 to 2020, in reality, the long-term trend since 2012 and 2009 (respectively, see **Figure 13**) for these regions show significant variation from 0 to 1 ppb. Within these margins, we would expect negligible differences in deleterious health and environmental effects directly. To contextualize this mixing ratio range, a study correlating air pollutant uptake from woodlands in the United Kingdom with improvements in health noted an SO_2 dose-response relationship, where every 3.8 ppb of SO_2 was associated with a 0.60% increase in all cause deaths.[2] From 0 to 1 ppb, there would be between 0-0.15% extra all-cause deaths at the most extreme bounds of variation (though in reality, year-over-year variations do not approach the extremes of this range). In addition, it is not likely to see a significant functional difference in $PM_{2.5}$ contribution via SO_2 oxidation within this variation, which another relevant metric for negative health effects.

We would expect Toronto's SO_2 emissions to be in between Windsor and Simcoe. From a historical perspective, we note that Toronto has been influenced by sulfur sources in the Greater Toronto Area (GTA), most notably coal-fired power generation. As we analyze the historical data set through earlier years, leading to more recent years, and remembering important sulfur-limiting regulations since the 1980s (especially with regards to sulfur generation from coal-fired power plants), we would expect that the amount of SO2 emissions in Toronto would decrease.[19] However, Toronto is still an urban area influenced by industry and traffic emissions, and so we expect a modest amount of SO_2 present in Toronto through the historical data set. We would also expect that Simcoe would have the lowest amount of SO_2 emissions. Since Simcoe is a more rural area, we would not expect significant local emissions of SO_2 from either industry or traffic. Any sulfur present in Simcoe is likely to be influenced by transport from the surrounding areas. Finally, we would expect Windsor to have the highest mixing ratio of SO2 in all three of the chosen sites. Windsor is a highly industrialized city as well as having close proximity to industry across the border in Detroit, Michigan, in addition to its proximity to other local industrialized Canadian cities, such as Sarnia, Ontario.

Most importantly, it seems that the difference between the three NAPS sites is not relevant now as it was in the past. In 2007, the difference between Windsor (urban) and Simcoe (rural) was 5.2 to 1.8 ppb respectively, meaning that an industrialized region's SO_2 mixing ratios were nearly 3x as much as rural mixing ratios, which lines up with theoretical expectations. In 2020, the recent mean mixing ratios for all 3 sites are again consistently varying between 0 and 1 ppb, and don't appear to be functionally different.

Particle sulfate is the second metric of interest for this historical data analysis. We can examine the historical trends for p-SO_4^{-2} for all 3 NAPS sites, though it is important to note that the sampling rate for p-SO_4^{-2} was far lower than SO_2. Instead of hourly averaged data, p-SO_4^{-2} provided a data point every few days; in addition, there were significant gaps throughout the years in p-SO_4^{-2} data. Overall, the reduced amount of data points resulted in increased variation and uncertainty in the particle sulfate data relative to SO_2. As a result, not every comparison made had statistical significance. One clear conclusion to draw from this data is the difference in mean p-SO_4^{-2} concentrations from the start of our analysis period to 2019.

For Toronto from 2003 to 2019, annual mean particle sulfate concentrations decreased from 3.2 to 0.9 μg/m^3, a reduction of 72%, with an annual max decrease of 27 to 3 μg/m^3 (see **Table 6**). For Windsor from 2004 to 2019, annual mean particle sulfate concentrations decreased from 4.0 to 1.1 μg/m^3, a reduction of 73%, with an annual max decrease of 14 to 2.5 μg/m^3 (see **Table 6**). For Simcoe from 2007 to 2019, annual mean particle sulfate concentrations decreased from 2.6 to 1.0 μg/m^3, a reduction of 62%, with an annual max decrease of 17 to 2.6 μg/m^3 (see **Table 6**).

From the beginning of the dataset there are some important conclusions to note. As expected, in 2007 (the earliest year common to all sites, see **Table 6**), Windsor had the highest p-SO_4^{-2} concentrations at 3.7 μg/m^3, owing to its close proximity to Sarnia and Detroit sulfur emissions sources, as well as its position on the southwesterly air transport corridor from the Ohio River Valley. Simcoe had the lowest p-SO_4^{-2} concentration at 2.6 μg/m^3, due to its rural, low-sulfur emissions profile. Toronto had the median p-SO_4^{-2} concentration of all three sites at 2.7 μg/m^3, likely due to its proximity to urban industrial emissions, but relative distance from

U.S. points sources when compared to Windsor. In the most recent year of data, 2019, the p-SO_4^{-2} mean concentrations for all 3 sites are nearly indistinguishable, with Windsor at 1.1 μg/m^3, Simcoe at 1.0 μg/m^3, and Toronto at 0.9 μg/m^3, suggesting that location urbanization is now possibly a relatively unimportant factor for p-SO_4^{-2}.

By the current AAQC standards, hourly $PM_{2.5}$ should not exceed 27 μg/m^3, and annual AAQC should not exceed 8.8 μg/m^3.[11] Given that roughly 25% of $PM_{2.5}$ is composed of sulfate, we can see that the period before 2015 shows annual and hourly $PM_{2..5}$ concentration exceedances for all 3 NAPS sites (where $PM_{2.5} \approx 4*$p-SO_4^{-2}), and that the period after 2015 shows no AAQC exceedances in this dataset (see **Figure 14**). Another important metric for the significance of $PM_{2.5}$ reductions comes from a Harvard study of 6 U.S. cities from 1979 to 2009, which evaluated the contribution of decreased $PM_{2.5}$ concentrations (specifically p-SO_4^{-2}) to reductions in annual deaths. It was shown that there was a linear correlation between decreasing $PM_{2.5}$ concentrations and annual deaths, and that particle sulfate had an equivalent toxicity to the average $PM_{2.5}$ particle component.[50] Lepeule et al. demonstrate that every 1 μg/m^3 decrease in average $PM_{2.5}$ concentration (presuming that the reduction is in toxic particles, such as sulfate) is associated with an approximately 1.4% reduction in annual all-cause deaths.[50] Applying this to our NAPS sites over the entire data set, we can then expect a 3.2% decrease in annual deaths for Toronto as a direct result of reduced p-SO_4^{-2} concentrations alone (-2.3 μg/m^3 from 2003 to 2019, see **Table 6**) , a 4.1% decrease for Windsor (-2.9 μg/m^3 from 2004 to 2019, see **Table 6**), and a 2.2% decrease for Simcoe (-1.6 μg/m^3 from 2007 to 2019, see **Table 6**).

The third metric of interest for this historical data analysis is SO_x. Related to SO_x is the p-SO_4^{-2}/SO_x ratio (X_{pSO4}). From 2003 to 2019, the annual Toronto SO_x mean decreased 85%, from 11 to 1.6 μg/m^3, while there was an 86% X_{pSO4} increase of 0.29 to 0.54 (see **Table 7**). For Windsor from 2004 to 2019, annual SO_x mean decreased 79%, from 16 to 3.3 μg/m^3, while there was a 38% X_{pSO4} increase of 0.24 to 0.33 (see **Table 7**). For Simcoe from 2007 to 2019, annual SO_x mean decreased 77%, from 7.5 to 1.7 μg/m^3, while there was a 69% X_{pSO4} increase of 0.29 to 0.54 (see **Table 7**). There is a general upwards trend for X_{pSO4} for all three sites (see **Figure 15**), though the trend for Windsor is not statistically significant. We expect that the

decrease in SO_x is largely correlated with the decrease in SO_2, given the correlation factor of r = 0.99, implying a nearly perfectly linear relationship. With this strength of correlation, and the weak statistical relationship between time and p-SO_4^{-2}, we can conclude that the decrease in SO_x over time is largely driven by a decrease in SO_2 associated with increased environmental regulations since the 1980s. Since atmospheric sulfur is dominated by SO_2 versus particle sulfate, it follows that SO_x trends match the general SO_2 trends.

We expected X_{pSO4} to be inversely proportional to the amount of locally emitted gas phase SO_2. Since the majority of SO_x is typically made-up of SO_2 emissions, with p-SO_4^{-2} being a byproduct of SO_2 oxidation (with only minor direct releases to the atmosphere as sulfuric acid and a fractional amount of $PM_{2.5}$), it follows that this ratio will be established by the relative impacts of local SO_2 emissions weighed against long range transport of p-SO_4^{-2}.

It was predicted that X_{pSO4} for Toronto would be in between Windsor and Simcoe, due to its moderate local SO_2 emissions and its influence from long range transport of emissions from both Sarnia, Windsor, Detroit, the Ohio River valley, and Sudbury. For Simcoe, we expected the highest X_{pSO4}, as Simcoe is a rural area with low local SO_2 emission, positioned in the southwesterly long-range air transport corridor from the Ohio River valley, which would contribute to high p-SO_4^{-2} concentrations. Finally, we expect Windsor to have the lowest X_{pSO4} of all the three sites, owing to its high local emissions of SO_2 and close proximity to point sources located in Detroit, Michigan. At the beginning of the data set, these expectations were matched by our data analysis, though Toronto and Simcoe were indistinguishable in 2019 (but both were still higher than Windsor, as expected). This suggests that there is a general trend of increasing X_{pSO4} following regulated SO_2 emissions, likely due to an increased relative significance of long-range transport of p-SO_4^{-2}, and that the importance of urban sources of sulfur (such as vehicles emissions form fossil fuel combustion, and other sources) has diminished. We speculate that, under the assumption that meteorological conditions have not changed significantly from 2003 to 2019, the rate of decrease for Ontario's sulfur emissions is greater than that of the surrounding US states, and that the sulfate detected at the monitoring stations is now more proportionally originating from US point sources.

There is a historic trend of seasonal significance for Toronto's annual SO_2 mixing ratio means, as seen in **Figure 16**. In the years before 2015, we typically saw the highest SO_2 mixing ratio annual means in the Winter season. This is explained, from an emissions perspective, by the reliance on coal-fired power plants for electricity in Ontario during this time period – we speculate that, as temperatures drop in the winter season, the importance of residential heating increases, resulting in an increased demand for power. As power usage increases, so does power plant output, which results in more coal-combustion-driven SO_2 emissions. This is combined with meteorological factors, as the colder weather results in temperature inversions with lower boundary layers, trapping pollutants below. This would increase the sampled SO_2 mixing ratios at the NAPS monitoring sites. Summer SO_2 means were historically the lowest pre-2015. While air conditioning usage would cause very high power consumption in the summer, the warmer temperatures likely elevated the boundary layer higher than any other season, reducing the detected SO_2 at the monitoring stations. After 2015, however, the seasonal differences become functionally negligible. Much like the overall SO_2 trends for Toronto, every seasonal mean varied between 0 and 1 ppb from 2016 onwards, with very little difference between individual seasons. In 2020, the differences between the winter and spring seasons are not statistically significant, indicating that any inter-seasonal gap in SO_2 mean mixing ratio is decreasing and is likely irrelevant to our current understanding of Ontario's sulfur trends.

Seasonal analysis was also performed for p-SO_4^{-2} in Toronto, though the only statistically significant conclusions were drawn in 2005, where the summer p-SO_4^{-2} means were higher than in the spring and winter (see **Figure 17**). This 2005 result is as expected – it has been established in the literature that particle sulfate formation is the highest in the summer.[16] For the other years, it is likely that, much like SO_2, seasonal differences are largely irrelevant in recent years.

When examining the differences between SO_2 in the daytime versus the nighttime, in the earliest years, we do note a clear increase in daytime SO_2 mean mixing ratios relative to the night (see **Figure 18**). For example, from 2003 to 2008, daytime SO_2 means were roughly 0.5-1 ppb higher than the nighttime. Much like the general trend in Toronto's SO_2, there was very little functional difference in daytime and nighttime SO_2 annual means from 2012 onwards, as

the means all varied from 0 – 1 ppb once again. We expect that the difference between the annual SO_2 means for the daytime and nighttime intervals is largely driven by anthropogenic activity. The daytime interval (8:00 AM - 8:00 PM) captures both the morning and evening periods of heavy commuter traffic. The location of the Toronto NAPS site, much like our sampling location at York University, is influenced by commuter traffic – there is a very close proximity to several major highways, including Ontario's Highway 401 (reportedly the busiest highway in the entire world, with an average daily traffic of over half a million vehicles a day).[51] There will also naturally be a relative increase in anthropogenic activities during the daytime hours, with an associated increase in power consumption and subsequent electricity generation-related SO_2 emissions, as seen by the Henschel et al. European cities' SO_2 study.[29]

One possible explanation for the overall reduction of SO_x in urbanized areas, as well as the decreased importance of daytime versus nighttime, is the reduction of sulfur content in gasoline and diesel fuel from 100s of ppm to less than 15ppm based on environmental regulation guidelines.[17] This is confirmed by examination of national SO_x inventories – across Canada in 2000, the estimated contribution of all transportation emissions to the total amount of emitted SO_x was 87,000 tonnes out of a total 910,000 tonnes (~9.6%).[52] In 2020, this proportion decreased sharply, and was responsible for 3,100 tonnes out of a total 190,000 tonnes (~1.6%).[52]

4.2 Conclusions from Current Sulfur and Particulate Data

We first evaluate the current SO_2 data measured at York University from August 12th, 2021, to October 18th, 2022. The measured mean SO_2 mixing ratio In Toronto is 0.37 ppb, with a maximum detected value of 27 ppb on June 16th, 2022, at 5:30 AM (see **Table 8 and Figure 20**). From the beginning of the historic dataset (2003) to our measurement period (2021-2022), the mean SO_2 mixing ratio in Toronto has decreased 87% from 2.9 to 0.37 ppb, and much like the 93% decrease from 2003 to 2020 (2.9 to 0.2 ppb), we interpret this as a functionally significant difference that is likely to have meaningful consequences in sulfate formation and human health effects. From our expected dose-response relationship, this potentially represents a 0.38% decrease in all-cause deaths.[2] From 2015 to 2022, mean SO_2 decreased 63% from 1.0 to

0.37 ppb, and from 2020 to 2022, mean SO_2 increased 85% from 0.2 to 0.37. While this increase from 2020 is statistically significant, in reality, it is not likely to have functionally significant consequences for air quality. As previously mentioned, Toronto SO_2 means have varied between 0 and 1 ppb since 2012, continuing a decade-long trend of mixing ratio stagnation. It is likely at this point we are seeing diminishing returns with the current set of environmental regulations. Note that comparisons between the historical dataset and the current dataset are not caveated by the fact that the NAPS site and the York University sampling locations are different.

A box plot of each month's SO_2 was displayed in **Figure 21**, and a month-over-month trend of SO_2 mean was displayed in **Figure 22**. As expected from previous results, we see that each month's mean SO_2 varied between 0 and 1 ppb, and there was very little correlation between time and SO_2 mixing ratio. Attempting to fit a linear trendline to the data showed an r^2 value of 0.05, indicating a correlation factor of r = 0.22, as well as very high variability unexplained by a linear regression model. One important conclusion apparent from the box plot was that June 2022 had an anomalously high 95th percentile range relative to other months, indicating a greater than expected amount of high pollution events. This will be investigated further in **Chapter 4.3**.

Seasonal and daytime/nighttime SO_2 trends were also investigated (see **Figures 23 and 24**). For the current time period, we found that the difference between each season's SO_2 mean was statistically significant, with the summer period SO_2 mean being the highest at 0.40 ppb, followed by the spring SO_2 mean at 0.37, the winter SO_2 mean at 0.36 ppb, and finally the autumn SO_2 mean being the lowest at 0.28. The seasonal means were all within 0.2 and 0.4 ppb, a range in which variation is not realistically likely to have any effects on health, the environment, or particle sulfate generation. Likewise, while the daytime and nighttime intervals showed a statistically significant difference, there was little functional difference in mean SO_2, as daytime (0.40 ppb) was only marginally higher than nighttime (0.32 ppb).

We next evaluate the current trends in particle sulfate as detected by the Aerodyne AMS from August 12th to August 25th, 2021. It is important to reemphasize that this short data

collection period does not necessarily represent the long-term trend of p-SO_4^{-2} concentrations in southern Ontario. The measured mean p-SO_4^{-2} concentration in Toronto is 0.60 μg/m^3, with a maximum detected value of 4.7 μg/m^3 on August 12th, 2021, at 5:20 PM. From the beginning of our historic dataset (2003) to our measurement period (August 2021), the mean p-SO_4^{-2} concentration in Toronto has decreased by 81% (a 2.6 μg/m^3 decrease), and from 2015, mean p-SO_4^{-2} concentration decreased by 60% (a 0.90 μg/m^3 decreases. From 2019, mean p-SO_4^{-2} decreased by a further 33% (a 0.30 μg/m^3 decrease). Referring again to Lepeule et al., we expect a 3.6% reduction in all-cause deaths from a 2003 to 2022 frame of reference, and a 1.3% reduction in deaths from 2015 to 2021, directly due to decreased p-SO_4^{-2} concentrations. From the end of the historical data set in 2019, we can expect a further 0.48% reduction in all-cause deaths based on our collected p-SO_4^{-2} dataset. Based on the trend of historic data, coupled with the collected data from this study, we can see that environmental regulations have worked to continually reduce particle sulfate concentrations in Toronto, though, in the most recent years, this trend has slowed as the rate of p-SO_4^{-2} reduction has decreased (see **Figure 14**).

SO_x was calculated from the AMS data as 1.6 μg/m^3. With the calculated SO_x mean, X_{pSO4} can be calculated as 0.38. Note that the timescales are different – mean SO_2 was calculated from the entire 15 months of data collected by the 43i, while mean p-SO_4^{-2} was calculated from the 3 months of data from the AMS and AIM-IC-MS. As such, mean SO_x is not fully representative of the entire time period of this study. When compared to 2019, Toronto SO_x is unchanged in the current time period, though X_{pSO4} has decreased, indicating that a greater proportion of total sulfur is made up of SO_2. Based on the historical data, there should be a continuing trend of increasing X_{pSO4} in Toronto that is not seen here. Theoretically, this likely implies a significant reduction in p-SO_4^{-2} and/or a significant increase in SO_2; in reality, however, the recent trends in the last few years show high SO_2 variability between 0 and 1 ppb, and a stagnation in the decrease of p-SO_4^{-2}. The strongest correlation factor for X_{pSO4} was with SO_2, where r = -0.76, and the weakest was with p-SO_4^{-2}, where r = -0.40, and so X_{pSO4} is more closely related to SO_2. Given the SO_2 variability, we expect significant volatility in the trend of year-over-year X_{pSO4}. The negative correlation between p-SO_4^{-2} and X_{pSO4} is unexpected;

logically, increasing p-SO_4^{-2} should increase X_{pSO4}, though the high variability in p-SO_4^{-2} could contribute to this.

Several additional species were detected by the AMS, including p-NO_3^-, p-NH_4^+, and p-organics, and were summed alongside p-SO_4^{-2} for a total approximation of $PM_{2.5}$ of 6.3 μg/m^3 (see **Table 10**). Of these species, the collective particle organics made up the majority of the average $PM_{2.5}$ concentration, at 4.9 μg/m^3, or 79% of total $PM_{2.5}$. The next highest proportion was p-SO_4^{-2}, previously shown as 0.60 μg/m^3, or 9.7%. This is followed by p-NH_4^+ at 0.55 μg/m^3, or 8.9%, and NO_3^- at 0.25 μg/m^3, or 4.0%. From our established literature values, based on Bell et al.'s analysis of the U.S. in 2007, we note a historical precedent where p-organics constitute 28% of total $PM_{2.5}$, p-SO_4^{-2} constitutes 26%, p-NO_3^- constitutes 12%, and p-NH_4^+ constitutes 11%, with total other particles constituting 24%.[16] We can see that, in our collected AMS data, the relative contribution of p-organics in 2021 was much higher than Bell's 2007 values, while both p-SO_4^{-2} and NO_3^- have decreased from these literature values. Finally, p-NH_4^+ has also slightly decreased compared to the literature value. Note that direct comparison is somewhat inaccurate, given that $PM_{2.5}$ is approximated as the sum of p-SO_4^{-2}, p-organics, p-NO_3^-, and p-NH_4^+ only.

Given the relatively small dataset we used for this analysis (roughly 2 weeks), any deviation from literature values can be reasonably explained as uncertainty. During this time period, the data was defined by 3 significant peaks (see **Figure 27**), which could skew the data based on the chemical composition of the air plumes that correspond to these peaks. For example, for the August 12th to 13th peak, there was a max value of 17 μg/m^3 and an average concentration value over 4 μg/m^3 for p-organics (compared to 24 μg/m^3 max and average concentration over 6 μg/m^3 for $PM_{2.5}$); we can theorize that, despite the fact that every component had a large peak during this time, this particular pollutant plume was dominated by particles with a large organic fraction, likely due to increased forest fire activity in Toronto during this time. More data would be needed to determine if the long-term proportional composition of $PM_{2.5}$ is consistent with these measured values (specifically, has the fraction of p-organics increased with a decreasing p-SO_4^{-2}, as suggested here), or if this single peak event has skewed our data. This constrained time period also does not account for seasonal

differences in particle composition, which has been well-established as a significant factor for variation in certain particulate species by Bell et al.[16]

Figures 25 and 29 show wind roses and pollution roses for SO_2 and p-SO_4^{-2} during their respective measurement periods. The SO_2 pollution rose was very similar to the wind direction versus frequency plot and shows the directions of influencing sources of SO_2. First, we see that the 255-270° and 165-180° sectors were the most notable, with the highest recorded SO_2 mixing ratios reaching above 25 ppb. Next, we see that the general southwest direction consistently had the highest mixing ratios compared to the other sectors. While there was a high frequency of northwest winds, this was not correlated with high SO_2 mixing ratios from the 270-15° range. The highest single point mixing ratio from the north sector was 11 ppb. Finally, there were a few high mixing ratio SO_2 points from the 75-90° range, with a single point maximum of 25 ppb. Like SO_2, the highest recorded p-SO_4^{-2} concentrations come from the southwest sector, evenly dispersed from the range of 180-270°. From our p-SO_4^{-2} pollution rose, we see that the majority of the detected p-SO_4^{-2} in the north sector is low concentration (≤ 2 μg/m^3).

It is likely that air plumes corresponding to a wind direction sector are either originating from or are highly influenced by our known sources. Thus, it is important to attribute these point sources to their respective sectors (see **Table 21**). We also provide a higher resolution image of our southern point sources to clearly differentiate them visually (see **Figure 40**). Again, these point sources are based on the 2020 SO_2 emissions inventory from the NPRI, listed in **Table 1**, and the 2017 NEI (see **Table 12**). Since SO_2 is a combustion byproduct of petroleum products, we also expect some minor contributions from major highways. In particular, there is a portion of Highway 401 southwest (210°) from York University that points in a straight line to our instruments, which notably overlaps with southwesterly long-range transport of sulfur.

Figure 40. Higher resolution Google Earth mapping of southern Ontario SO_2 point sources, from 195-240°. A marker has been placed at the Highway 401 section aligned with York University.

Table 21. Sector breakdown of SO_2 point sources, including surrounding major highways and broad U.S. sources. Sources organized in sector by relative distance from York University.

Sector	Sources
0-60°	Highway 407
75-90°	Bowmanville Cement Plant, Picton Plant
90-195°	New York, Pennsylvania
195-225°	Highway 401, Highway 403, Highway 407, Mississauga Cement Plant, Stelco Inc. Hamilton, Birla Carbon Canada Ltd., Arcelor Mittal Dofasco, Dundas Operations, Imperial Oil Nanticoke Refinery, Stelco Inc. Lake Erie, Ohio
225-240°	Highway 401, Michigan (Detroit), Ohio, Indiana
240-255°	Imperial Oil Sarnia Refinery Plant, Cabot Canada Ltd. Chemicals, Sarnia Manufacturing Plant, Michigan (Detroit), Indiana
255-300°	Michigan
300-330°	Algoma Steel Inc., Resolute Forest Products
330-360°	Cooper Cliff Nickel Refinery, Copper Cliff Smelter, Sudbury Integrated Nickel Operations Smelter

Based on these sources, we can see that the most significant contributors to SO_2 are, apparently, New York, Pennsylvania, and Michigan. In reality, we expect this to be slightly inaccurate, as the wind direction is only a rough approximation of origin sector (in the total meteorology data, there is an uncertainty of approximately 15-20° on each measurement, based on the provided standard deviation of the wind direction data). The most probable contributors are likely shifted over by a sector, making the most important contributors to Toronto's SO_2 are the Highway 401, Hamilton steel refineries, the Nanticoke petroleum refinery, the Sarnia petroleum refinery, and Cabot Canada Ltd. In addition, there is some moderate contribution from Sudbury's metal refineries and the Bowmanville cement factory.

We can see that the most significant contributors to p-SO_4^{-2} are likely to be similar to SO_2, given that both species are affected most strongly by transport from the southwest sector, with some smaller contribution from the northern sector. Additionally, we expect that distant sources are more important contributors, given that it takes time for SO_2 to oxidize to particle sulfate. U.S. Point sources are also more relevant for p-SO_4^{-2}, given their distance, and the most important sources almost entirely consist of coal-fired power plants **(see Table 12**). The relative rate of SO_2 oxidation to p-SO_4^{-2} is given as the lifetime (the time for a chemical species to reduce to 1/e of its initial value). For a simple estimate of p-SO_4^{-2} formation, we will ignore the rate of deposition of SO_2 for the lifetime calculation. The lifetime, τ, of SO_2 will be estimated as the rate of chemical conversion to p-SO_4^{-2} by the OH radical (assuming a typical 1.1 - 5 x 10^6 molecules/cm^3 for [•OH])[53] under dry conditions, where k = 6.0 x 10^{-13} cm^3 $molecule^{-1}$ s^{-1} at normal room pressure and temperature:

$$\tau_{SO_2} = \frac{1}{k_{SO_2 : \cdot OH} * [\cdot OH]} \quad (\boldsymbol{Eq.\ 19})$$

With our assumed OH radical concentration range, $\tau_{SO2} \approx 4 – 17$ days. After 1 lifetime, roughly 63% of SO_2 will be converted into p-SO_4^{-2}, giving an approximate conversion rate of 0.2 – 0.7% per hour within the first lifetime. Within 24 hours of transport, up to 17% of SO_2 could be converted by the dry pathway alone, and up to 34% within 48 hours, which could be significant enough to be detected by the AMS.

As previously mentioned, this is a dry conservative estimate of SO_2 lifetime. In reality, the majority of oxidation to p-SO_4^{-2} will occur through the ozone and peroxide aqueous pathway under high RH regimes. Since RH is highly variable throughout a day, it is difficult to estimate an SO_2 lifetime for the wet ozone-peroxide oxidation pathway. Some literature values report up to 10% conversion of SO_2 per hour under periods of high temperature and relative humidity.[54] Additionally, it is expected that the p-SO_4^{-2} formation rate would increase at night, where RH is higher, in association with the presence of more clouds and fog. Thus, p-SO_4^{-2} is largely produced from distant sources under high cloud and fog meteorology scenarios, with lesser contributions from local facility emissions. We do also expect some direct sulfate formation from SO_2 and vehicle exhaust, and so p-SO_4^{-2} concentrations are dependent on both distant sources and local vehicle emissions, such as from the surrounding highways.[55] Since sulfur content in fuels have decreased over the last few decades, it is possible that the contribution of highways will be minor.

Local chemical production facilities in the GTA and Hamilton metal refineries are most likely lesser sources of p-SO_4^{-2} in Toronto as detected at York University (these sources are typically 1-6 hours of air plume transport away, though this is highly dependent on wind speed, see **Figure 41**), except possibly for days with extremely high relative humidity or very low wind speeds. The highest concentration p-SO_4^{-2} plumes originate from the southwest; Sarnia and Michigan point sources may be far enough away for significant oxidation to occur, though it is more likely that contributions from the Ohio River Valley (consistently a day or greater away) are more impactful. Northern contributions are frequent, but not high concentration; highly sulfur emitting metal refineries in Sudbury are distant sources that could contribute to particle sulfate concentrations in Toronto, though the concentrations are lower than expected. Given the wide area of forest cover between Toronto and Sudbury, we may see significant vegetative deposition of SO_2 and p-SO_4^{-2} on a given plume's long path to York University, as the dry deposition velocity for fine particles and SO_2 has been observed to be significantly higher for vegetation versus grasslands and arable crop land.[56, 57]

Chapter 4.3 Analysis of High Sulfur Pollution Events and Transport Effects

To fully grasp the nature of the contribution of long-range transport versus local source emissions, we need to examine the high pollution event HYSPLIT trajectories, as seen in **Figures 32 and 33**, as well as **Tables 13 and 15**. As previously established, HYSPLIT trajectories are a much more accurate way to track the path of a pollution plume from its origin versus wind sector analysis. As such, we have isolated several periods of high pollutant concentrations and mixing ratios and ran HYSPLIT back trajectories for each of these periods to determine the origin of these plumes. To support the p-SO_4^{-2} trajectories, we can also examine the SO_2 and carbon monoxide mixing ratios for the time period alongside the average p-SO_4^{-2} concentration

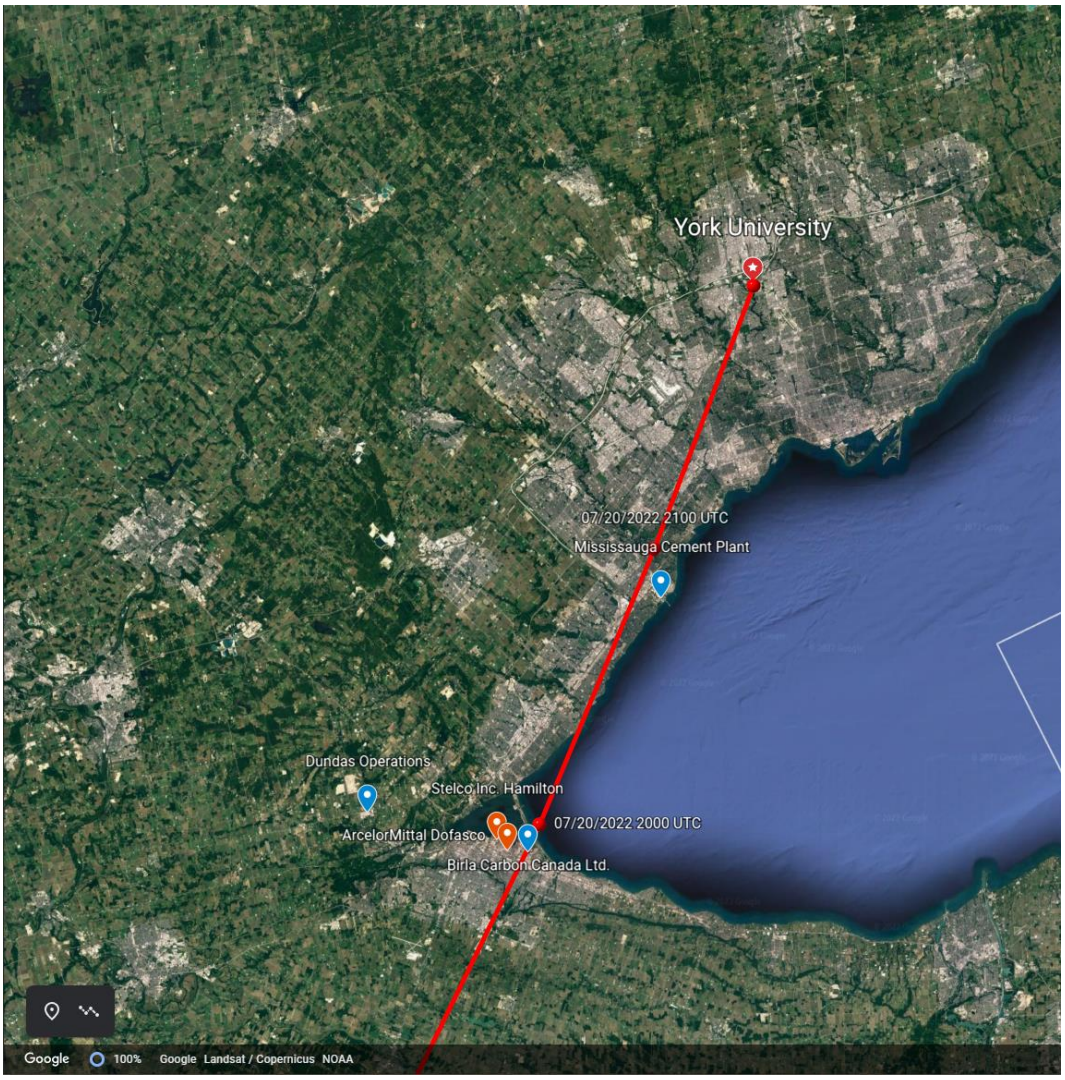

Figure 41. Sample south HYSPLIT trajectory from 7/20/2022 with hourly UTC timestamps on Google Earth.

in an attempt to estimate the degree of SO_2 oxidation and distance traveled for each detected particle mass. RH values collected by the EMOS stations are averaged from local data, and do not fully explain the meteorological history of the travelling aerosol mass (i.e., exposure to clouds and fog), which is more important for explaining the relative influences of dry- and wet-oxidation pathways. Each species' HYSPLIT trajectories are highly susceptible to lake breeze effects which can skew HYSPLIT trajectories. Since there are few p-SO_4^{-2} events, we will discuss each pollution event individually. Conversely, there are many SO_2 events, and they will be discussed in aggregate according to HYSPLIT sector.

Note that p-SO_4^{-2} is assumed to be solely oxidized SO_2 emissions, ignoring directly released $PM_{2.5}$ and sulfuric acid. We can justify this approximation based on the sulfuric acid capture efficiency of significant point sources; according to the NPRI, almost 90% of sulfuric acid produced by facilities in Canada is captured, and either disposed of or transferred to other facilities for use as a reagent.[12] Additionally, 2020 inventory estimates from the NPRI show 111,070 tonnes of SO_2 emitted in Ontario, versus 1,124 tonnes of sulfuric acid and 8063 tonnes of $PM_{2.5}$ released to the atmosphere, which is roughly a 35x factor of SO_2 to sulfuric acid.[12]

Event 1 was a southwesterly trajectory (see **Table 13)**. This trajectory had the highest p-SO_4^{-2} concentrations recorded in the entire dataset. X_{pSO4} is significantly higher than the mean, indicating that this plume was dominated by particle sulfate versus SO_2. The HYSPLIT trajectory traveled west of the GTA point sources and south of the Sarnia point sources, originating in the Ohio River Valley (see **Figure 33**). Since the CO was average and the trajectory does not travel along Highway 401, we conclude that traffic emissions are not a likely source of p-SO_4^{-2}. A possible conclusion is that the source of this southwestern plume was from Ohio and Indiana; we speculate that prevailing westerly wind transport of midday coal-fired power plant emissions were responsible for this p-SO_4^{-2} high pollution event, such as the Luminant Miami Fort Station in Ohio and the Rockport Power Plant in Indiana (see **Table 12**), though SO_2 point sources in the GTA cannot be fully eliminated as a possibility.

Event 2 was a westerly trajectory (see **Table 13**). X_{pSO4} is significantly higher than the mean X_{pSO4}, indicating that this plume was dominated by particle sulfate versus SO_2. The

HYSPLIT trajectory travels north of the Sarnia point sources and originates near the border of Michigan and Indiana (see **Figure 33**). The CO was average, and the trajectory does not travel along Highway 401, so contributions from traffic are expected to be minor. A likely origin of this western plume was from Indiana, possibly originating from East Chicago sources (ArcelorMittal and Cokenergy, see **Table 12**), though it is more likely that the most significant sources of emissions were the Sarnia petroleum and chemical production facilities.

Event 3 was a northerly trajectory (see **Table 13**). X_{pSO4} is significantly higher than the mean X_{pSO4}, indicating that this plume was dominated by particle sulfate versus gas-phase SO_2. The HYSPLIT trajectory traveled just southwest of and originated near the Sudbury metal refineries (see **Figure 33**). The CO was average, and the trajectory does not travel along Highway 401, so contributions from traffic are expected to be minor. It is likely that the source of this high particle sulfate event was Sudbury metal refineries, combined with a rapid oxidation pathway. This was a nocturnal event, which increases RH relative to the daytime, supporting this local-source emission and high RH oxidation pathway conclusion.

There is one additional explanation: wildfires are significant sources of $PM_{2.5}$ emissions, including a small fraction of sulfate release, and increase particle sulfate conversion from precursor SO_2.[58] 2021 was a particularly high year for Ontario wildfires, with 1198 total fires across the entire season, compared to 268 in 2022, and the 10-year average of 825.[59] To estimate the effect of wildfires on particulate matter, we use smoke data as a tracer, based on NOAA's HMS Smoke data (see **Figure 42**). It can be seen that, on the northern origin high p-SO_4^{-2} event, there was significantly more atmospheric smoke due to wildfire activity than on other events. It is difficult to ascertain exactly how much of the detected particle matter is from wildfires and how much is from Sudbury smelters based on the AMS measurement alone, though given the severity of the wildfires (the smoke from northern Ontario was visible from Toronto), it is likely that the wildfires are the most important contributor to this event.

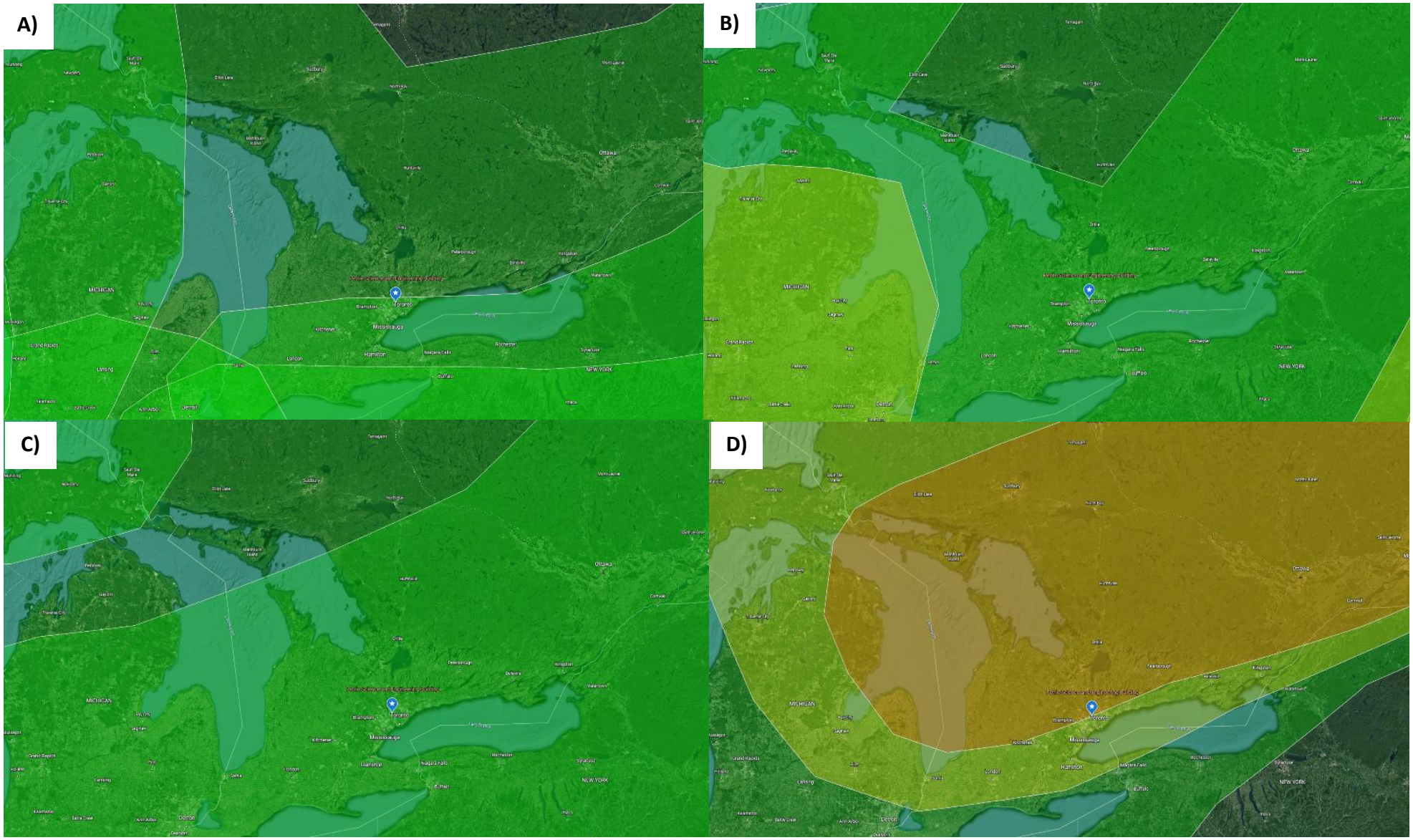

Figure 42. NOAA HMS Smoke overlays for 3 days of high p-SO_4^{-2} concentrations, and 1 'clean' day of low sulfur a comparison baseline. Overlay A) is from August 31st, 2021, a 'clean' pollutant day. Overlay B**)** is from August 12th, 2021, a southerly trajectory. Overlay C) is from August 13th, 2021, a westerly trajectory. Overlay D) is from August 20th, 2021, a northerly trajectory. A blue marker represents York University.

Event 4 was a southerly trajectory detected by AIM-IC-MS (see **Table 13**). X_{pSO4} is higher than the mean, indicating a moderate elevation of p-SO_4^{-2} relative to SO_2. Though the trajectory does travel along the Highway 401, the CO was average, and the majority of the plume was detected overnight when vehicle traffic would be low, so vehicle emissions are likely negligible. The HYSPLIT trajectory traveled directly over the Hamilton metal refineries, GTA chemical production facilities, the Nanticoke Imperial Oil petroleum refinery, and Ohio, and originating in West Virginia (see **Figure 32**). Given the high relative SO_2, we expect significant near-source oxidation of Ontario SO_2 point sources to p-SO_4^{-2}. We therefore conclude that the source of this southerly plume was likely Hamilton metal refineries and the Nanticoke petroleum refinery, with some significant influence from GTA chemical production and the Gavin Power Plant in Ohio (see **Table 12**).

Event 5 was a southerly trajectory detected by AIM-IC-MS (see **Table 13**). X_{pSO4} is higher than the mean, representing a high elevation of p-SO_4^{-2} relative to SO_2. The HYSPLIT trajectory traveled west of the GTA point sources, south of the Sarnia sources, over Ohio, and ending near the border of Indiana and Ohio (see **Figure 32**)**.** The trajectory does not travel along the Highway 401, the CO was below average, and the plume was detected overnight when vehicle traffic would be low, so vehicle emissions are likely negligible. We conclude that the primary source for this high p-SO_4^{-2} event is likely Indiana power generation plants, such as the Rockport Power Plant, the Petersburg Generating Station, and the Duke Energy - Gibson Plant (see **Table 12**). There may be some small influences from Michigan power plants (DTE Energy – Trent and Monroe Power Plants, St. Clair Power Plant), and the Luminant Fort Miami Power Station in Ohio (see **Table 12**).

Event 6 was a southerly trajectory detected by AIM-IC-MS (see **Table 13).** There was an X_{pSO4} of 0.22, which is significantly lower than mean X_{pSO4}, indicating a very low proportion of p-SO_4^{-2} relative to SO_2. CO was 0.36 ppm, which is significantly higher than the average recorded value. The HYSPLIT trajectory traveled over the Hamilton metal refineries, GTA chemical facilities, and the Nanticoke petroleum refinery, and originated just outside Detroit, Michigan (see **Figure 32**). X_{pSO4} is very low (indicating a high amount of local SO_2 emissions); thus, we expect significant near-source oxidation of Ontario SO_2 point sources to p-SO_4^{-2}. The trajectory

does travel along the Highway 401, the CO was far higher than average, and the plume was detected in the morning during heavy commuter traffic, so vehicle emissions are probable contributors to this pollution event. We conclude that the primary source for this high p-SO_4^{-2} event is rapid oxidation of SO_2 emissions from Hamilton metal refining facilities and GTA chemical production facilities, supported by SO_2 undergoing in-exhaust oxidation from vehicle emissions. There may be some supporting contributions from Michigan power generation, namely the DTE Energy – Monroe Power Plant (see **Table 12**).

Sector analysis is not useful for our p-SO_4^{-2} high pollution events, when compared to individual event analysis (see **Table 14**). Since there is only a single event for the north and west sectors, and no events for the east sector, there is no strong basis for comparison, as more data is needed to form proper trends. The only pertinent conclusion from our p-SO_4^{-2} sector analysis is the 'event count' parameter, which indicates that the majority of events originated from the south, as expected from our p-SO_4^{-2} pollution rose (see **Figure 29**).

There were 6 p-SO_4^{-2} high pollution events in total. Out of these 6, 4 originated from the west, 1 originated from south, and 1 originated from the north. While we do technically differentiate between the west and south trajectories based on the previously established angular parameters, in reality, they all follow the same, broad, southwesterly origin path. This will be a common finding between both p-SO_4^{-2} and SO_2; there is a wide overlap between the south and west HYSPLIT trajectories, often traversing over Lake Erie, and so we speculate that air plumes carrying pollution follow the prevailing westerlies from the Ohio River Valley to Toronto. It is known that prevailing westerlies are responsible for intercontinental pollution transport from the trans-Pacific Area to the United States, especially for particulate species.[60] In addition, these same prevailing westerlies are known to transport air pollution from the Ohio River Valley into Ontario.[61] Not all south and west trajectories overlap, however. There is a distinction between the overlapping southwestern trajectories originating from the Ohio River Valley, western trajectories crossing over Sarnia and Detroit, Michigan, and southern trajectories crossing over Hamilton, Nanticoke, New York, and Pennsylvania.

For the SO_2 HYSPLIT sector analysis (see **Table 16**), there were generally very few differences in any of the analyzed parameters across the sectors; we found that there were no statistically significant differences in mean mixing ratios for both SO_2 and CO across all 4 directional sectors. The major difference between each sector of analysis was the 'event count' parameter, which is a metric of the frequency of origin for our high pollution events. It was discovered that the majority of the detected SO_2 events originated in the west (N = 17), followed closely by the south (N = 15). The north sector was far lower than the west and south directions (N = 5), followed closely by the east sector, which was the most infrequent direction of origin (N = 3). This aligns with our expectations from the meteorological data (see **Figure 25**).

As mentioned previously, there is a significant amount of overlap between the south and west sectors, with indications of a southwesterly transport corridor originating from the direction of the Ohio River Valley seen in the SO_2 HYSPLIT trajectory map (see **Figure 33**). It can be seen that 6 of our 17 'west' events (events 3, 7, 11, 19, 21, and 31, see **Table 15**) are actually southwesterly origin events influenced by Hamilton metal refineries, GTA chemical production facilities, the Nanticoke petroleum refinery, and possibly some nearby Michigan power generation plants (see **Table 13**). A common feature of these events is that they did not travel past Lake Erie within the last 24 hours, indicating that is more probable that the origin of these events were local sources. Using additional HYSPLIT trajectories run for more than 24 hours could further elucidate the movement of these air plumes, but for the purposes of this study, the trajectories were kept at a constant timescale to better compare with one another (note that timestamps could be displayed for each individual trajectory to display the total run time, but this would significantly hinder the visual clarity of our figures).

Another 8 west events (events 1, 2, 6, 16, 23, 24, 26, and 38, see **Table 15**) originated directly to the west and are influenced by Sarnia's point sources as well as Michigan power plants (namely the St. Clair Power Plant, Erikson Power Plant, and the J.H. Campbell Generating Station). A final 3 west events (events 5, 13, and 14, see **Table 15**) skewed slightly to the north, and are likely influenced by very-near sources of SO_2, such as the Mississauga cement plant, and supported by Sudbury metal refineries and highway emissions, as these sources tended to originate in the north but reach York University by approaching from the south and west.

Of the 14 southern sources, 7 appeared to originate from the common southwesterly origin, as previously mentioned (events 8, 9, 22, 27, 28, and 30, see **Table 15**), while the other half of the events (events 10, 12, 25, 29, 34, 35, and 36, see **Table 15**) originated from Pennsylvania and West Virginia, or more commonly, followed non-linear paths around the GTA without travelling significantly laterally (see **Figure 33**). Regardless of origin, all of the southern sources (barring a single western-skewed trajectory, event 28, with missing CO data and an unclear origin, see **Table 15**) were influenced by Hamilton metal refineries, GTA chemical production facilities, and the Nanticoke petroleum refinery. The southwestern trajectories had some probable supporting influences from Ohio power generation sources, such as the JM Stuart Station, the Luminant Miami Fort Station, and the William H. Zimmer Power Station (see **Table 12**). The most southern trajectories were likely supported by the Cardinal Operating Co. Power Plant in Ohio, and the Keystone Power Plant, the Homer City Generating Station, the Seward Power Plant, and the Conemaugh Generating Station in Pennsylvania (see **Table 12**).

The 5 northern trajectories (events 4, 17, 18, 20, and 39, see **Table 15**) are most probably influenced by the Sudbury metal refineries, though the relationship is not completely clear. The highest detected CO mixing ratio of the northern trajectories was 0.25 ppm (event 17), followed by 0.24 ppm (event 4), with the remainder being below the average value of 0.21 ppm (see **Table 15**). It is possible that on these 2 days there was some influence from the nearby Highway 407, since these trajectories occurred in the morning during periods of expected commuter traffic, though the CO mixing ratio is not very high relative to the average. We can conclude that, in the absence of any other likely sources, distant Sudbury metal refineries were largely responsible for the northern SO_2 high pollution events, despite the high deposition rate of SO_2 in the large region of dense vegetation between Toronto and Sudbury (i.e., the travel path of Sudbury SO_2 emissions to our instruments).

The 3 eastern trajectories (events 15, 32, and 33, see **Table 15**) are skewed somewhat south, likely due to lake and land breeze effects, or possibly the resolution of HYSPLIT's meteorology data (see **Figure 33**). There may be some close influence from the GTA chemical production facilities, namely the Mississauga Cement Plant, though the greatest contributor of eastern SO_2 is most likely the Bowmanville Cement Plant, with some contributions from the

Leigh Hanson Materials Ltd. Picton Plant, and the RED Rochester LLC. and Cayuga Operating Company LLC. power generation sources in New York (see **Table 12**). CO data is only available for 2 of the 3 trajectories, and both of these trajectories show CO mixing ratios close to the average, and so it is unlikely that vehicle emissions are a significant contributor to eastern origin SO_2 in Toronto.

There were 7 detected high pollution events (events 3, 6, 9, 11, 16, 23, 34, see **Table 15**) with a significant elevation of CO (defined here as 10σ greater than the background (≥ 0.26)). 5 of these 7 events had a westerly HYSPLIT origin, and 2 had a southerly HYSPLIT origin. All of these events travel along either Highway 401, or Highway 407.

There was a small but notable seasonal dependence on the detected SO_2 high pollution event count (see **Table 17**), where it was found that there significantly more high pollution events in the summer period (N = 14) versus any other season (autumn: N = 8, winter: N = 2, spring: N = 4). While it appeared that the mean SO_2 mixing ratio of high pollution events was higher in the summer, it was not possible to establish a statistically significant difference.

June 2022, in particular, had the highest number of high pollution events compared to any other month, with over a quarter of the events taking place during this month (10/39, see **Table 15**). As seen in the monthly box plot for SO_2 (see **Figure 21**), the 95^{th} percentile data range is far higher in June 2022 than any other month; the frequency of high pollution events in this month contributed to this outlier. Of these 10 events, 5 originated in the west (events 19, 21, 23, 24, and 26), 3 originated in the south (events 22, 25, and 27), and 2 originated in north (events 18 and 20). As expected, the primary contributors to these June events were Hamilton metal refineries, GTA chemical production facilities, Sarnia petroleum and chemical production facilities, as well as some minor contributions from Michigan and Ohio power plants. Only event 23 had a CO mixing ratio significantly above the average of 0.21 ppm; this event had a CO mixing ratio of 0.31 ppm and passed close to Highway 401, though the nocturnal timing of the event makes conclusion of aggregated vehicle emissions suspect. It is more likely that there were some distant influences from Sarnia and Michigan.

Two of the three 2022 Ontario Special Air Quality Statements (SAQS, a warning issued during short-term, high-health-risk, atmospheric pollution periods such as forest fires) were issued in this month, on June 21st, 2022, and June 25th, 2022 (the third occurred after our collected dataset, on October 24th, 2022).[62] This coincides with 3 of our detected high pollution air quality events, and immediately precedes our maximum detected mixing ratio of 27 ppb on June 26th, 2022. In 2021, before our data collection began, there were 2 SAQS, on June 6th, and on July 19th. As an aside, there were no Smog and Air Health Advisories for 2021 and 2022 (a special air quality warning issued for long-term, high-health-risk, atmospheric pollution periods).[63]

4.4 Sarnia Field Study

From our Sarnia field study, we calculated from our mass-balance equation that the SO_2 emissions rate (based on the average of our quantitative transects) for July 21st and July 22nd, 2022, was 0.18 tn/hr (95% CI [0.16, 0.20]), or 4,320 kg/day. We used the NPRI SO_2 emissions inventory from 2002 to 2021 to estimate the hourly emissions rate for Sarnia from the last 2 decades as a reference point (see **Figure 39**). It is important to reiterate that directly comparing an annual emissions inventory with a 2-day mass balance estimation will make for an incompatible analysis. Extrapolating the 2-day estimation to an entire year will not provide an accurate count of the total SO_2 emitted, though averaging a yearly emissions total from an inventory to an hourly rate could provide a rough basis for comparison.

Similar to the general trend of Ontario SO_2, the Sarnia emissions rate has stagnated since 2010. Based on the NPRI estimate, the average Sarnia SO_2 emissions rate was 2.1 tonnes/hr since 2015, the year of implementation of the most recent set of Ontario environmental regulations. Compared to this average, Sarnia SO_2 emissions have decreased by 91% from the last 10-year-average to 2022. This would be a dramatic decrease not replicated by our general trend of SO_2 data in Ontario. Our initial conclusion would be that our estimated emissions rate is far lower than we should expect; to investigate this result, we will examine the various factors affecting our estimate.

Firstly, the emissions rate was calculated from a single field study consisting of only two days of analysis. The mass-balance equation is highly dependent on local meteorological conditions, which are themselves dependent on season; notable variables include temperature, wind speed, and boundary layer height. The temperature has a lesser effect than other meteorological parameters (e.g., reducing the ambient temperature by 30° C would only affect the integral sum by ~0.02), and the wind speed was not low, which means that other factors would be responsible for underestimation. Boundary layer height estimates are the most nebulous factor for our mass-balance equation; our first estimate is based on a model, with a high relative uncertainty, while the second estimate is based on ceilometer measurements, which originated from nearby Windsor, not in Sarnia itself. For example, based on the upper ranges of our estimate from the NCEP North American Regional Reanalysis Product model, the boundary layer height on July 21st may have been as high as 2750 m, which corresponds to a calculated emissions rate estimate of 0.67 tonnes/hr (assuming that this would be the only boundary layer estimate). This extreme example would still demonstrate a 68% decrease in Sarnia SO_2 emissions, indicating that there are still other factors to consider.

Another consideration from the narrow window of the field campaign is that unforeseen factors may skew the data. Sarnia SO_2 emissions are almost entirely based off of 4 specific point sources - over these 2 days, if anything interfered with the operation of these facilities, we may see a random and uncontrolled reduction in apparent SO_2 emissions (e.g., if, for some reason, the Imperial Oil petroleum refinery had a significant reduction in production).

The final consideration is that the extreme decrease in estimated SO_2 emissions could be partially expected. There was a specific amendment to the 1990 Ontario Environmental Protection Act (*O. Reg. 530/18*) made on February 25th, 2022, specifically targeting petroleum refinery SO_2 emissions.[19] By this amendment, Imperial Oil (both Sarnia and Nanticoke), Shell (Sarnia/Corunna), and Suncor's (Sarnia) petroleum refineries would be required to reduce their sulfur emissions by 80% across the province, and by 90% in Sarnia specifically.[19] By the estimates of the regulations, these listed facilities would decrease their SO_2 emissions by about 20% in 2 months (from the decision date of February 25th, 2022) through the use of SO_2 reducing additives in the petroleum refining process, and the banning of sulfurous fuels used in

the refining process.[19] These facilities will also have established emissions limits to be adhered to by December 2028, capping at 225 kg of SO_2 per day. The projected 90% reduction would align with our observed estimation of the decrease in SO_2 emission rate, though it is likely too early to observe proper adherence to these theoretical limits. There is also a discrepancy between the regulations and the observed emissions measurements; 225 kg/day for 4 facilities in Sarnia would be a limit of 900 kg/day, or 0.04 tn/hr, which is actually a ~98% projected reduction in SO_2 emissions. It is possible that the 91% observed decrease is as expected from the actions prescribed in the newest legislation, and that the remaining ~7% reduction in emissions will be more difficult to achieve, requiring more years of effort.

There are a few other relevant observations from our Sarnia field study. First, we find our known point sources correlated well with our driven transects' detected emissions. By labeling the peak concentrations of SO_2 on our transect maps (see **Figures 34 and 35**), and overlaying forward HYSPLIT trajectories, we note that the peak of our pollutant plumes are almost perfectly aligned with our point sources. This demonstrates that the sources identified in our NPRI inventory are still the most relevant SO_2 emitters in Sarnia. We can also track the individual peaks to specific point sources, though the Imperial Oil petroleum refinery and the Cabot Canada Ltd. chemical production facility are too close together to be spatially resolved by HYSPLIT. We find that, as expected, the Imperial Oil/Cabot Canada (~10% of Ontario's total 2020 emissions, see **Table 1**) combined source is responsible for our peak emissions on both days of the field study, according to our HYSPLIT trajectories.

Transect 3 on the first day of the field study is important to highlight (see **Figures 36 and 38**). The peak SO_2 appears to be diminished relative to the later transects; conventional understanding would indicate that it should have higher detected SO_2 mixing ratios relative to Transects 4 and 5, as it should be somewhat less dispersed. This could indicate an inconsistent emission rate from the source during the midday, which in turn would cause a slight underrepresentation of the estimated emission rate.

During the course of the field study, significant local plumes of SO_2 were observed, emitting from our highlighted point sources. Specifically, on July 22nd, 2022, we observed an air

plume emitted from Imperial Oil/Cabot Canada Ltd. with a detected SO_2 mixing ratio of over 200 ppb; to contextualize this value with a personal anecdote, we noticed that as we drove through the plume, there was a distinct, sulfurous flavour to the air inside our vehicle. This 200 ppb mixing ratio could exceed the AAQC, if it remained at this level for at least 10 minutes. Due to the mobile nature of our study, we could not remain in location and observe the mixing ratio over time; as such we cannot conclusively determine if there was an AAQC exceedance in this location, or if it was a brief refinery flare that quickly subsided. Sustained SO_2 emissions of this caliber could have significant deleterious health effects on the surrounding population centre

This 200 ppb plume does provide a valuable case study for the reduction and dispersion of an emitted SO_2 plume over distance, as it is easily tracked through our transects. The 200 ppb peak was detected in Transect 1, then decreased to 16 ppb 2 km away in Transect 2, followed by 8 ppb 7 km away in Transect 3, and finally detected at 7 ppb 15 km away in Transect 4 (see **Figure 37 and Table 20**). We can see that, as expected, the decrease in SO_2 over distance stagnated as the dispersion of the plume became well-mixed up to the boundary layer. In just 20 km, however, the peak SO_2 mixing ratio had reduced by 97%. While the rate of dissipation is heavily dependent on meteorological conditions, in general, we can see that the dispersion of peak SO_2 emissions will result in a rapid decline in detected mixing ratios within 2-20 km. This has critical implications for our analysis of long-range transport effects on Toronto's SO_2 mixing ratio. If a sufficiently high-SO_2-mixing-ratio plume, such as the 200 ppb peak detected during our study, were to travel from Sarnia, it may be detected in Toronto, but it would require optimal meteorological conditions. As such, transported high pollution event SO_2 is either from a close source, or is a significantly high mixing ratio emission coupled with favourable wind and weather conditions to sustain rapid air plume transport. Otherwise, we would expect extinction of the plume through a combination of deposition and oxidation during transit.

Chapter 5 – Conclusions

5.1 Summary

In summation, we note statistically significant differences in SO_2, p-SO_4^{-2}, SO_x, and X_{pSO4} when comparing the current data to the historical data. In Toronto, we observed an 87% decrease in mean SO_2 mixing ratio from 2003 to 2022 (2.9 to 0.37 ppb, see **Table 5**). While comparisons made with the earliest years in the historical dataset are functionally significant, more recent trends have headed towards stagnation, varying between 0 and 1 ppb since 2012. For Toronto in particular, the historical dataset demonstrates a linear correlation in the decrease of annual SO_2 mean (see **Figure 13**) until 2012, and since then, there is no clear upwards or downwards trend (including the current data). Additionally, there were no observed correlations for seasonal and daytime/nighttime intervals in the current time period.

A similar result can be seen for p-SO_4^{-2}, where the earliest years of the NAPS data for Toronto shows a linear decrease in annual mean concentration until 2008, after which this rate of decrease appears to stagnate. After 2008, there is a weak, downward trend in annual mean p-SO_4^{-2} concentration to the current time period (see **Figure 14**). The 2021 mean was 0.60 µg/m^3, an 81% decrease from 2.6 µg/m^3 in 2003. From this decrease, we expect that there was a 2.8% reduction in all-cause deaths over this time interval. There is a single historical correlation of p-SO_4^{-2} with seasonal variation, as particle sulfate was highest in the summer of 2005 (aligning with literature expectations) though a larger seasonal trend cannot be ascertained. Additional particle data was collected by the AMS (p-organics, p-NH_4^+, p-NO_3^-), and it was found that p-organics were higher than expected compared to the literature value, and all other particles were lower than expected. Our confidence in our AMS and AIM-IC-MS particulate data conclusions is hindered by the low quantity of data.

The trend in SO_x followed a linear decrease until 2012, at which point there was a weak downward trend year-over-over year with recent stagnation, to our current SO_x mean of 1.6 µg/m^3. This resembles a hybrid of the SO_2 and p-SO_4^{-2} trends across the historic and current time periods. X_{pSO4} has decreased in recent years from 0.54 in 2019 to 0.36 in 2022. X_{pSO4} has a moderate negative correlation with SO_2 (r = -0.76), and unexpectedly, a weak negative

correlation with p-SO_4^{-2} (r = -0.40). This is likely an invalid conclusion, indicative of the high variability in the available particle sulfate data (since, in isolation, an increase in p-SO_4^{-2} would theoretically correlate with a higher X_{pSO4}).

Based on our pollution roses, we can see that the most significant sectors of origin for SO_2 and p-SO_4^{-2} are from the south and the west. In general, we see influence from local GTA point sources, such as Hamilton metal refineries, GTA and Sarnia chemical production facilities, and petroleum refineries in Nanticoke and Sarnia, with likely minor influences from local highways. There is also moderate influence from the north sector, associated with Sudbury metal refineries.

The majority of high pollution events also originated in the south and west sectors, with a common overlap in the southwest, which is speculated to be influenced by a prevailing westerly wind transporting pollutants from the Ohio River Valley. SO_2 high pollution events were again associated with GTA point sources, most notably Hamilton metal refineries, GTA chemical production facilities, and the Nanticoke petroleum refinery, with some partial influence from distant Sudbury metal refineries and Sarnia petroleum and chemical production facilities. There is also a segment of the Highway 401 that, when traced with high carbon monoxide mixing ratios, is a probable minor contributor to Toronto SO_2 mixing ratios. Note that SO_2 has been shown to rapidly and non-linearly decrease in mixing ratio with distance from the source, and so the contribution of the Sarnia and Sudbury point sources require highly concentrated air plumes under favourable meteorological conditions to reach Toronto. US point sources in Michigan, Ohio, Indiana, Pennsylvania, and New York (see **Table 12**) may have some minor contributions to Ontario's SO_2, though the transport distance of these point sources to Toronto make significant influence unlikely. One notable exception is the St. Clair Power Plant in Michigan, which is directly adjacent to Sarnia and emits more SO_2 per year than any other point source listed in this analysis (see **Tables 1 and 12**), and so we expect comparable or even greater influence than Sarnia point sources. There is also a seasonal dependence for the number of detected high pollution events, as the summer months (particularly June 2022, coinciding with two Ontario SAQS alerts) had the highest event count by far.

Particle sulfate high pollution events were largely associated with the aforementioned GTA point sources (possibly related to differences in RH), long-range transport from Sarnia, Sudbury, Michigan, Ohio, and Indiana, and in-exhaust oxidation of vehicle emissions of SO_2. U.S. coal-fired power plants, namely the Ohio Luminant Miami Fort Station and William H. Zimmer Power Plant, the Michigan DTE Energy – Monroe and Trenton Power Plants and St. Clair Power Plant, and the Indiana Rockport Generating Station, are likely major contributors to Ontario's p-SO_4^{-2}. Unusually high wildfire activity in the summer of 2021 was likely a partial contributor to northern origin p-SO_4^{-2}.

The calculated emissions for Sarnia based on our mobile mass-balance method field study was 0.18 tn/hr (95% CI [0.14, 0.22]), or 4,300 kg/day. There was a 91% reduction in Sarnia SO_2 emissions from the previous 10-year average, based on the NPRI data. The most significant likely contributor to the SO_2 reduction is the February 2022 Environmental Protection Act regulation amendment that immediately mandated sulfur-reducing additives added to Ontario petroleum facilities, while also banning sulfurous refinery fuels. The limited time period for the field study increases the uncertainty of our estimate as it applies to the trend of SO_2 emission rates in Sarnia.

Overall, we can see a historic trend of sulfur reductions in Ontario, particularly in Toronto. Environmental regulations enacted in 2015 have not shown a significant effect, as both SO_2 and p-SO_4^{-2} have plateaued in recent years in Toronto, with the majority of sulfur reductions resulting from previous decades of regulations. The major contributors to Ontario's SO_2 are Hamilton metal refineries, GTA chemical production facilities, the Nanticoke petroleum refinery, and some minor contributions from traffic emissions, Sarnia petroleum and chemical production facilities, coal-fired power plants in Michigan, Ohio, Pennsylvania, and Indiana. The major contributors to Toronto's p-SO_4^{-2} are Sarnia petroleum and chemical production facilities, Hamilton and Sudbury metal refineries (particularly in high-RH regimes), long-range transport from power plants in Ohio, Michigan, and Indiana, and wildfire activity to the north. Much like the February 2022 petroleum regulations, sector-based reduction targets are the most effective approach to control sulfur emissions; for example, metal refining facilities emit more SO_2 than

any other industry in Ontario, and so specific measures to capture sulfur more efficiently from metal smelting processes would be effective.

5.2 Future Work

There are a number of future steps that need to be taken to reinforce this study. The main limitation to our research was the relatively fixed location of the data collection; outside of our 2-day Sarnia field study, the entirety of this study was conducted on-site at York University. In order to draw any conclusions about the effects of pollutant transport, a number of necessary assumptions were continually made, assisted with atmospheric transport modeling via NOAA HYSPLIT. For instance, on any given high pollution event, we take our best estimate of the pollutant source based on the proximity of inventory point sources to our trajectory and support our estimates with metrics such as carbon monoxide mixing ratios. The issue with this approach, however, is the uncertainty associated with each conclusion. Without comprehensive field work, it is not possible to conclusively track and determine our pollutant plumes from their respective sources. The Sarnia field study, for instance, helped elucidate the transport dynamics of Sarnia SO_2 point sources. We would still need more research to track plumes all the way to York University, to fully understand the dissipation rate of SO_2 pollution.

A more aggressive approach to field campaigns would help confirm the speculative theories made in this study with respect to sulfur plume origins. In particular, direct downwind measurements made in Hamilton, Mississauga, Nanticoke, and Sudbury are necessary to confirm the current contributions of our historic inventory point sources, as well as the experimental lifetimes of sulfur plumes (factoring in deposition rates over distance traveled for our specific topographies, dispersion effects, and the oxidation rates relative to relative humidity). Quantifying the relationship between emitted SO_2 mixing ratios from the source and detected emissions in Toronto is essential for confirming the most important contributors to Ontario's atmospheric sulfur. It would also be useful to confirm the presence of the southwesterly air pollution transport corridor speculated in this study, as this is critical to understanding the consequences of long-range transport from U.S. coal-burning emissions.

There are several important considerations for these further field studies. First, it would be useful to expand the dimensions of our analysis. In addition to measuring SO_2 mixing ratios with the Thermo Fisher 43i instrument, we could also take field measurements of p-SO_4^{-2} by using a mobile Aerodyne AMS, known as a Compact-ToF-AMS. As we move downwind of the source, we could directly evaluate the conversion rate of SO_2 to p-SO_4^{-2} with respect to time and relative humidity and meteorological factors. Another consideration is the type of vehicle used – an aircraft campaign would help cover a lot more distance in our measurements when compared to a ground vehicle method, which helps accurately determine the decrease in sulfur from the emission site to York University.

Increasing the amount of data available in our study would reinforce the conclusions made. Specifically, collecting AMS data for the entire study period, and ensuring that the AMS was calibrated, would allow for more confidence in our p-SO_4^{-2} analysis and direct comparison with the entire SO_2 dataset. There should also be an element of reproducibility; in particular, it would be prudent to repeat our Sarnia field study, especially given the uncertainty in the pollution decrease observed from our historical dataset to our field study. If our observations are repeatedly seen across multiple field studies, we could make a stronger conclusion about the effects of environmental regulation on reducing sulfur emissions.

References

1. Aas W. et al. Global and regional trends of atmospheric sulfur. *Nature Scientific Reports,* **2019**, *953*, 1-11.
2. Powe, N. A., Willis, K. G. Mortality and Morbidity Benefits of Air Pollution (SO_2 and PM_{10}) Absorption Attributable to Woodland in Britain. *Journal of Environmental Management* 2004, *70*, 119-128.
3. Burnett R. T. et al. Effects of Low Ambient Levels of Ozone and Sulfates on the Frequency of Respiratory Admissions to Ontario Hospitals. *Environmental Research* **1994**, *65*, 172-194
4. Xing Y., Xu Y., Shi M., Lian Y. The impact of PM2.5 on the human respiratory system. *J Thorac Dis*. **2016,** *8*, 69-74.
5. Atkinson R. W. et al. Acute effects of particulate air pollution on respiratory admissions: results from APHEA 2 project. Air Pollution and Health: a European Approach. *Am J Respir Crit Care Med* **2001**, *164*, 1860-1866.
6. Watmough S. A., Aherne J., Eimers C., Dillon P. J. Acidification at Plastic Lake, Ontario: Has 20 Years Made a Difference? *Water Air Soil Pollut.* **2007**, *7*, 301-306.
7. Kunzli N. et al. Breathless in Los Angeles: The Exhausting Search for Clean Air. *Am J Public Health,* **2003,** *93*, 1494–1499.
8. Davis D., Bell M., Fletcher T. A look back at the London smog of 1952 and the half century since. *Environmental Health Perspectives,* **2002**, *110*.
9. Husain L. et al. Long-term trends in atmospheric concentrations of sulfate, total sulfur, and trace elements in the northeastern United States. *Journal of Geophysical Research* **2004,** *09*, 1-12.
10. Fairbridge, P. Measurement of Wintertime SO_2 at York University, *report for CHEM 4000*, **2005.**
11. Ontario Ministry of the Environment. Ontario's Ambient Air Quality Criteria. Ontario Government Website. https://www.ontario.ca/page/ontarios-ambient-air-quality-criteria. (Accessed October 7th, 2022).

12. National Pollutant Release Inventory. NPRI Data. https://pollution-waste.canada.ca/national-release-inventory/ (Accessed October 7th, 2022).
13. Chou C. Sulfur in coals: A review of geochemistry and origins. *International Journal of Coal Geology*, **2012**, *100*, 1-13.
14. Carn S. et al. Sulfur dioxide emission from Peruvian copper smelters detected by the Ozone Monitoring Instrument. *Geophysical Research Letters,* **2007**, *34*, n.p.
15. Gardiner K. et al. Occupational exposure to carbon monoxide and sulphur dioxide during the manufacture of carbon black. *Ann Occup. Hyg.,* **1992**, *36*, 363-372.
16. Bell et al. Spatial and Temporal Variation in $PM_{2.5}$ Chemical Composition in the United States for Health Effects Studies. *Environ Health Perspect*. **2007**, *115*, 989-995.
17. Ontario Consolidated Laws. R.R.O. 1990, Reg. 361: SULFUR CONTENT OF FUELS. *Environmental Protection Act.* https://www.ontario.ca/laws/regulation/900361 (Accessed October 7th, 2022).
18. Government of Canada. Sulfur in Gasoline Regulations. Government of Canada Website. https://laws-lois.justice.gc.ca/eng/regulations/SOR-99-236/page-1.html#h-1029237 (Accessed October 7th, 2022)
19. Ontario Consolidated Laws. R.R.O. 1990, O. Reg. 530/18: AIR POLLUTION – DISCHARGE OF SULFUR DIOXIDE FROM PETROLEUM FACILITIES. *Environmental Protection Act.* https://www.ontario.ca/laws/regulation/180530 (Accessed October 7th, 2022).
20. Canagaratna M. R. et al. Chemical and Microphysical Characterization of Ambient Aerosols with the Aerodyne Aerosol Mass Spectrometer. *Mass Spectrometry Reviews*, **2007**, *26*, 185-222.
21. Finlayson-Pitts B. J., Pitts J.: Chemistry of the Upper and Lower Atmosphere, Academic Press, San Diego, California, United States, 2000.
22. Hazi Y., Heikkinen M.S.A., Cohen B. S. Size distribution of acidic sulfate ions in fine ambient particulate matter and assessment of source region effect. *Atmospheric Environment,* **2003,** *37*, 5403-5413.

23. Hoyle C.R. et al. Aqueous phase oxidation of sulphur dioxide by ozone in cloud droplets. *Atmos. Chem. Phys.*, **2016**, *16*, 1693-1712.

24. Kunen S. M., Lazrus A. L., Kok G. L., Heikes B. G. Aqueous oxidation of SO2 by hydrogen peroxide. *Journal of Geophysical Research*, **1983**, *88,* 3671-3674.

25. Jia M. et al. Inverse Relations of PM2.5 and O3 in Air Compound Pollution between Cold and Hot Seasons over an Urban Area of East China. *Atmosphere* **2017**, *59,* 1-12.

26. Brown et al. Variability in Nocturnal Nitrogen Oxide Processing and Its Role in Regional Air Quality. *Science*, **2006**, *311*, 67-69.

27. Wang J., et al. Fast sulfate formation from oxidation of SO2 by NO2 and HONO observed in Beijing haze. *Nature Communications*, **2020**, *11*, 1-7.

28. Kasper A., Puxbaum H. Seasonal Variation of SO2, HNO3, NH3 And Selected Aerosol Components At Sonnblick (3106 m a.s.l.). *Atmospheric Environment,* **1998***, 32,* 3925-3939

29. Henschel S. et al. Ambient air SO2 patterns in 6 European cities. *Atmospheric Environment***, 2013**, *79*, 236-247.

30. Paulot F., Fan S., Horowitz L. W. Contrasting seasonal responses of sulfate aerosols to declining SO2 emissions in the Eastern U.S.: Implications for the efficacy of SO2 emission controls. *Geophysical Research Letters*, **2016**, *44*, 455-464.

31. Environment and Climate Change Canada. NAPS Program Data Mart. Environment and Climate Change Canada Website. https://data-donnees.ec.gc.ca/data/air/monitor/national-air-pollution-surveillance-naps-program/?lang=en. (Accessed October 10th, 2022).

32. Ontario Ministry of the Environment. Air Quality Ontario. Ontario Ministry of the Environment Website. http://www.airqualityontario.com/. (Accessed October 14th, 2022).

33. Government of Canada. National Air Pollution Surveillance Program. Government of Canada Website. https://www.canada.ca/en/environment-climate-change/services/air-pollution/monitoring-networks-data/national-air-pollution-program.html. (Accessed October 10th, 2022)

34. ThermoFisher Scientific. Model 43i-TLE Instruction Manual, 2015. ThermoFisher Scientific Website. https://www.thermofisher.com/order/catalog/product/43ITLE. (Accessed October 10th, 2022).
35. Aerodyne Research Inc. AMS Aerosol Mass Spectrometer Systems. Aerodyne Research Inc. Website. https://www.aerodyne.com/wp-content/themes/aerodyne/fs/Aerosol%20Mass%20Spectrometer%20Systems_2.pdf. (Accessed October 10th, 2022).
36. He L. et al. Submicron aerosol analysis and organic source apportionment in an urban atmosphere in Pearl River Delta of China using high-resolution aerosol mass spectrometry. *Journal of Geophysical Research,* **2011**, *116*, 1-15.
37. Environment and Climate Change Canada. Historical Climate Data. https://climate.weather.gc.ca/. (Accessed October 16th, 2022).
38. Stull R., *Practical Meteorology: An Algebra-Based Survey of Atmospheric Science,* no ed.; Univ. of British Colombia, 2017.
39. Karion A. et al. Methane emissions estimate from airborne measurements over a western United States natural gas field; Supplemental. *Geophysical Research Letters*, **2013**, *40*, 4393-4397.
40. Stull R., *An Introduction to Boundary Layer Meteorology*, no ed.; Springer, 1988.
41. University of Colorado Jimenez Group. TOF-AMS. University of Colorado Website. https://cires1.colorado.edu/jimenez-group/ToFAMSResources/ToFSoftware/. (Accessed October 11th, 2022).
42. Stein A. F. et al. NOAA's HYSPLIT Atmospheric Transport and Dispersion Modeling System. *Bulletin of the American Meteorological Society* **2015**, *96,* 2059-2077
43. Picarro. Cavity Ring-Down Spectroscopy (CRDS). Picarro Website. https://www.picarro.com/company/technology/crds. (Accessed October 11th, 2022).
44. Joudan S., Clouthier J., VandenBoer T., Young C. Application of a novel online ion chromatography-mass spectrometry method to measure organic acids in particulate matter in Toronto, Canada. In prep.

45. Taylor, P. Background of EMOS. (Accessed February 22nd, 2023). https://www.yorku.ca/pat/weatherStation/background.html

46. DeCarlo, P. F. et al. Field-Deployable, High-Resolution, Time-of-Flight Aerosol Mass Spectrometer. *Anal. Chem* **2006**, *78*, 8281-8289.

47. Seinfeld, J. H.; Pandis, S. N. *Atmospheric Chemistry and Physics: From Air Pollution to Climate Change*, 2nd ed.; John Wiley & Sons, Inc., 2006.

48. Environmental Protection Agency. 2017 National Emissions Inventory. (Accessed December 9th, 2022). https://www.epa.gov/air-emissions-inventories/2017-national-emissions-inventory-nei-data#dataq

49. Justus C. G., Mikhail A. Height Variation of Wind Speed and Wind Distribution Statistics. *Geophysical Research Letters*, **1976**, *3*, 261-264.

50. Lepeule J., Laden F., Dockery D., Schwartz K. Chronic Exposure to Fine Particles and Mortality: An Extended Follow-up of the Harvard Six Cities Study from 1974 to 2009. *Environmental Health Perspectives*, **2012**, *120*, 965-970.

51. U.S. Department of Transportation. Long-Life Concrete Pavements in Europe and Canada - Chapter 2: Pavement Selection Strategies. USDT Website. https://international.fhwa.dot.gov/pubs/pl07027/llcp_07_02.cfm (Accessed November 4th, 2022).

52. Environment and Climate Change Canada. Canada's Air Pollutant Emissions Inventory Report 2022: Sulphur Oxides (SO_x). Government of Canada Website. (Accessed February 26th, 2023).

53. Hewitt, C. N., Harrison, R. Tropospheric concentrations of the hydroxyl radical - a review. *Atmospheric Environment* **1985**, *19*, 545-555.

54. Eatough D. J., Caka F. M., Farber R. J. The Conversion of SO_2 to Sulfate in the Atmosphere. *Israel Journal of Chemistry* **1994**, *34*, 301-304.

55. Liu T. et al. Formation of secondary aerosols from gasoline vehicle exhaust when mixing with SO2. *Atmos. Chem. Phys.* **2016**, *16*, 675-689.

56. Gallagher M. et al. Measurements and parameterizations of small aerosol deposition velocities to grassland, arable crops, and forest: Influence of surface roughness

length on deposition. *Journal of Geophysical Research* **2002,** *107*, 4154-4162.

57. Hayden K. et al. New methodology shows short atmospheric lifetimes of oxidized sulfur and nitrogen due to dry deposition. *Atmos. Chem. Phys.* **2021**, *21*, 8377-8392.
58. Reid J. S., Koppmann R., Eck T. F., Eleuterio D. P. A review of biomass burning emissions part II: intensive physical properties of biomass burning particles. *Atmos. Chem. Phys.* **2005**, *5*, 799-825.
59. Ontario Government. Forest Fires. Ontario Government Website. https://www.ontario.ca/page/forest-fires#section-5 (Accessed November 9th, 2022).
60. Wang K. et al. Modeling intercontinental air pollution transport over the trans-Pacific region in 2001 using the Community Multiscale Air Quality modeling system. *Journal of Geophysical Research* **2009**, *114*, 1-23.
61. Zheng, Y., Hopke P. K. A study of the sources of acid precipitation in Ontario, Canada. *Atmospheric Environment* **1989**, *23*, 1499-1509.
62. Ontario Ministry of the Environment. Special Air Quality Statements (SAQS). Ontario Ministry of the Environment Website (Accessed November 12th, 2022).
63. Ontario Ministry of the Environment. Smog and Air Health Advisories (SAHA). Ontario Ministry of the Environment Website (Accessed November 12th, 2022).